Limits of Voronoi Diagrams

Limieten van Voronoi Diagrammen

(met een samenvatting in het Nederlands)

Proefschrift

door

Roderik Cornelis Lindenbergh

geboren op 12 juni 1970, te Aerdenhout

promotor: Prof. Dr. D. Siersma
copromotor: Dr. W. L. J. van der Kallen

Faculteit der Wiskunde en Informatica
Universiteit Utrecht

Contents

Chapter 1

Introduction.

In this thesis we study sets of points in the plane and their Voronoi diagrams, in particular when the points coincide. We bring together two ways of studying point sets that have received a lot of attention in recent years: Voronoi diagrams and compactifications of configuration spaces. We study moving and colliding points and this enables us to introduce 'limit Voronoi diagrams'. We define several compactifications by considering geometric properties of pairs and triples of points. In this way we are able to define a smooth, real version of the Fulton-MacPherson compactification. We show how to define Voronoi diagrams on elements of these compactifications and describe the connection with the limit Voronoi diagrams.

Voronoi diagrams and supermarkets.

Consider all supermarkets in a city. We divide the city in sectors by considering the closest supermarket: all people in the sector of some supermarket are closer to this supermarket than to any other supermarket. The *Voronoi diagram* of the supermarkets is this subdivision of the city into sectors. The *Voronoi cell* of one supermarket is just the sector of the supermarket. An example of a Voronoi diagram of six supermarkets, numbered 1 to 6, is given in Figure 1.1.
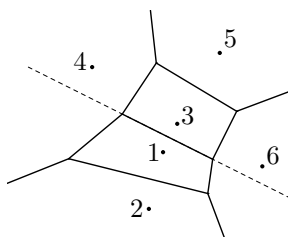
Figure 1.1: The Voronoi diagram of six supermarkets, labeled $1, 2, 3, 4, 5, 6$.

In the figure we see some boundaries, for example the boundary between supermarket 1 and supermarket 3. People living on this boundary are at equal distance between those supermarkets. The boundary is part of a line, the dotted line in the picture, which is called the *bisector* of 1 and 3, because on one side of the line people are closer to supermarket 1 and on the other side people are closer to supermarket 3. So, the bisector divides the plane into two sectors or *half-planes*. The sector containing supermarket 1 is called *Voronoi half-plane* $vh(1,3)$ and the sector on the other side of the bisector is Voronoi half-plane $vh(3,1)$. We can express the sector $V(1)$ of supermarket 1 in terms of these Voronoi half-planes:

$$V(1) \;=\; vh(1,2) \cap vh(1,3) \cap vh(1,4) \cap vh(1,5) \cap vh(1,6) \qquad (1.1)$$

Of course this formula just states that you are in the sector of supermarket 1 if you are closer to supermarket 1 than to 2, closer to supermarket 1 than to 3, etcetera. If we want to code the bisector of 1 and 3, we need only two ingredients: one point on the bisector and the *angle* that the bisector makes with the horizontal line. This will be important later on.

Driving supermarkets: changing Voronoi diagrams.

In the Dutch countryside food is supplied by little supermarket lorries, or supervans. These vans drive through the countryside looking for customers. In the part of the countryside we are considering there are five supervans. If we know their positions at a certain moment, we can determine the Voronoi diagram of the five vans at that moment. But, if the vans drive continuously the Voronoi diagram of the vans changes continuously as well. In Chapter 4 we model these driving supervans and their changing Voronoi diagrams. For every supervan there is a curve that gives at any time t the position of the supervan. If we want to know the Voronoi diagram at time t, we specify t in the curves describing the position of the vans. Using positions given by the curves we compute the Voronoi diagram.
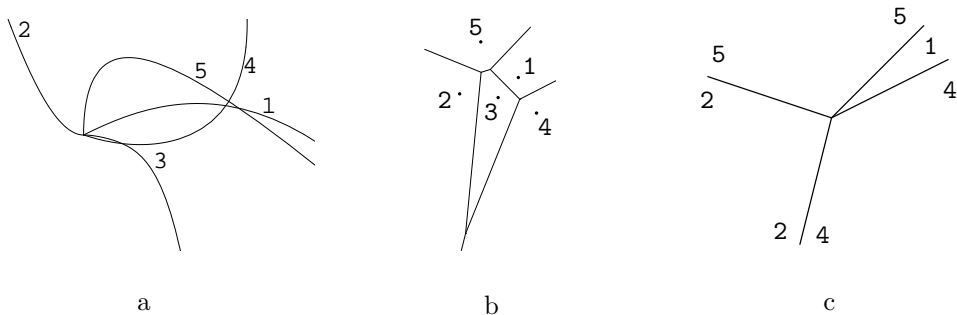

Figure 1.2: a. The positions of five driving supervans before collision. b. The Voronoi diagram of the vans, just before collision, and c. at collision.

There is only one problem. At one day a very unfortunate accident happens: all vans run into each other at $t = 0$. How should we define the Voronoi diagram of the vans at $t = 0$? In this particular example we decide to analyze the situation just before the accident happens. That is, we let time run backwards and investigate what is going on for small negative t. The route covered by the five vans before the accident is shown in Figure 1.2.a. A Voronoi diagram of the positions of the vans just before the accident is given in Figure 1.2.b.

Our strategy is to define a Voronoi diagram at $t = 0$ that is consistent with the situation just before $t = 0$. We call such a diagram a 'limit Voronoi diagram' and an example of this that resembles the Voronoi diagram in Figure 1.2.b is shown in Figure 1.2.c. Compare the two diagrams. Note that the directions of the outgoing edges in the two diagrams are very similar. The Voronoi cell of van 3, in the middle of the diagram of Figure Figure 1.2.b seems to have completely disappeared in Figure 1.2.c. These two remarks address questions that we answer in Chapter 4 and the chapters after that: what information is needed to to create a diagram as shown in figure 1.2.c? And, can we still say something about the Voronoi cells that seem to disappear in the limit, like the cell of van 3?

Voronoi diagrams for coinciding points.
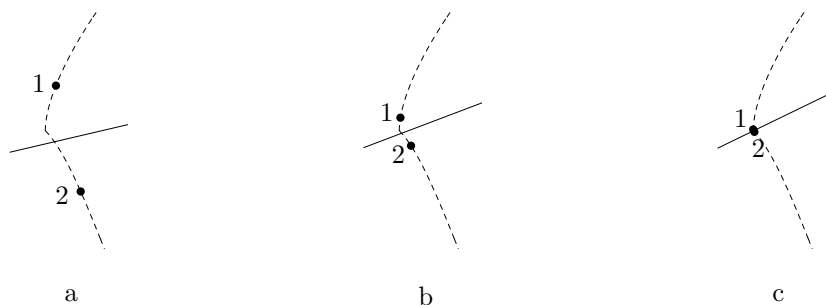
Figure 1.3: The Voronoi diagram of two coinciding points.

We restrict ourselves for a moment to the case of two points, p_1 and p_2. The position of each point at time t is given by a curve. Suppose that the two points meet at $t = 0$. Such situation is shown in Figure 1.3.a-c. In Figures 1.3.a and b, the two points are still distinct. Therefore we can draw the line l_{12} that passes through both points. This line makes some angle α_{12} with the horizontal axis. So this angle α_{12} is in some sense the *angle* of the points p_1 and p_2. As the positions of the points depend on time t, the angle α_{12} also depends on time, that is $\alpha_{12} = \alpha_{12}(t)$. The Voronoi diagram of points p_1 and p_2 is determined by the line at equal distance from the points p_1 and p_2. That line is exactly the bisector of p_1 and p_2: the line perpendicular to line l_{12} passing through the middle of the line segment 12. If p_1 and p_2 coincide, we define the middle of the line segment 12 as the point $p_1 = p_2$

itself. And we define the angle $\alpha_{12}(0)$ as the limit for small negative t of $\alpha_{12}(t)$. Now we define the bisector at $t = 0$ in terms of this angle and this middle point. That is, the bisector of $p_1 = p_2$ is the line passing through $p_1 = p_2$ perpendicular to the direction $\alpha_{12}(0)$. But this implies that we have created a Voronoi diagram for the two coinciding points p_1 and p_2!

We drop this particular example but conclude the following: we can define a limit Voronoi diagram for two coinciding points p_1 and p_2 if we know the following information:

  – the position $p_1 = p_2$ of the coinciding points.
  – an angle α_{12} mod 2π.

In this way we can define a limit Voronoi diagram for an arbitrary number of co-inciding points as well: as long as we have for every pair of coinciding points p_i and p_j a position $p_i = p_j$ and an angle α_{ij}, we can define the bisector of p_i and p_j. And, using the bisector we can determine the two Voronoi half-planes $vh(p_i, p_j)$ and $vh(p_j, p_i)$. Now we are done, as any Voronoi cell can be expressed as an intersection of half-planes, as we saw in Equation 1.1.

We work along these lines in Chapter 4. For example, the curves describing the positions of the two points $p_1 = p_1(t)$ and $p_2 = p_2(t)$ in Figure 1.3 are given by $p_1(t) = (t^2, t + t^2 - .3t^3)$ and $p_2(t) = (t, -t - 3t^2 + 2t^3)$. We only allow curves given by pairs of polynomials in t. We call points described by such curves *polynomial sites*. After having defined Voronoi diagrams for polynomial sites we show how to determine the Voronoi diagrams without having to compute all bisectors.

First we assume that we have a set of n polynomial sites that all coincide at $t = 0$. So, this is the situation in Figure 1.2.a, where five polynomial sites cluster together. Leaving out polynomial site $p_3(t)$ in the beginning will not change the shape of the limit diagram as we see in figure 1.2.c. We show in Section 4.5 which sites exactly can be left out without changing the boundary of the diagram. So, we want to characterize those sites that are somehow in the interior of the cluster. Of course we could as well characterize the sites that are on the exterior of the cluster. This is done in terms of the convex hull of the sites in the cluster for small enough positive t.
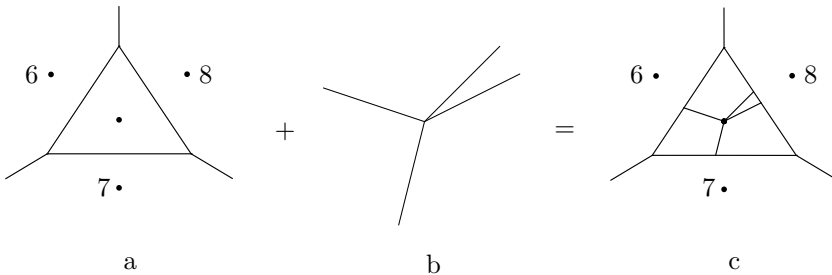

Figure 1.4: Plugging Voronoi diagrams.

For a general set $S(t)$ of n polynomial sites, the boundary of the Voronoi diagram at

$t = 0$ is determined by *plugging*. We demonstrate plugging in Figure 1.4 where we compute the Voronoi diagram of $S(t) = \{p_1, \ldots, p_8\}$, for $p_6 = (-3, 2)$, $p_7 = (0, -3)$ and $p_8 = (3, 2)$. The other polynomial sites form a cluster in the origin. In fact we used this cluster already for the supervan example in Figure 1.2. The cluster locations of $S(t)$ at $t = 0$ are the distinct positions of the sites at $t = 0$. So, we have four cluster locations. The Voronoi diagram of the cluster locations is given in Figure 1.4.a. Next, the cell of every cluster location is filled, if necessary. Three cells in our example correspond to a single point, so no filling is needed there. The limit Voronoi diagram of the points clustering in the origin, is shown in Figure 1.4.b. We simply plug this diagram in the appropriate cell in order to obtain the limit Voronoi diagram of $S(t)$. The result is shown in Figure 1.4.c.

The limit Voronoi diagrams are really new diagrams: in general they can not be realized as classic Voronoi diagrams, for example Figure 1.4.c. In classic Voronoi diagrams, every Voronoi cell has positive area, for example. This is not true for limit Voronoi diagrams.

Compactifications of configuration spaces.

A collection of n points in $\mathbb{R}^2$ is often called a *configuration*. The *configuration space* of n distinct points in $\mathbb{R}^2$ is just the space that consists of all possible configurations of n distinct, ordered points. Suppose for example that $n = 3$. Any element of the configuration space consists of three lebeled points $p_1, p_2, p_3 \in \mathbb{R}^2$ such that: p_1 is distinct from p_2; p_1 is distinct from p_3; and p_2 is distinct from p_3. A natural way of describing the configuration (p_1, p_2, p_3) is by listing the coordinates of p_1, p_2, and p_3. But if we list all six coordinates in single file, we obtain an element $c = (p_1, p_2, p_3)$ in $\mathbb{R}^6$. That is, the configuration space of three distinct point in the plane is part of a six dimensional space. In fact it is six dimensional, as almost all elements of $\mathbb{R}^6$ can be seen as some configuration (p_1, p_2, p_3) of three distinct points.

We are interested in the Voronoi diagram of n points in the plane. That is, we want to define a Voronoi diagram for every configuration in a configuration space of n points. We are especially interested in possible Voronoi diagrams for point sets that contain coinciding points. We call such point sets *degenerate* configurations. The idea of a compactification of a configuration space is as follows: we want to construct a space that encodes all possible configurations of n distinct points, both non-degenerate and degenerate. Degenerate configurations should be on the boundary of this space. By adding this boundary the degenerate configurations are incorporated. For a bounded space, adding the boundary is the same as compactifying, which explains the name 'compactification'. One important reason to compactify is the hope to be able to extend some definition, in our case the definition of Voronoi diagram, to the degenerate configurations. This extension would give access to limit objects which in our case are limits of Voronoi diagrams.

We denote the set of ordered n tuples of all pairwise distinct points in the plane by $CONF_n$. Although this is not very useful for us, an easy example is the compactifica-

tion $(\mathbb{R}^2)^n$ of the configuration space $CONF_n$ itself. The problem with this compactification is that it gives very little information on degenerate configurations: for two coinciding points $p_1 = p_2$, the only point that is added by compactifying is the point (p_1, p_2). Consider the two points $p_1(t)$ and $p_2(t)$ where $p_2(t) = p_1(t) + t(\cos\alpha, \sin\alpha)$. If t goes to zero, $p_2(t)$ will coincide with $p_1(t)$. Describe the Voronoi diagram of $p_1(0)$ and $p_2(0)$ as in Figure 1.3. Then every distinct value of α corresponds to a distinct direction of the bisector of the points $p_1(0)$ and $p_2(0)$. But this means that there is not one Voronoi diagram corresponding to $p_1(0) = p_2(0)$ but a complete collection of diagrams, parameterized by α mod 2π.

Compactifying using angles.

By now, the attentive reader should be convinced that it is not a strange idea to use angles for a suitable compactification. In Chapter 5 we may consider all angles between n points: we start with n distinct, labeled points in the plane. For every two points p_i and p_j with $i < j$ we consider the directed line l_{ij} passing through the two points. This line makes some angle α_{ij} mod 2π with the horizontal axis. The *angle map* ψ_{DA_n} maps a configuration of n distinct points to the $\binom{n}{2}$ directed angles α_{ij} with $i < j$. Let T be a triangle with vertices 1, 2 and 3. If we know the angles α_{12}, α_{13} and α_{23}, we know in fact the shape of the triangle T. So, $\psi_{DA_3}(CONF_3)$ describes in a way all distinct triangles on three points. We describe explicitly this image $\psi_{DA_3}(CONF_3)$ in Chapter 5. We explain the consequences of the action of the symmetric group S_3 on the labels of the three vertices. Finally we give geometric interpretations of boundary points of $\psi_{DA_3}(CONF_3)$ in terms of degenerate configurations.

The first compactification that we encounter is CDA_n, the *compactification* of *directed angles*. This space is defined as the closure of the graph of the angle map ψ_{DA_n}, so a point $\gamma_n \in CDA_n$ consists of n points and $\binom{n}{2}$ angles between those points. If γ_n is a boundary point of CDA_n, then not all points need to be distinct. In any case we know for every two points $p_i, p_j \in \gamma_n$ an angle α_{ij} and the position(s) $p_i \neq p_j$ or $p_i = p_j$. This implies that for γ_n a Voronoi diagram $V(\gamma_n)$ is defined.

In Chapter 6 we prove a continuity theorem for Voronoi diagrams of data sets from CDA_n. It states essentially that two data sets $\gamma_n, \eta_n \in CDA_n$ that are close in the Euclidean metric, have Voronoi diagrams whose boundaries are close in the Hausdorff metric. The Hausdorff metric is very suitable to compare images. Two sets A and B in the plane are within Hausdorff distance r iff r is the smallest number such that any point of A is within distance r from some point in B and vice versa.

An algebraic description: from angles to slopes.

The line through the points (x_1, y_1) and (x_2, y_2) is given algebraically by the equation

$$y - y_1 \;=\; \frac{y_2 - y_1}{x_2 - x_1}(x - x_1) \tag{1.2}$$

The quantity $\frac{y_2 - y_1}{x_2 - x_1}$ is of course the *slope* of the line. Instead of writing down the angle α_{ij} for every two points p_i and p_j, we consider all slopes a_{ij}. It turns out that there exists an algebraic relation between the six possible slopes for four distinct points p_0, p_1, p_2 and p_3. This relation is called the *six-slopes* formula, compare Figure 1.5. The formula is given by $\Delta_{0123} = 0$, where

$$\Delta_{0123} = (a_{01} - a_{12})(a_{02} - a_{23})(a_{03} - a_{13}) - (a_{01} - a_{13})(a_{02} - a_{12})(a_{03} - a_{23}).$$

We prove in Chapter 5 that there also exists a *triangle* formula. This is a relation $t_{ijk} = 0$ between slopes and x-coordinates of the points p_i, p_j, and p_k. So by now we have two formulas involving points and slopes: one holds for any three points and the other holds for any four points. Suppose we have some configuration c of points and slopes such that all triangle formulas and all six-slopes formulas hold. A question that we consider in Chapter 5 is the following: is such configuration c always a limit of non-degenerate configurations. To that end we introduce a variety that consists of exactly those configurations such that all triangle formulas and all six-slopes formulas hold. That is: the algebraic variety T_n is just the set of zeroes common to all triangle formulas and all six-slopes formulas. It serves as an algebraic counterpart of the compactification CUA_n of *undirected angles*. We prove that T_n is not a smooth variety and give a geometric interpretation for the non-singular configurations.
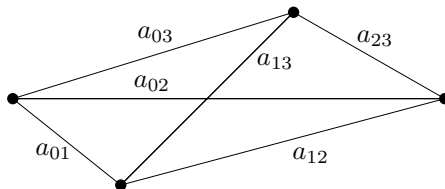
Figure 1.5: For four distinct points the six-slopes formula holds.

A smooth and clickable compactification.

Look at Figure 1.2 again. On the right, a limit Voronoi diagram of the points $p_1, \ldots, p_5$ is displayed. For every point p_i a Voronoi cell is visible, except for p_3. One could say that the Voronoi cell $V(p_3)$ is so small that we cannot see it. A solution in this case could be to rescale or magnify the picture somehow until the cell $V(p_3)$ becomes visible. After magnifying enough we would get a picture that is very similar to Figure 1.2.b In more complicated configurations we might need to rescale or zoom in several times at several positions in order to distinguish every cell.

This shows the need of a 'clickable' compactification on which we can define 'clickable' Voronoi diagrams. An example is given in Figure 1.6. In the top 'screen', six points are visible. But the two points in the middle are in fact clusters of points.
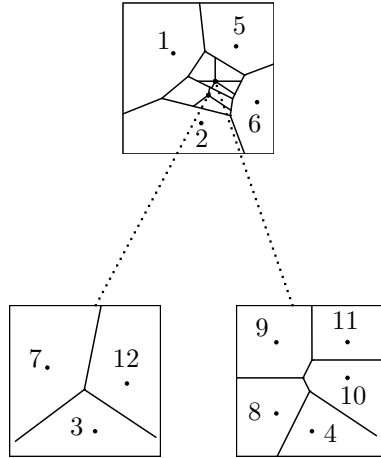
Figure 1.6: A clickable Voronoi diagram in a clickable configuration.

One cluster consists of the points p_3, p_7 and p_{12}. This can be 'seen' by clicking on the cluster: The bottom left screen appears, displaying these points separately. The bottom right screen appears after clicking on the other cluster and displays the points p_4, p_8, p_9, p_{10} and p_{11}.

The Fulton-MacPherson compactification is a well-known compactification of the configuration space of n distinct labeled points that has such a 'clickable' structure. To analyze Voronoi diagrams we do not need the full generality of this compactification. That is why we construct a real version of this compactification, incorporating some ideas of Kontsevich-Soibelman. Let $c \in CONF_n$ be some configuration of n distinct points. Kontsevich and Soibelman write down both the angles α_{ij} between any two points, and, for every ordered triple of points (p_i, p_j, p_k), the ratio $\beta_{ij}^{ik} = \frac{|p_i - p_k|}{|p_i - p_j|}$. They take the closure of the image of $CONF_n$ under the map that assigns all angles and ratios to a set of distinct points. This results in a manifold with corners $FM_2(n)$.

In Chapter 7 we show how to adapt their approach so that the resulting compactification is a smooth manifold. Instead of just a ratio, we write down a *hook* for every triple of points. A hook h_{ij}^{ik} consists of this ratio β_{ij}^{ik} together with an angle α_{ij}^{ik} between the legs of the hook, cf. Figure 1.7. We define a space XAH_n as the closure of the image of $CONF_n$ under the map

$$\psi_{AH_n}: \quad CONF_n \quad \rightarrow \quad (\mathbb{R}/\pi\mathbb{Z})^{\binom{n}{2}} \times ((-\infty, \infty] \times \mathbb{R}/2\pi\mathbb{Z})/\sim_k)^{6\binom{6}{3}},$$
$$(p_1, \ldots, p_n) \quad \mapsto \quad ((\alpha_{ij})_{1 \leq i < j \leq n}, (\beta_{ij}^{ik}, \alpha_{ij}^{ik})), \quad i, j, k \text{ pairwise distinct}$$

where $\sim_k$ denotes the identification of $(\beta_{ij}^{ik}, \alpha_{ij}^{ik})$ with $(-\beta_{ij}^{ik}, \alpha_{ij}^{ik} + \pi)$.

Any point $x \in XAH_n$ that is added to $CONF_n$ by taking the closure has some ratio $\beta_{ij}^{ik}(x)$ equal to zero. We think of these points as corresponding to degenerate
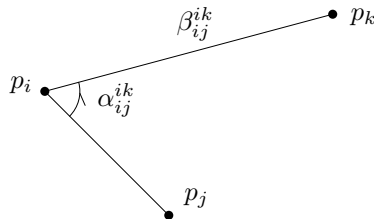
Figure 1.7: The hook $h_{ij}^{ik} = (\beta_{ij}^{ik}, \alpha_{ij}^{ik})$ hinged at p_i from p_j to p_k. The little arrow indicates the positive direction.

configurations, that is, configurations that have some coinciding points. We exploit these zero ratios to define a series of *screens* corresponding to x. A screen is just a copy of the plane $\mathbb{R}^2$. In Figure 1.6 for example, there are three screens. We 'fill' these screens with the degenerate configuration. We can do it so that any two points in the configuration are separated in at least one screen. Moreover, the process is such that it shows how to write XAH_n locally as the graph of a function. This proves that XAH_n is indeed a smooth manifold.

The close connection between XAH_n and the manifold with corners FM_2 has two immediate applications. First of all there is Theorem 7.65 that reveals the corner structure of FM_2: the corners appear automatically if we describe the natural map from FM_2 to XAH_n.

Moreover, we can apply this same method of defining and filling screens to the manifold with corners $FM_2(n)$. That is, we add a family of screens to a degenerate configurations $x \in FM_2(n)$. But $FM_2(n)$ contains all angles mod 2π between two points. Therefore we can, without ambiguities, define a clickable Voronoi diagram as shown in Figure 1.6 for every $x \in FM_2(n)$. We conclude Chapter 7 by showing how to jump between several descriptions and models in this thesis. Suppose we start with some $x \in XAH_n$, for example. We can always construct a set $S(t)$ of polynomial sites $\{p_1(t), \ldots, p_n(t)\}$ with the following property: if we write down all angles and ratio's for the sites in $S(t)$, we exactly obtain x.

Comparing prices: higher order Voronoi diagrams.

In what preceded we have extended Voronoi diagrams by limit Voronoi diagrams. Another extension or generalization of the classic Voronoi diagrams are the *higher order* Voronoi diagrams. We discuss some results on higher order Voronoi diagrams in Chapter 3.

People in the Netherlands like to compare prices. That is, they have no fixed supermarket, but frequent the, say, five closest supermarkets to pick the bargains. For those people we have to divide the city into different sectors that we call 5-sectors.

In one 5-sector, the five closest supermarkets are the same. So, if people know which 5-sector they live in, they know the five closest supermarkets. An example is given in Figure 1.8. In Figure 1.8.a the 6 supermarkets of above are displayed again. In Figure 1.8.b the four different 5-sectors are drawn. So, in sector 13456, the five closets supermarkets are supermarkets 1, 3, 4, 5 and 6. Or, if we put it the other way around: in 5-sector 13456, supermarket 2 is the most far away supermarket. This diagram is the *fifth order* Voronoi diagram of the six supermarkets.
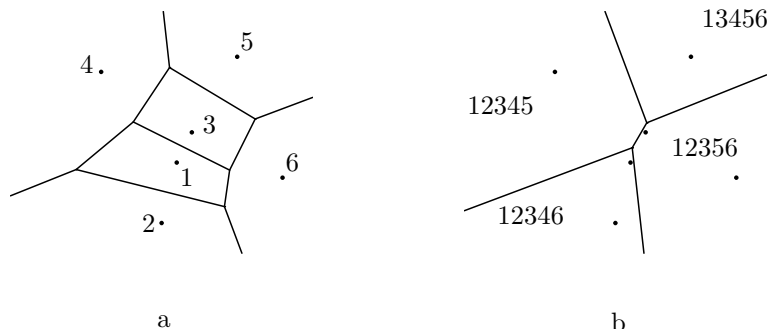
Figure 1.8: a. The Voronoi diagram of six supermarkets $1, \ldots, 6$, and b. the fifth order Voronoi diagram of the same supermarkets.

Note that in Figure 1.8.b only four distinct 5-sectors are present. This implies that two supermarkets (which ones?) are nowhere the most far away supermarket. We can change however the position of the supermarkets in such a way that every supermarket is somewhere the most far away supermarket. (How to do this? Put the supermarkets on the vertices of a convex 6-gon.) This shows that if we change the position of the supermarkets, the set of 5-sectors may change as well. In Chapter 4 we write down all 5-sectors. Moreover, we write down all 4-sectors, all 3-sectors and all 2-sectors. And we add all 1-sectors and all 6-sectors, although they are trivial (why?). If we collect everything we get a collection of subsets of $\{1, 2, 3, 4, 5, 6\}$. Or more general: we start with a set S of n distinct points in the plane. The *Voronoi poset* $\Pi(S)$ consists exactly of those subsets of $\{1, \ldots, n\}$ that have a non-empty Voronoi cell.

Although the 5-sectors may change if we change the position of the supermarkets, there are certain invariants. An invariant is just a number that is independent of the position of the supermarkets. In Theorem 3.24 we prove for example the following: suppose the number of supermarkets is odd. Then the number of odd sectors equals the number of even sectors. Or more formal: for almost every configuration S the total number of cells in all even order Voronoi diagrams of S equals the total number of cells in all odd order Voronoi diagrams of S.

Chapter 2

Voronoi diagrams.

In this chapter we give a short introduction to Voronoi diagrams. Most material covered in this chapter can be found in good books on computational and discrete geometry. A very readable general introduction to computational geometry is the book by De Berg, Kreveld, Overmars and Schwarzkopf, see [BKOS]. The book by Edelsbrunner, see [Ed], is more in-depth, but less suited as an introduction. Okabe, Boots and Sugihara wrote a monograph on Voronoi diagrams for a broad audience, see [OBS]. Most recent is the chapter on Voronoi diagrams written by Aurenhammer and Klein in the Handbook of Computational Geometry ([AK]). Some concepts that are used in the rest of this thesis are shortly discussed in an overview paper on computational topology, cf. [DEG].

Apparently, Dirichlet in 1850 and Voronoi in 1908, cf. [Vo], were the first that used a notion of Voronoi diagram. They considered Voronoi diagrams of regular point sets, associated to quadratic forms. Consult [CF] for a recent and recommendable book on Voronoi diagrams of quadratic forms.

2.1 Convex hull.

A subset A of the plane is **convex** if for any two points $p, q \in A$ the line segment pq is contained in A as well. The **convex hull** $CH(A)$ of a set A is the smallest convex set containing A. Any two non-coinciding points $p = (p_x, p_y)$ and $q = (q_x, q_y)$ define two **hull half-planes** hh_{pq} and hh_{qp} where:

$$hh_{pq} \quad := \quad \{r = (r_x, r_y) \in \mathbb{R}^2 \mid \mathrm{Det}(p, q, r) \geq 0\}.$$

The determinant $\mathrm{Det}(p, q, r)$ is given by:

$$\mathrm{Det}(p, q, r) \quad = \quad \begin{vmatrix} 1 & p_x & p_y \\ 1 & q_x & q_y \\ 1 & r_x & r_y \end{vmatrix}.$$

Let S be a finite set of distinct points in $\mathbb{R}^2$. We can write $CH(S)$ as an intersection of hull half-planes. More precisely, $CH(S)$ equals the intersection of those half-planes defined by points in S that contain all points of S

$$CH(S) \quad = \quad \bigcap_{p_i, p_j \in S} \{h_{p_i p_j} \; : \; S \subset h_{p_i p_j}\}.$$

As a non-empty intersection of half-planes, $CH(S)$ is a convex polygon. We can represent this polygon by listing its consecutive vertices in clockwise order. In this way $CH(S)$ corresponds to a cyclically ordered list of points from S.
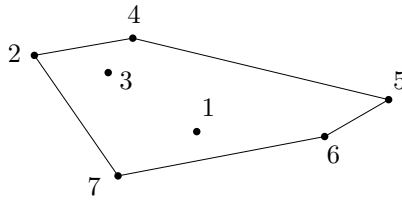
Figure 2.1: The convex hull of the points $1, \ldots, 7$.

Example 2.1
In Figure 2.1, $CH(S) \leftrightarrow \{2, 4, 5, 6, 7\}$.

Suppose the points in S start moving around in the plane. Assume that at the start of the motion, no three points in S are collinear. A small enough disturbance of the points in S does not change the ordered list of points of $CH(S)$. Only when a point p_k passes a convex hull edge $p_i p_j$, the list changes (simultaneously $\text{Det}(p_i, p_j, p_k) = 0$). We call this change in $CH(S)$ a **convex hull event**.

2.2   Voronoi diagram.

Start again with a set $S = \{p_1, \ldots, p_n\}$ of n distinct points in the plane. The **Voronoi cell** $V(p_i)$ of a point $p_i \in S$ is defined as

$$V(p_i) := \{q \in \mathbb{R}^2 : d(p_i, q) \; \leq d(p_j, q), \; i \neq j\}.$$

Here, $d(p, q)$ denotes the ordinary Euclidean distance between p and q. Note that we define a Voronoi cell as a closed subset of $\mathbb{R}^2$, in contrast to the choice made in [Ed, BKOS]. The **Voronoi diagram** $V(S)$ of S is the family of subsets of $\mathbb{R}^2$ consisting of the Voronoi cells and all of their intersections. The boundary of a Voronoi cell consists of **Voronoi edges** and **Voronoi vertices**. A point $q \in \mathbb{R}^2$ is on the Voronoi edge $e(p_i, p_j)$ if $d(q, p_i) = d(q, p_j)$ and $d(q, p_k) \geq d(q, p_i)$ if $k \neq i, j$.

A point $q \in \mathbb{R}^2$ is a Voronoi vertex if it is present on at least two Voronoi edges. A circle C is an **empty circle** with respect to S if there are no points of S inside the circle. For any three points p_i, p_j, and p_k, that are not collinear, there exists a unique circle C_{ijk} passing through p_i, p_j, and p_k. A circle C_{ijk} is a **Voronoi circle** if it is an empty circle.
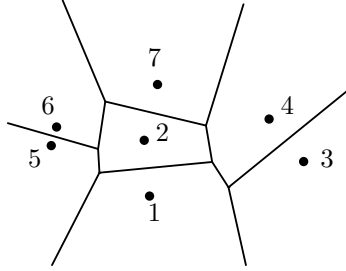
Figure 2.2: The Voronoi diagram of some points $1, \ldots, 7$.

Lemma 2.2
$q \in \mathbb{R}^2$ *is a Voronoi vertex if and only if q is the center of a Voronoi circle.*

Proof. [BKOS], Theorem 7.4. ∎

The **bisector** $B(p_i, p_j)$ of two points p_i and p_j is the line equi-distant to p_i and p_j. It is perpendicular to the line segment $p_i p_j$ passing through $\frac{1}{2}(p_i + p_j)$. A point q is in the **Voronoi half-plane** $vh(p_i, p_j)$ if it is not closer to p_j than to p_i:

$$vh(p_i, p_j) \quad = \quad \{q \in \mathbb{R}^2 \mid d(q, p_i) \leq d(q, p_j)\}.$$

As a consequence, the Voronoi half-plane $vh(p_i, p_j)$ is bounded by the bisector $B(p_i, p_j)$. Any Voronoi cell is an intersection of half-planes

$$V(p_i) \quad = \quad \bigcap_{j \neq i} vh(p_i, p_j).$$

Therefore, any Voronoi cell $V(p_i)$ is convex and is either bounded or unbounded.

Lemma 2.3
$V(p_i)$ *is unbounded if and only if $p_i \in \delta CH(S)$, where $\delta CH(S)$ denotes the boundary of the convex hull $CH(S)$.*

Proof. [OBS], Property V2. ∎

Lemma 2.4
Let p_i, p_j and p_k be three distinct points that are not collinear. Let c be the center of the circle through p_i, p_j and p_k. Then:

$$c \quad = \quad B(p_i, p_j) \cap B(p_i, p_k).$$

Proof. The point c is equi-distant to p_i, p_j and p_k.   ■

2.3   Topological changes.
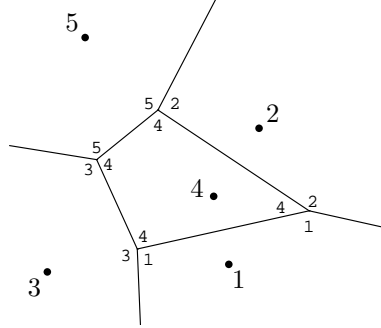
Figure 2.3: A diagram of type $\{134, 142, 245, 354\}$.

Definition 2.5
*Let $V(S)$ be a Voronoi diagram. Represent every vertex x of $V(S)$ as an ordered list
of labels of the points of S on the Voronoi circle $C(x)$ of x. The order of the labels
corresponds to the cyclic, clockwise order of the points on $C(x)$. The set of all these
lists is the* **type** *of the Voronoi diagram $V(S)$.*

Example 2.6
A diagram of type $\{134, 142, 245, 354\}$ is depicted in Figure 2.3.

A point set S is in **general position** iff no three points are collinear and no four
points are cocircular. If S is in general position, then every Voronoi circle has exactly
three points on its boundary. When the points in S start to move around in the
plane, the type of $V(S)$ changes exactly when the configuration of empty circles
changes. This can happen generically in two ways.
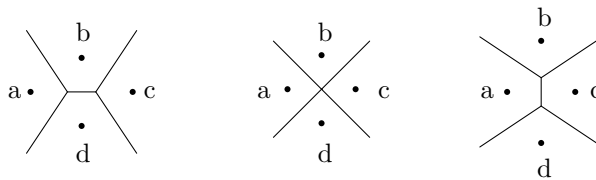
Figure 2.4: A circle event.

The first is when two empty circles C_{abd} and C_{bcd} coincide. This is a **circle event**,

see Figure 2.4. Before the event, a, b, c, and d define two empty circles C_{abd} and C_{bcd}. If c moves to the left in the leftmost figure, a, b, c and d become cocircular. If c continues moving left, one arrives in the situation of the rightmost figure, where C_{abc} and C_{acd} are the empty circles. The corresponding change in type is given by:

$$\{\ldots, abd, bcd, \ldots\} \quad \rightarrow \quad \{\ldots, abcd, \ldots\} \quad \rightarrow \quad \{\ldots, abc, acd, \ldots\}.$$
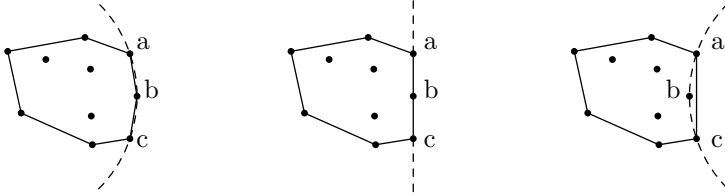
Figure 2.5: A convex hull event.

The other way by which the type of a Voronoi diagram can change is by means of a convex hull event, see Figure 2.5. Consider the circle defined by the points a, b and c. In the figure on the left, $b \in \delta CH(S)$. The circle C_{abc} contains all other points of S in its interior. Suppose b moves to the left. At some stage, b passes through the line segment ab. At this moment, the circle C_{abc} swaps over, and becomes empty, as in the picture on the right. This means that in the type of $V(S)$, an extra term acb appears.

2.4 Delaunay triangulation.
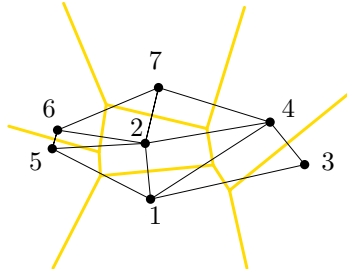
Figure 2.6: The Delaunay triangulation of the points introduced in Figure 2.2.

Starting from a Voronoi diagram $V(S)$ we define the **Delaunay graph**, $DG(S)$, of S. The vertices of $DG(S)$ are exactly the points in S. Two vertices p_i and p_j are connected by an edge in $DG(S)$ exactly if there exists an edge $e(p_i, p_j)$ of positive length in the Voronoi diagram $V(S)$. Let $D(S)$ be the straight line embedding of

the Delaunay graph $DG(S)$. For point sets S that are in general position, $D(S)$ triangulates the convex hull $CH(S)$. For this reason, the straight line embedding $D(S)$ of the Delaunay graph $DG(S)$ is called the **Delaunay triangulation** of S. This terminology is also used for point sets S that are not in general position. In the latter case $D(S)$ is not necessarily a triangulation. An example of a Delaunay triangulation is presented in Figure 2.6.

The Delaunay triangulation $D(S)$ is **dual** to the Voronoi diagram $V(S)$ in the following sense: vertices in the Voronoi diagram correspond to faces in the Delaunay triangulation, while Voronoi cells correspond with vertices of $D(S)$. As a consequence, the effect of a convex hull event and a circle event on the Delaunay triangulation $D(S)$ is easily found. At the convex hull event depicted in Figure 2.5 a triangle T_{abc} appears in the Delaunay triangulation $D(S)$. Moreover, for any triple of points p_i, p_j, and p_k in a point set S it follows that p_i, p_j, and p_k gives a triangle in $D(S)$ if and only if the circle C_{ijk} is a Voronoi circle. Indeed, in the circle event of Figure 2.4 an edge bd of the Delaunay triangulation flips over in an edge ac. This proves the following lemma.

Lemma 2.7
Let S be a set of distinct points in $\mathbb{R}^2$ in general position. The type of the Voronoi diagram $V(S)$ is the list of triangles in the Delaunay triangulation $D(S)$.

The following characterization of Delaunay triangulations explains why Delaunay triangulations are often used in the generation of altitude maps and contour plots. The **minimal angle** of a triangulation is the smallest angle that occurs in any of the triangles of the triangulation. In Figure 2.6, the minimal angle is the angle $\angle 526$.

Lemma 2.8
*Let S be a point set in general position. The Delaunay triangulation $D(S)$ is that triangulation that maximizes the minimal angle over all triangulations of S.*

Proof. [BKOS], Theorem 9.9.   ■

2.5   Geometric transformations.

2.5.1   The lifting transformation.

There is an easy correspondence between Delaunay triangulations of point sets in $\mathbb{R}^2$ and convex hulls in $\mathbb{R}^3$: the **lifting transformation**. This transformation is established by the map

$$\psi : \quad \begin{array}{ccc} \mathbb{R}^2 & \to & \mathbb{R}^3, \\ (x,y) & \mapsto & (x,y,x^2+y^2). \end{array}$$

It maps a point in the plane onto a point of the paraboloid P defined by $z = x^2 + y^2$, see Figure 2.7. The map ψ has two properties that are important to us.
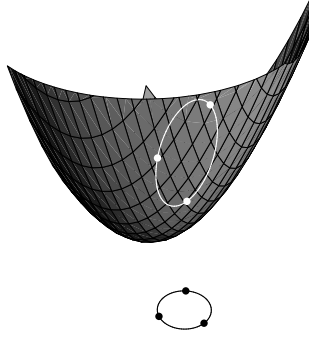
Figure 2.7: Lifting (x, y) to $(x, y, x^2 + y^2)$.

Lemma 2.9
Let C be a circle in the xy-plane.
  (i) $\psi(C) = P \cap H_C$, *where H_C is a plane in $\mathbb{R}^3$.*
  (ii) *A point q is inside C if and only if $\psi(q)$ below H_C.*

Proof. The proof follows directly from combining the equation of a circle in the plane and the equation of the paraboloid P. ∎

Let S be a set of points in the xy-plane and S' the set of images of the points in S on the paraboloid P. By Lemma 2.9, ψ maps empty circles defined by S onto faces of the lower convex hull of S'. Therefore, the projection of the lower hull faces of $CH(S')$ onto the xy-planes gives exactly the Delaunay triangulation $D(S)$.

Let S be a set of n points in general position. A subset A of k points of S is a **k-set** if it can be separated from the complementary set $B = S \setminus A$ of $n - k$ points by a plane V_A. Here we say that V_A **separates** A from B if V_A can be oriented so that all points in A are on the positive side of A, while all points of B are on the negative side. Lemma 2.9 shows that any set of k points contained in a circle in $\mathbb{R}^2$ can be mapped to a k-set in $\mathbb{R}^3$.

2.5.2   Mapping points to planes.

A set of n planes $\mathcal{V}$ defines a subdivision of $\mathbb{R}^3$ into connected pieces of dimension $0, 1, 2$ or 3. This subdivision is the **arrangement** $\mathcal{A}(\mathcal{V})$ of $\mathcal{V}$. Arrangements form a topic of their own, cf. [OT]. We assume that any point in any plane $V_i \in \mathcal{V}$ for $i = 1, \ldots, n$ can be written as $(x, y, f_{\mathcal{V}_i}(x, y))$, for some linear function $f_{\mathcal{V}_i} : \mathbb{R}^2 \to \mathbb{R}$. That is, $\mathcal{V}$ consists of non-vertical planes only. We say that $p = (p_x, p_y, p_z) \in \mathbb{R}^3$ is **above** plane $\mathcal{V}_i$ iff $p_z > f_{\mathcal{V}_i}(p_x, p_y)$; similarly for **below**. The **k-level** of the arrangement $\mathcal{A}(\mathcal{V})$ consists of those points in $\mathbb{R}^3$ above or in $k - 1$ planes and below or in $n - k$ planes of $\mathcal{V}$. The n-level of an arrangement $\mathcal{A}(\mathcal{V})$ is also called the **upper envelope** of $\mathcal{A}(\mathcal{V})$.
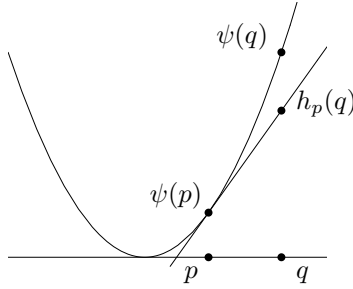
Figure 2.8: Lifting points to planes.

Using the map ψ again, we show that we can determine the Voronoi diagram of a set S of points in $\mathbb{R}^2$ by computing the boundary of an upper envelope in $\mathbb{R}^3$. Consider Figure 2.8 that demonstrates the principle one dimension lower. To any point p in a fixed point set S we associate a plane h_p in $\mathbb{R}^3$. That is, we map p to the unique plane h_p tangent to the paraboloid P at the point $\psi(p)$. Lemma 2.10 shows that the set of planes $\{h_p \mid p \in S\}$ completely encodes the relative distances of points $q \in \mathbb{R}^2$ to points in S.

Lemma 2.10
Let $q \in \mathbb{R}^2$ and let $h_p(q)$ be the intersection of the vertical line through q and the plane h_p. Then

$$d(q,p)^2 \quad = \quad \psi(q) - h_p(q).$$

Proof. An easy computation or [Ed], Observation 13.3.   ∎

Applying this result, we compute the Voronoi diagram $V(S)$ as follows. Let $q \in \mathbb{R}^2$. Suppose that q is in the interior $V(p_i)^\circ$ of the Voronoi cell $V(p_i)$. By Lemma 2.10 this is equivalent to h_{p_i} being the first hyperplane that one encounters from the set $\{h_{p_j} \mid p_j \in S\}$ if one goes downwards in negative vertical direction, starting from $\psi(q)$. But this means that $V(S)$ is exactly the projection of the boundary of the upper envelope of the arrangement $\{h_{p_j} \mid p_j \in S\}$ on $\mathbb{R}^2$.

We can connect the Delaunay triangulation $D(S)$ of a point set S with the lower convex hull of a set S'. Meanwhile the Voronoi diagram $V(S)$ can be obtained from the upper envelope of an arrangement. Remember that the Delaunay triangulation $D(S)$ is dual to the Voronoi diagram $V(S)$. By now it may not come as a surprise, that there exists a duality transfer from lower convex hulls to upper envelopes and vice versa. For more information consult [Ed, BKOS].

Chapter 3

A Voronoi poset.

Given a set S of n points in general position, we consider all k-th order Voronoi diagrams on S, for $k = 1, \ldots, n$, simultaneously. We recall symmetry relations for the number of cells, number of vertices and number of circles of certain orders. We introduce a poset $\Pi(S)$ that consists of the k-th order Voronoi cells for all $k = 1, \ldots, n$, that occur for some set S. We prove that there exists a rank function on $\Pi(S)$ and moreover that the number of elements of odd rank equals the number of elements of even rank of $\Pi(S)$, provided that n is odd.

3.1 Introduction.

The dynamics of Voronoi diagrams in the plane is well understood. When $n - 1$ points are fixed and one point is moving continuously somewhere inside the convex hull, combinatorial changes of the Voronoi diagram correspond to changes in the configuration of empty circles, see Chapter 1 and [AGMR] for example. Changes in the configuration of non-empty circles correspond to combinatorial changes of higher order Voronoi diagrams. Here the k-th order Voronoi diagram associates to each subset of size k of generating sites that region in the plane that consist of points closest to these k sites.

We consider all k-th order Voronoi diagrams simultaneously for k between 1 and n. We do so by introducing the Voronoi poset $\Pi(S)$ of a set S of n distinct sites in the plane. The poset consists of all sets of labels that correspond to a subset of sites that defines some non-empty Voronoi cell in some k-th order Voronoi diagram.

Higher order Voronoi diagrams have been investigated by numerous people. Many results are published in an article by D.T. Lee, see [Le]. A survey is given in Edelsbrunners book on algorithms in combinatorial geometry, see [Ed]. In Chapter 1 we have introduced k-sets and we have shown that there exists a map ψ that changes the point inside circle relation in $\mathbb{R}^2$ into a point below hyperplane relation in $\mathbb{R}^3$.

It turns out that these circles containing points serve as a 'building block' for higher order Voronoi diagrams as we discuss in full detail in Section 3.2. As a consequence, formulas counting k-sets in $\mathbb{R}^3$ can be applied in the counting of vertices, edges and cells of higher order Voronoi diagrams. Instead of considering circles that contain a fixed number of, say, k points, one can also consider circles that contain at most k points. This is done in [GHK].

Let T be a set of n points in $\mathbb{R}^3$ in general position that are the vertices of a convex polytope. Sharir, [Sh], Lemma 4.4 and Clarkson and Shor, [CS], Theorem 3.5 prove that the number of k-sets of T is given by $2(k+1)(n-k-2)$. They prove this formula using probabilistic methods that we do not discuss here.
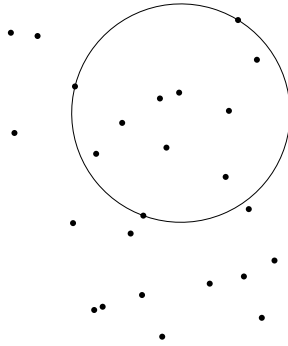
Figure 3.1: An invariant for circle configurations.

This formula can also be derived in the context of k-th order Voronoi diagrams from Lee's results as has been observed by several people, see again Clarkson and Shor, [CS] or Andrzejak et al. , [AAHSW]. We give this derivation explicitly and state in Theorem 3.18 that

$$c_i + c_{n-i-3} \quad = \quad 2(i+1)(n-i-2),$$

where c_i denotes the number of circles defined by a set S of n points in general position in the plane, containing exactly i points of S. For an illustration, see Figure 3.1. Moreover we explicitly derive similar formulas for the number of cells f_k in the k-th order Voronoi diagram $V_k(S)$, see Lemma 3.16, and the number of vertices v_k, see Lemma 3.17, in $V_k(S)$.

$$
\begin{aligned}
f_k + f_{n-k+1} &= 2k(n-k+1)+1-n, \\
v_k + v_{n-k} &= 4k(n-k).
\end{aligned}
$$

These 'symmetry relations' are independent of the particular position of the sites in S, provided S is in general position: while the number of cells in some k-th order Voronoi diagram may change, depending on the configuration, the sum of the

number of cells in the k-th order diagram and the number of cells in the $(n-k+1)$-th diagram remains constant.

In Section 3.3 we introduce the Voronoi poset mentioned above and prove that $\Pi(S)$ has a rank function. As an application of the symmetry relations we prove in Theorem 3.24 that the number of elements of odd rank in $\Pi(S)$ equals the number of even rank, provided that n is odd.

The Voronoi poset of a set S of n moving points seems a natural object to study as changes of the poset occur exactly at those moments where S is not in general position. As there are tight connections between higher order Voronoi diagrams, k-levels in certain arrangements in $\mathbb{R}^3$ and certain k-sets in $\mathbb{R}^3$, the study of the Voronoi poset may have applications in these areas as well.

3.2 Higher order Voronoi diagrams.

3.2.1 Definition of k-th order Voronoi diagram.

Let $S = \{p_1, \ldots, p_n\}$ be a set of n distinct points in $\mathbb{R}^2$ in general position. Let $0 \leq k \leq n$. For every point p in the plane we ask for the k nearest points from S. That is, we look for a subset $A \subset S$, such that

$$|A| = k, \qquad \forall x \in A, \quad \forall y \in S - A : \quad d(p, x) \quad \leq \quad d(p, y).$$

For two points in $\mathbb{R}^2$, we define a half-plane

$$h(x, y) := \{p \in \mathbb{R}^2 \mid d(x, p) \leq d(y, p)\}.$$

The **Voronoi cell** of $A \subset S$ of **order** $|A|$ is the intersection of half-planes

$$V(A) := \bigcap_{x \in A, \ y \in S - A} h(x, y),$$

whenever this intersection is not empty. As an intersection of half-planes, $V(A)$ is a convex polygon.

Remark 3.1
It is left as an exercise to the reader to show that assuming general position implies that a Voronoi cell is not a line segment or a single point.

The **k-th order Voronoi diagram** is the subdivision of $\mathbb{R}^2$, induced by the set of Voronoi cells of order k. For later purposes, we identify the k-th order Voronoi diagram with the set of non empty k-th order Voronoi cells.

$$V_k(S) := \{V(A) \mid A \subset S, \ |A| = k, \ V(A) \neq \emptyset\}.$$
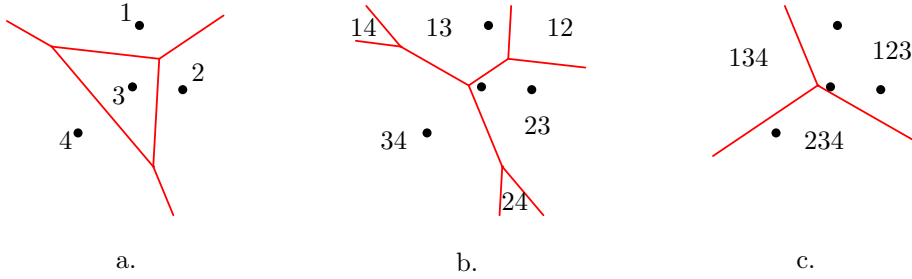
Figure 3.2: A first, second and third order Voronoi diagram.

Example 3.2

Let $S = \{(45, 86), (76, 40), (40, 42), (1, 9)\}$. Figure 3.2.a. shows the first order Voronoi diagram. The second order diagram is shown in Figure 3.2.b. and the third order diagram in Figure 3.2.c. All non-empty Voronoi cells are indicated by their generators. Note that not all possible triples occur.

Remark 3.3

A planar graph that represents a point-face dual of the k-th order Voronoi diagram can be constructed as follows, cf. [AS]. Write down for every $A \subset S$ with $|A| = k$ and $V_k(A) \neq \emptyset$ its **centroid** $c(A)$, defined by $c(A) = (1/k) \sum_{p \in A} p$. Two centroids $C(A)$ and $c(B)$ are connected by an edge exactly iff $V_k(A)$ and $V_k(B)$ share an edge.

3.2.2   Circles and higher order Voronoi diagrams.

In this section, we state some elementary properties of higher order Voronoi diagrams. Every edge in $V_k(S)$ is part of some bisector $B(a,b)$, with $a, b \in S$. The Voronoi vertices are exactly those points that are in the centers of the circles determined by three points from S. Therefore, under our general position assumption, every Voronoi vertex has valency three. The following theorem describes the local situation around a Voronoi vertex. The symbol $\odot_{a,b,c}$ denotes the circle passing through the points a, b, and c.

Theorem 3.4

Let x be the center of $\odot_{a,b,c}$, for $a, b, c \in S$, let

$$H \quad = \quad \{ \, z \in S \mid d(x, z) < d(x, a) \, \},$$

and let $k = |H|$. Then x is a Voronoi vertex of $V_{k+1}(S)$ and $V_{k+2}(S)$. The Voronoi edges and cells that contain x are given in Figure 3.3. Moreover, all Voronoi vertices are of this form.

Proof. [De], Theorem 1 and Theorem 2.   ∎
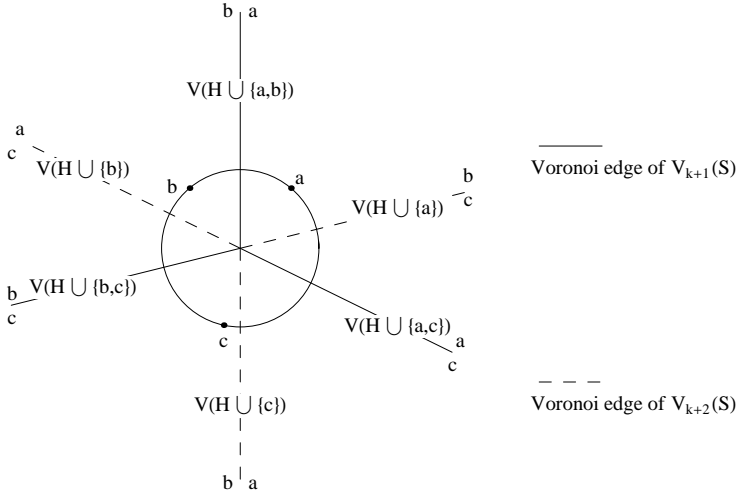
Figure 3.3: The Voronoi diagram around x.

Let a, b, c and H be as defined in Theorem 3.4. We define the **order** of a circle $\bigodot_{a,b,c}$ as $|H|$. Notation: $|\bigodot_{a,b,c}| := |H|$. An **order k Voronoi circle** $\bigodot_{a,b,c}$ is a circle through three points a, b and c from S that contains exactly k points from $S - \{a, b, c\}$. In fact, from all $\binom{n}{3}$ Voronoi circles $\bigodot_{a,b,c}$ and all sets $H_{a,b,c}$, compare Theorem 3.4, almost enough information is provided to construct all k-th order Voronoi diagrams $V_k(S)$ for $k = 1, \ldots, n-1$.

Algorithm 3.5
Voronoi diagrams of all orders.

Input: set S of n points in general position.
Output: all k-th order Voronoi diagrams $V_k(S)$ for $k = 1, \ldots, n-1$.
  1: Compute all circles $\bigodot_{a,b,c}$ defined by S.
  2: Compute all sets $H_{a,b,c}$ defined by S.
  3: Take all circles of order $k-1$ and order $k-2$. The centers of these circles are exactly the vertices of $V_k(S)$.
  4: Theorem 3.4 gives for every vertex the three incident edges and the three incident cells.
  5: Two vertices are connected by an edge iff the two vertices have two incident cells in common. Skip the edge if it is used.
  6: Edges that are not skipped are unbounded edges. Their direction and orientation still have to be computed. The direction is simply the direction of the bisector containing the edge. The orientation follows from Figure 3.3.

Remark 3.6
Denote the number of circles of order k by c_k and the number of vertices in a k-th

order Voronoi diagram by v_k. As a consequence of Theorem 3.4 we get

$$v_k \quad = \quad c_{k-1} \; + \; c_{k-2}. \tag{3.1}$$

3.2.3   Counting vertices, edges and cells.

The following theorem shows that the total number of vertices, edges and Voronoi cells does not depend on the positions of the points in S, assuming general position.

Theorem 3.7
Let v_k, e_k, and f_k denote the number of vertices, edges and cells in $V_k(S)$ for some set S of size n in general position. The total number of vertices, edges and cells in the Voronoi diagram of all orders are as follows.
  (i) $\sum_{k=1}^{n} v_k = \frac{1}{3}n(n-1)(n-2)$.
  (ii) $\sum_{k=1}^{n} e_k = \frac{1}{2}n(n-1)^2$.
  (iii) $\sum_{k=1}^{n} f_k = \frac{1}{6}n(n^2+5)$.

Proof. We prove the three claims.
   (i)   Every circle center defined by three distinct sites from S is a Voronoi vertex in some k-th and $(k+1)$-th order Voronoi diagram. As there are $\binom{n}{3}$ distinct circles, the first claim follows.
   (ii)   Consider the arrangement of bisectors $\mathcal{A}(S)$. Fix one bisector $B(a,b)$. As S is in general position, we may assume that the bisector $B(a,b)$ is divided into $n-1$ line segments by the Voronoi circle centers $abx_3, abx_4, \ldots, abx_n$, where we write $S = \{a, b, x_3, \ldots, x_n\}$. Every line segment is an edge in some k-th order Voronoi diagram. As there are $\binom{n}{2}$ distinct bisectors, claim *(ii)* follows.
  (iii)   The Euler formula, $v_k - e_k + f_k = 1$, holds for every order. Therefore

$$\sum_{k=1}^{n} f_k \quad = \quad n + \sum_{k=1}^{n} e_k - \sum_{k=1}^{n} v_k,$$

which completes the proof.   ∎

The number of vertices, edges and cells in $V_k(S)$ depends on the configuration of S as the ordinary Voronoi diagram shows. The following theorem gives expressions for these numbers. Let f_k^{∞} denote the number of unbounded cells in the k-th order Voronoi diagram. By definition $f_0^{\infty} := 0$.

Theorem 3.8
Let S be in general position. Then the number of vertices, edges and cells in the k-th order Voronoi diagram can be expressed as follows.
  (i) $v_k = 2(f_k - 1) - f_k^{\infty}$.
  (ii) $e_k = 3(f_k - 1) - f_k^{\infty}$.
  (iii) $f_k = (2k-1)n - (k^2 - 1) - \sum_{i=1}^{k} f_{i-1}^{\infty}$.

Proof. [Ed, Le]. ∎

Note that $f_n = 1$. Substituting $k = n$ in the expression for f_k in Theorem 3.8 yields the following equation for the total number of unbounded cells:

$$\sum_{i=1}^{n} f_{i-1}^{\infty} = n(n-1). \tag{3.2}$$

The unbounded cells in the k-th order Voronoi diagram can be characterized as follows: let $\overline{pq}$ denote the line segment with endpoints p and q and l_{pq} the line through p and q.

Property 3.9
A cell $V(A)$ of the k-th order Voronoi diagram $V_k(S)$ is unbounded if and only if one of the following two conditions holds.
 (i) There exists a line l that separates A from $S - A$.
 (ii) There exist two consecutive points p and q, with $p, q \in S - A$, on $\delta CH(S - A)$ such that the points in $A - \overline{pq}$ are in the open half plane defined by l_{pq} opposite to $CH(S - A)$.

Proof. [OBS], Property OK4. ∎

Under the general position assumption, we only need to consider condition *(i)* in Property 3.9. It is clear that in this case the following symmetry holds:

$$f_k^{\infty} = f_{n-k}^{\infty}. \tag{3.3}$$

3.2.4 Circle events and hull events.

In Section 2.3 we have discussed the type of a Voronoi diagram in connection with circle events and convex hull events. We generalize these notions to k-th order Voronoi diagrams. Let S be a set of points in general position and fix some $k \in 1, \dots, n$. As in [Le] we call a Voronoi vertex of $V_k(S)$ **old** if its corresponding circle has order $k - 2$ and **new** if its corresponding circle has order $k - 1$. We will also use the words old and new to indicate order $k - 2$ and order $k - 1$ circles with respect to $V_k(S)$.

Example 3.10
In the classic or first order diagram, vertices correspond with empty circles, so all vertices are new.

Represent every vertex x of $V_k(S)$ as an ordered list of labels of the points of S on the $k - 1$ or $k - 2$ order Voronoi circle $C(x)$ corresponding to x. Order the labels as in Definition 2.5. The **type** of a k-th order Voronoi diagram $V_k(S)$ consists of

two lists: a list of ordered labels of old vertices and a list of ordered labels of new vertices.

Example 3.11
Consider the configuration in Figure 3.5.a. The circles 124 and 143 are empty, while the circles 123 and 243 both contain one point. Therefore, the type of the second order Voronoi diagram is given by: $\{\{124, 143\}, \{123, 243\}\}$.

Suppose that the points in S start moving. S is in general position, as long a no four points are cocircular and no three points are collinear. If four points become cocircular, then two circles C_{abd} and C_{bcd}, both surrounding a subset $T \subset S$ of size $|T| = k$, coincide and change into two circles C_{abc} and C_{acd}, see Figure 2.4. This corresponds to a change of the Voronoi vertices abd and bcd into Voronoi vertices abc and acd in both $V_{k+1}(S)$ and $V_{k+2}(S)$. This is the generalization of a circle event and is called a **k-th order circle event**. So, a zero order circle event is just a circle event.
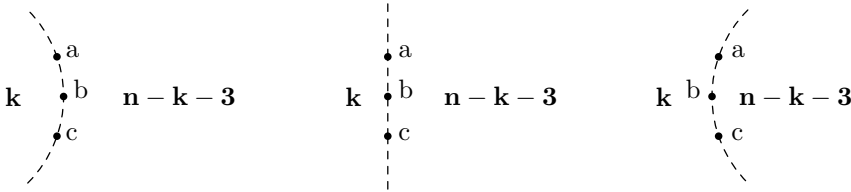
Figure 3.4: A k-th order convex hull event.

If three points become collinear, an order k circle abc changes into an order $n - k - 3$ circle abc, see Figure 3.4. This implies that the vertex abc disappears in $V_{k+1}(S)$ and $V_{k+2}(S)$ and appears in $V_{n-k-1}(S)$ and $V_{n-k-2}(S)$. This is the generalization of a hull event and is called a **k-th order hull event**. So, a zero order hull event is just a hull event. At a k-th order circle event the type of $V_{k+1}(S)$ and $V_{k+2}(S)$ changes. At a k-th order hull event, the type of $V_{k+1}(S), V_{k+2}(S), V_{n-k-1}(S)$ and $V_{n-k-2}(S)$ changes.

3.3   The Voronoi poset.

3.3.1   Definition and examples.

Fix a labeling of the sites in S and identify a set of sites $A \subset S$ that defines a non-empty Voronoi cell $V(A)$ with the set of labels $L(A) \subset [n]$ of the sites in A. A subset L of $[n]$ may or may not correspond to some Voronoi cell $V(A_L)$. For $k = 1$ we retain the ordinary Voronoi diagram, which implies the correspondence

$$V_1(S) \;\leftrightarrow\; \{\{1\}, \{2\}, \dots, \{n\}\}.$$

We define $V_0(S) = \{\emptyset\}$. The set $\{\{1, \ldots, n\}\}$ corresponds to $V_n(S)$. We consider the set of all Voronoi cells that appear for a given set S of points and call the set of corresponding labels the **Voronoi poset** $\Pi(S)$ of S:

$$\Pi(S) := \bigcup_k \{ L(A) \mid V(A) \in V_k(S) \}.$$

This definition also makes sense when we drop the general position assumption.

We order the elements in the poset by set inclusion of the sets $L(A)$. This yields a partially ordered set. For more on partially ordered sets consult [Zi]. The poset is bounded since we have the empty set as $\hat{0}$, the unique minimal element, and the set $[n]$ as $\hat{1}$, the unique maximal element. In general, a poset is called **graded** if it is bounded and if every maximal chain has equal length. We show that $\Pi(S)$ is graded. Below we give an example showing that $\Pi(S)$ is in general not a lattice.

Property 3.12
$\Pi(S)$ *is graded.*

Proof. We show that $r(L(A)) = |L(A)|$ is a **rank function** for $\Pi(S)$. A rank function maps an element x from a poset to a unique level in such a way that the level corresponds to the length of any maximal chain from x to $\hat{0}$. Let $L(A) \in \Pi(S)$, with $|L(A)| = k$. Every point $x \in V(A)$ has all k points from A as its k nearest neighbors. Order those points with respect to their distance to x. As we assumed general position it is always possible to change the choice of x in such a way that this order is strict. By removing at each step the furthest point still available, we obtain a chain of length k that descends to $\hat{0}$. ∎

We analyze the two smallest cases, assuming general position.

Example 3.13
For $n = 3$ there is one poset, the full poset on $[3]$. That is,

$$\Pi_3(S) = \{\emptyset, 1, 2, 3, 12, 13, 23, 123\}.$$

Example 3.14
For $n = 4$ there are two essentially distinct posets as is evident from the circles defined by four points. Since $n = 4$, Voronoi circles are of order one or two. Eulers formula rules out four circles of order one. At the same time less than two circles would not yield enough cells in the first order diagram.

Figure 3.5.a has two empty Voronoi circles. Clearly, subset 23 is the only subset of $[4]$ missing, leaving us with :

$$\Pi_4(S_1) = \{\emptyset, 1, 2, 3, 4, 12, 13, 14, 24, 34, 123, 124, 134, 234, 1234\}.$$

This example shows that the Voronoi poset is in general not a lattice. A lattice requires that every two elements of the poset have a unique minimal upper bound.
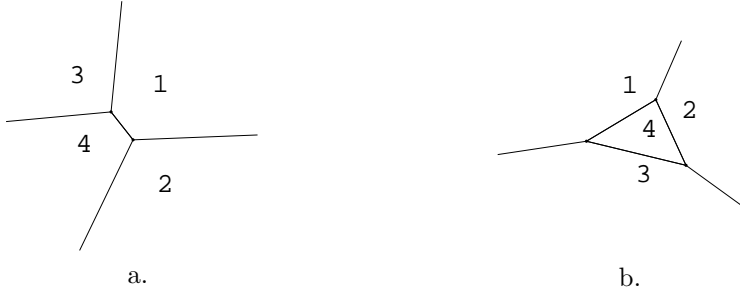
Figure 3.5: The two distinct first order Voronoi diagrams.

In this example, the elements 2 and 3 have two minimal upper bounds, namely 123 and 234.

In Figure 3.5.b. there are three empty Voronoi circles. The cell 123 cannot appear in the third order diagram, but all other subsets of [4] do appear, thus:

$$\Pi_4(S_2) = \{\emptyset, 1, 2, 3, 4, 12, 13, 14, 23, 24, 34, 124, 134, 234, 1234\}.$$

3.3.2   The order complex of the Voronoi poset.

The standard way to associate a topological space to a finite poset $(P, \leq)$ is by means of the **order complex** $\Delta(P)$ of the poset, see [Bj, Wa]. The order complex is the simplicial complex of all nonempty chains of P. A **chain** of P of **length** k is a totally ordered subset

$$x_0 \; < \; x_1 \; < \; x_2 \; < \; \ldots \; < \; x_k,$$

of elements $x \in P$. The well-known **geometric realization** associates a topological space with a simplicial complex.

As a Voronoi poset on a set of n points $p_1, \ldots, p_n$ always has a unique maximal element $\{1, \ldots, n\}$, the geometric realization of the order complex is a cone and therefore contractible. This shows that the topological space that we have associated with S is homotopy equivalent with a point, and therefore not very interesting.

More promising is to consider the complement, that is the **anti Voronoi poset** $aP(S)$, consisting of those subsets of $\{1, \ldots, n\}$ that are not in the Voronoi poset. Another possibility is to consider the arrangement of bisectors.

3.4   Symmetry relations.

Given a set S of sites, we count for every order k the number of vertices v_k, the number of edges e_k and the number of non empty Voronoi cells f_k. The **f-vector**

of $\Pi(S)$ is the vector $\{f_1, f_2, \ldots, f_n\}$. The c- and e-vector are defined analogously. Note that the f-vector of $\Pi(S)$ may change if the position of the sites in S changes.

Example 3.15
Consider the two configurations S_1 and S_2 on four points, presented in Example 3.14. The f-vector of $\Pi(S_1)$ equals $(1, 4, 5, 4, 1)$, while the f-vector of $\Pi(S_2)$ equals $(1, 4, 6, 3, 1)$.

3.4.1 Symmetry in the number of cells.

It turns out that a symmetry exists in the f-vectors.

Lemma 3.16
Consider the f-vector of $\Pi(S)$, where $|S| = n$. Then $f_k + f_{n-k+1}$ is a constant independent of the position of the points in S. More precisely,

$$f_k + f_{n-k+1} \;=\; 2k(n-k+1) + 1 - n. \tag{3.4}$$

Proof. We apply Theorem 3.8 to f_k and f_{n-k+1}:

$$f_k + f_{n-k+1} \;=\; (2k-1)n - k^2 + 1 - \sum_{i=1}^{k} f_{i-1}^{\infty}$$

$$+ \;\; (2(n-k+1) - 1)n - (n-k+1)^2 + 1 - \sum_{i=1}^{n-k+1} f_{i-1}^{\infty},$$

$$= \;\; 2kn - 2k^2 + 2k + 1 - n + n(n-1) - \Big(\sum_{i=1}^{k} f_{i-1}^{\infty} + \sum_{i=1}^{n-k+1} f_{i-1}^{\infty} \Big).$$

We join the two sums by applying Symmetry Equation 3.3. and evaluate the result by using Equation 3.2.

$$\sum_{i=1}^{k} f_{i-1}^{\infty} + \sum_{i=1}^{n-k+1} f_{i-1}^{\infty} \;=\; \sum_{i=1}^{n} f_{i-1}^{\infty} \;=\; n(n-1).$$

The lemma follows from combining the two equations above. ∎

3.4.2 Symmetry in the number of vertices.

A similar equation holds for the number of vertices of a collection of Voronoi diagrams $V_k(S)$, for $k = 1, \ldots, n-1$.

Lemma 3.17
Let S be a set of points in general position with $|S| = n$. Let v_k denote the number of vertices in the k-th order Voronoi diagram. Then:

$$v_k + v_{n-k} \;=\; 4k(n-k) - 2n. \tag{3.5}$$

Proof. Using Theorem 3.8 we write $v_k + v_{n-k}$ in terms of numbers of cells. Next we regroup and apply Symmetry Equation 3.3. After applying Theorem 3.8 we combine using symmetry again. Finally, using $\sum_{i=1}^{n} f_{i-1}^{\infty} = n(n-1)$ completes the proof.

$$
\begin{aligned}
v_k + v_{n-k} &= 2(f_k - 1) - f_k^{\infty} + 2(f_{n-k} - 1) - f_{n-k}^{\infty}, \\
&= 2(f_k + f_{n-k} - 2 - f_k^{\infty}), \\
&= 2(n^2 - 2n + 2kn - 2k^2 - (\sum_{i=1}^{k} f_{i-1}^{\infty} + \sum_{i=1}^{n-k} f_{i-1}^{\infty} + f_k^{\infty})), \\
&= 2(n^2 - 2n + 2kn - 2k^2 - \sum_{i=1}^{n} f_{i-1}^{\infty}), \\
&= -2n + 4kn - 4k^2, \\
&= 4k(n-k) - 2n. \qquad\blacksquare
\end{aligned}
$$

3.4.3   Symmetry in the number of Voronoi circles.

Recall that the order of a Voronoi circle equals the number of points of S contained in its interior. We define the **c-vector** of S as the vector

$$
c(S) \quad = \quad \{c_0, c_1, \ldots, c_{n-3}\},
$$

where c_i denotes the number of circles of order i. The following theorem states that for n arbitrary points in general position, the number of circles containing exactly i points on their inside plus the number of circles containing exactly i points on their outside is constant. We prove this by applying the above results.

Theorem 3.18
Consider the c-vector of $\Pi(S)$, where $|S| = n$. Then $c_i + c_{n-i-3}$ is a constant independent of the position of the points in S. More precisely,

$$
\begin{aligned}
c_i + c_{n-i-3} &= 2(i+1)(n-2-i), \qquad\qquad\qquad (3.6) \\
&= 2i(n-i-3) + 2(n-2).
\end{aligned}
$$

Proof. We prove the theorem by induction.

[i=0].   We use the **lifting transformation**. This transformation changes the point-inside-circle relation in 2-dimensional space in a point-below-plane relation in 3-dimensional space. See also Section 2.5.1. The lifting transformation map ϕ is defined by

$$
\begin{aligned}
\phi : \quad \mathbb{R}^2 \quad &\to \quad \mathbb{R}^3, \\
(x, y) \quad &\mapsto \quad (x, y, x^2 + y^2).
\end{aligned}
$$

It lifts points in the plane to the unit paraboloid in three-space. As every circle defined by S in the plane contains only three points from S, every hyperplane defined by $\phi(S)$ contains only three points from $\phi(S)$ as well. The number c_0 of empty

circles of S in the plane equals the number of facets of the lower hull of $\phi(S)$ in three dimensions. At the same time, the number c_{n-3} of circles that contain all other points of S equals the number of facets of the upper hull of $\phi(S)$. All images of points in S under ϕ are part of the convex hull of $\phi(S)$. Since the convex hull of a point set of n points consists of $2n - 4$ facets, if every facet is a triangle, see [BKOS], Theorem 11.1, the claim follows.

[induction step]. We deduce the expression for $c_k + c_{n-k-3}$ by applying Equation 3.1, followed by combining Lemma 3.17 and the induction hypothesis:

$$
\begin{aligned}
c_k + c_{n-k-3} &= c_{k-1} + c_k + c_{n-k-3} + c_{n-k-2} - (c_{k-1} + c_{n-k-2}), \\
&= v_{k+1} + v_{n-(k+1)} - (c_{k-1} + c_{n-k-2}), \\
&= 2(2(k+1) - 1)(n - (k+1)) - 2(k+1) \\
&\quad - (2(k-1+1)(n-2-(k-1))), \\
&= 2(k+1)(n-2-k). \qquad \blacksquare
\end{aligned}
$$

Let $\tilde{f}_k := f_k + f_{n-k+1}$ and $\tilde{c}_i := c_i + c_{n-i-3}$. By the **reduced f-vector**, denoted $\tilde{f}$, we mean the vector of $\tilde{f}_k$'s for all distinct k. That is

$$
\tilde{f} \quad := \quad \{\tilde{f}_0, \tilde{f}_1, \ldots, \tilde{f}_{\lfloor \frac{n-1}{2} \rfloor}\}.
$$

$\tilde{c}$ is defined similarly. As a consequence of Lemma 3.16 and Theorem 3.18, $\tilde{f}$ and $\tilde{c}$ are only dependent on n.

Example 3.19

As an example we present the reduced f- and c-vectors for $n \in \{3, \ldots, 12\}$.

n	$\tilde{f}$	$\tilde{c}$
3	(4, 6)	(2)
4	(5, 9)	(4)
5	(6, 12, 14)	(6, 8)
6	(7, 15, 19)	(8, 12)
7	(8, 18, 24, 26)	(10, 16, 18)
8	(9, 21, 29, 33)	(12, 20, 24)
9	(10, 24, 34, 40, 42)	(14, 24, 30, 32)
10	(11, 27, 39, 47, 51)	(16, 28, 36, 40)
11	(12, 30, 44, 54, 60, 62)	(18, 32, 42, 48, 50)
12	(13, 33, 49, 61, 69, 73)	(20, 36, 48, 56, 60)

Remark 3.20

Computer calculations did not suggest any similar symmetry relation for the number of edges.

3.4.4   Relations between cells and circles.

Corollary 3.21
$\tilde{f}_i = \tilde{f}_0 + \tilde{c}_{i-1} = \tilde{c}_{i-1} + n + 1.$

Proof. This follows directly from Lemma 3.16 and Theorem 3.18.   ∎

Property 3.22
*Let f_i^∞ denote the number of unbounded cells in the i-th order diagram and let c_i
denote the number of circles of order i:*

$$f_i^\infty + (c_{i-1} - c_{i-2}) \;=\; 2(n - i). \tag{3.7}$$

Proof. We prove the property by induction.

[i=1] c_{-1} is zero by definition. The number of vertices v_1 in the first order Voronoi
diagram equals the number of circles of order zero, c_0. The claim follows from
applying Theorem 3.8:

$$\begin{aligned}
f_1^\infty + (c_0 - c_{-1}) &= f_1^\infty + v_1, \\
&= f_1^\infty + 2(f_1 - 1) - f_1^\infty, \\
&= 2(n - 1).
\end{aligned}$$

[induction step]   Assume we have proved that

$$f_i^\infty + (c_{i-1} - c_{i-2}) \;=\; 2(n - i).$$

We rewrite this, by using induction, as

$$c_{i-1} \;=\; 2ni - i(i+1) - \sum_{k=1}^{i+1} f_{k-1}. \tag{3.8}$$

Evaluate $c_i - c_{i-1}$:

$$\begin{aligned}
c_i - c_{i-1} &= (c_i + c_{i-1}) - 2c_{i-1}, \tag{3.9} \\
&= v_{i+1} - 2c_{i-1}, \\
&= 2(f_{i+1} - 1) - f_{i+1}^\infty - 2c_{i-1}.
\end{aligned}$$

Substituting this expression for $c_i - c_{i-1}$ and applying Theorem 3.8 and Equation
3.8 proves the claim:

$$\begin{aligned}
f_{i+1}^\infty + (c_i - c_{i-1}) &= 2(f_{i+1} - 1 - c_{i-1}), \\
&= 2(n - i - 1). \quad\quad\quad ∎
\end{aligned}$$

Corollary 3.23
The c-vector totally determines the f-vector. The correspondence is given by

$$f_k \;=\; n - k + 1 + c_{k-2}.$$

Proof. Applying Equation 3.7 we get

$$\sum_{i=1}^{k} f_{i-1}^{\infty} \quad = \quad (k-1)(2n-k) - c_{k-2}.$$

The claim follows from evaluating Theorem 3.8 using the expression above. ∎

3.5 Even versus odd order cells.

Given a grading on a set of objects, it is common to consider the **Poincaré polynomial** $P(t)$ of the grading. The i-th coefficient of this polynomial equals the number of objects of grade i. In our case, the objects are the elements of the Voronoi poset $\Pi(S)$, while the grading is given by the rank function on the poset. Recall that the rank of an element x in $\Pi(S)$ is just the order k of the Voronoi diagram in which x occurs as a cell. The i-th coefficient of the Poincaré polynomial $P(t)$ is given by f_i, as f_i gives the number of cells in the i-th order diagram $V_i(S)$. So, the Poincaré polynomial $P(t)$ of $\Pi(S)$ with respect to our rank function is given by

$$P(t) \quad = \quad f_0 + f_1 t + f_2 t^2 + \cdots + f_n t^n.$$

As an application of the symmetry relations we compare the number of cells in the even order Voronoi diagrams with the number of cells in the odd order diagrams. In terms of the Poincaré polynomial $P(t)$ of above, the following result can also be formulated as

$$P(-1) \quad = \quad 0.$$

Theorem 3.24
Let S be a set of points in general position with $|S| = n \geq 3$. Assume n is odd. In this case, the number of cells in the even order Voronoi diagrams equals the number of cells in the odd order Voronoi diagrams.

Proof. Write $\tilde{f}_i \ = \ f_i + f_{n-i+1}$. We show that $A = 0$, where:

$$A \quad = \quad -f_0 + f_1 - f_2 + \cdots - f_{n-1} + f_n.$$

So A is the number of cells in the odd order diagrams minus the number of cells in the even order diagrams:

$$A \quad = \quad -f_0 + \tilde{f}_1 + \frac{1}{2}\tilde{f}_{\frac{n+1}{2}} + t_n,$$

where

$$t_n \quad := \quad \sum_{i=2}^{\frac{n-1}{2}} (-1)^{i+1} \tilde{f}_i.$$

Clearly, $f_0 = 1$, as f_0 counts the empty set. $\tilde{f}_1$ is the number of points in S plus the number of cells in $V_n(S)$, so $\tilde{f}_1 = n + 1$. Applying Equation 3.4 gives:

$$\tilde{f}_{\frac{n+1}{2}} \quad = \quad -(-1)^{\frac{n+1}{2}} \frac{n^2 + 3}{4}.$$

Straightforward calculations show that:

$$t_n \quad = \quad (-1)^{\frac{n+1}{2}} \frac{n^2 + 3}{4} - n,$$

from which it follows that:

$$A \quad = \quad -1 + n + 1 - (-1)^{\frac{n+1}{2}} \frac{n^2 + 3}{4} + (-1)^{\frac{n+1}{2}} \frac{n^2 + 3}{4} - n \quad = \quad 0. \qquad \blacksquare$$

The claim of Theorem 3.24 does not hold when n is even. However, the following result does hold.

Lemma 3.25

Let S be a set of points in general position, with $|S| = n \geq 3$. Assume n is even. Let $A(S)$ denote the number of cells in the odd order Voronoi diagrams minus the number of cells in the even order diagram. Then:

$$n \equiv 0(4) \quad \Rightarrow \quad A(S) \text{ odd.}$$
$$n \equiv 2(4) \quad \Rightarrow \quad A(S) \text{ even.}$$

Proof. Similar computations as in the proof of Theorem 3.24. $\qquad \blacksquare$

Note that as $v_k = c_{k-1} + c_{k-2}$ it follows immediately that:

$$\sum_{k=1}^{n-1} (-1)^{k+1} v_k \quad = \quad 0,$$

for all n, where v_k denotes the number of vertices in the k-th order Voronoi diagram.

Chapter 4

Limits of Voronoi diagrams.

The Voronoi diagram of a set S of n distinct points in $\mathbb{R}^2$ associates to a point $p \in S$ that part of the plane that is closer to p than to any other point in S. In this chapter we assume that the position of any of the n points in $S = S(t)$ is given by a pair of polynomials in one parameter t, such that no two points are represented by the same pair of polynomials. We call the elements of $S(t)$ polynomial sites. In this setup it is possible that sites coincide at, say, $t = 0$. We define a Voronoi diagram $V(S(0)) := \lim_{t \downarrow 0} V(S(t))$. That is, $V(S(0))$ is defined as a limit diagram in a particular sense of the ordinary Voronoi diagram of the positions, at small positive t, of the polynomial sites. We show how to extend the notion of type to polynomial sites. This enables us to determine the combinatorics of $V(S(0))$. It turns out that in general some sites can be omitted without changing the boundary of the Voronoi diagram $V(S(0))$. We characterize those sites that can not be omitted and present an efficient algorithm to determine these sites together with the boundary of the Voronoi diagram.

4.1   Introduction.

Whenever Voronoi diagrams are studied, it is assumed that all points defining the diagram are distinct. We call these points sites. In the case of dynamic Voronoi diagrams, where the sites are moving continuously over time, the assumption above means that sites are not allowed to coincide at any moment. In this chapter we investigate in one particular setting what happens when we do allow sites to coincide in the plane.

We consider a set

$$S(t) = \{p_1(t), \ldots, p_n(t)\},$$

of n sites in the plane such that the position of site p_i at time t is given by a pair of polynomials in t, one for every coordinate. That is, both the movement of the x-

and the y-component are described by a polynomial in $\mathbb{R}[t]$.

In fact we do not have to restrict ourselves to sites described by pairs of polynomials: the theory developed in this chapter works whenever the movement of both the x- and y-component of all sites is described by functions that can be expanded as a convergent Taylor series. For the sake of simplicity we restrict ourselves to polynomials however.

In Chapter 1 we have described the Voronoi diagram of a set of distinct sites both in terms of half-planes and of empty circles. To check whether some point q is in a given half-plane $h(p_1, p_2)$ or inside a circle $c(p_1, p_2, p_3)$ for $p_1, p_2, p_3 \in \mathbb{R}^2$ boils down to evaluating the sign of an easy polynomial expression $f_h(p_1, p_2, q)$ or $f_c(p_1, p_2, p_3, q)$. The main idea of this chapter is to replace p_i for $i = 1, 2, 3$ and q by $p_i(t), q(t) \in \mathbb{R}[t]^2$ and to evaluate the sign of the coefficient of the lowest degree term in $f_h(p_1(t), p_2(t), q(t))$ and $f_c(p_1(t), p_2(t), p_3(t), q(t))$, at $t = 0$. In this way we define a Voronoi diagram $V(S(t))$ at $t = 0$, even if sites do coincide at $t = 0$. For a set of sites that coincide at $t = 0$ we regard $V(S(0))$ as the limit diagram $\lim_{\epsilon \downarrow 0} V(S(\epsilon))$. We develop this arithmetic for polynomial sites in all details in Section 4.2.

Here we add a warning: we can define a limit Voronoi diagram at $t = 0$ that is consistent with small positive t or small negative t. In general these two approaches give distinct results. Examples will be presented in the main text of this chapter.

There is a similarity between our approach and a well-known technique in computational geometry that is used to avoid computations involving degenerate input. In this technique, a set of distinct points that is not in general position is perturbed slightly in such a way that it is in general position after perturbation. For example, three points that are collinear before perturbation will not be collinear anymore after perturbation. As a consequence it is possible for a *generic* algorithm, that is, an algorithm that can only handle points in general position, to handle the input and compute the wished geometric structure, e.g. a Voronoi diagram. Such generic algorithms are in general much easier than algorithms for arbitrary input as a lot of degenerated cases can be ignored. In the so-called *Simulation of Simplicity* technique, cf. [EM, Ed2], polynomials in the variable ϵ are added to points of a set of distinct, degenerated points in such a way that evaluation of the new points for small enough ϵ produces a point set that is in general position. An overview on robust geometric computation is given in [Ya].

In Section 4.3 we extend the definition of type, see Definition 2.5, to a set of polynomial sites $S(t)$ at $t = 0$, provided that $S(0)$ fulfills some general position assumptions. This type gives us a complete combinatorial structure that matches with the combinatorial structure of the Voronoi diagram $V(S(t))$ for small enough positive t.

In Section 4.4 we define a Voronoi diagram for n not necessarily distinct points in the plane and $\binom{n}{2}$ angles between those points. We apply this definition to introduce Voronoi diagrams for a set of polynomial sites $S(t)$ at $t = 0$. The resulting Voronoi diagram or polynomial sites matches with the ordinary Voronoi diagram of the positions of the sites at small positive t. In this section we also give the connection between half-planes and Voronoi circles defined by $S(t)$ at $t = 0$, thereby connecting

the notion of type to polynomial sites diagrams.

The shape of a Voronoi diagram is defined as the union of the boundaries of the Voronoi cells. It turns out that in general some sites in a set $S(t)$ of polynomial sites can be omitted without changing the shape of the Voronoi diagram of $S(t)$. A question that we pose is how to determine this shape efficiently and how to characterize those sites that do determine the shape. We answer this question by splitting up the problem into two parts.

First we consider in Section 4.5 the shape of the Voronoi diagram of one cluster of polynomial sites at $t = 0$. By an l-cluster we mean a set of polynomial sites such that the positions of all sites coincide at one location l at $t = 0$. Lemma 4.35 fully classifies the sites $p_i(t)$ in the cluster such that $\text{area}(V(p_i(0))) > 0$ at $t = 0$.

The second part of the question is solved by Lemma 4.41. This lemma states that the shape of the Voronoi diagram at $t = 0$ of an arbitrary set of polynomial sites can be found as follows. First, compute the ordinary Voronoi diagram of all distinct locations at $t = 0$. Second, plug in the cell of location l, the shape of the Voronoi diagram of the l-cluster.

Section 4.6 shows that a lot of combinatorics can be hidden in the edges of the shape of the Voronoi diagram. In Section 4.7 we demonstrate the theory developed in the former section by a somewhat bigger example. We conclude this chapter in Section 4.9 with some remarks on generalizations to k-th order Voronoi diagrams and shortcomings of this setup.

4.2 Preliminaries.

We define half-planes and circles for polynomial sites. A **polynomial site** $p(t) = (p(t)_x, p(t)_y)$ consists of a pair of polynomials $p(t)_x, p(t)_y \in \mathbb{R}[t]$. Two polynomial sites $u(t)$ and $v(t)$ are called **distinct** if they represent distinct elements in $\mathbb{R}[t] \times \mathbb{R}[t]$. Throughout this section assume that $S(t) = \{p_1(t), \ldots, p_n(t)\}$, where every $p_i(t)$ a polynomial site and $p_i(t)$ distinct from $p_j(t)$ as a polynomial site whenever $i \neq j$.

Remark 4.1
The notions in this section are introduced so that they match the situation for ordinary points in the plane obtained by substituting a very small *positive* value of t in the set $S(t)$ of polynomial sites.

4.2.1 Polynomial lines and their directions.

Let $u(t)$ and $v(t)$ be two distinct polynomial sites. The **polynomial line** $l_{uv}(t)$ is defined by

$$l_{uv}(t) \quad := \quad \begin{vmatrix} 1 & u(t)_x & u(t)_y \\ 1 & v(t)_x & v(t)_y \\ 1 & x & y \end{vmatrix} \quad \in \quad \mathbb{R}[t, x, y].$$

The **ruling coefficient** $\mathrm{rc}(f(t))$ of a polynomial $f(t) \in \mathbb{R}[t]$ is the coefficient in its lowest degree term. The **ruling sign** $\mathrm{rs}(f(t))$ is the sign of the ruling coefficient $\mathrm{rc}(f(t))$. We define the **direction** ϕ_{uv} of the polynomial line $l_{uv}(t)$ at $t = 0$ as the argument of the point

$$(\cos \phi_{uv}, \sin \phi_{uv}) \quad = \quad \lim_{t \downarrow 0} \left(\frac{d(t)_x}{\mid d(t)_x \mid}, \frac{d(t)_y}{\mid d(t)_y \mid} \right)$$

where $d(t) = (d(t)_x, d(t)_y) = v(t) - u(t)$. Note that ϕ_{uv} is determined up to multiples of 2π. We often use that value of ϕ_{uv} that lives in $(-\pi, \pi]$.

Example 4.2
Let $u(t) = (t, t)$ and $v(t) = (-t, t^2)$. Then $l_{uv}(t) = t^2 + t^3 + tx - t^2x - 2ty$. Putting $l_{uv}(t)$ equal to zero yields an ordinary line for every $t \neq 0$. As $d(t) = v(t) - u(t) = (-2t, -t + t^2)$, we have $\lim_{t \to 0} \frac{d(t)_y}{d(t)_x} = \frac{1}{2}$. The direction of $l_{uv}(t)$ at $t = 0$ is given by $\arctan(\frac{1}{2}) - \pi$, however, as the ruling sign $\mathrm{rs}(d(t)_x)$ equals -1.

Remark 4.3
Note that this definition of ϕ_{uv} indeed matches with the direction of the directed line that passes first through $u(t)$ and then through $v(t)$ for small positive t. For a definition that would match with small negative t, we should take into account the odness or evenness of the power of the lowest degree term of $l_{uv}(t)$.

Example 4.4
Let u and v be as in Example 4.2. For small negative t, the direction of the line l_{uv} that passes first through $u(t)$ and then through $v(t)$ is close to $\arctan(\frac{1}{2})$. If we multiply both $u(t)$ and $v(t)$ by t, that is change $u(t)$ into $u(t) = (t^2, t^2)$ and $v(t)$ into $v(t) = (-t^2, t^3)$, then the direction of l_{uv} for small negative t and for small positive t both are close to $\arctan(\frac{1}{2}) - \pi$.

4.2.2   Collinearity.

Let $u(t), v(t)$ and $w(t)$ be three polynomial sites. As long as the sites do not coincide we can analyze whether they are collinear. Consider the determinant $D(t)$ given by

$$D(t) \quad = \quad D_{u,v,w}(t) \quad = \quad \begin{vmatrix} 1 & u(t)_x & u(t)_y \\ 1 & v(t)_x & v(t)_y \\ 1 & w(t)_x & w(t)_y \end{vmatrix}.$$

We call the three sites **collinear** if $D(t)$ is the null polynomial. Otherwise let $\mathrm{rs}(D(t))$ denote the ruling sign of $D(t)$. If $\mathrm{rs}(D(t)) = 1$, we say that $w(t)$ is on the **left** of the polynomial line $l_{uv}(t)$ at $t = 0$, and if $\mathrm{rs}(D(t)) = -1$, we say that $w(t)$ is on the **right**.

Example 4.5
$u(t) = (0, -t)$, $v(t) = (-t, 0)$, $w(t) = (t, -2t)$. Then $D(t) = 0$, so u, v, and w are collinear at $t = 0$.

Example 4.6
Change w to $w(t) = (t - t^2, -2t)$. Now $D(t) = t^3$, so w is on the left of the polynomial line $l_{uv}(t)$ at $t = 0$.

Example 4.7
For small negative t, the site $w(t)$ is on the right of l_{uv}. If we change $w(t)$ into $w(t) = (t - t^3, -2t)$, then $w(t)$ is on the left of $l_{uv}(t)$ for small negative t while it is still on the right for small positive t.

4.2.3   The center of a circle.

Let $u(t)$, $v(t)$, and $w(t)$ be polynomial sites such that $u(t)$, $v(t)$, and $w(t)$ are not collinear at $t = 0$. Let $D = D(t)$ be the determinant of above and let $d = d(t)$, and $e = e(t)$ be the determinants given by

$$
d = - \begin{vmatrix} u(t)_x^2 + u(t)_y^2 & u(t)_y & 1 \\ v(t)_x^2 + v(t)_y^2 & v(t)_y & 1 \\ w(t)_x^2 + w(t)_y^2 & w(t)_y & 1 \end{vmatrix}, \quad e = \begin{vmatrix} u(t)_x^2 + u(t)_y^2 & u(t)_x & 1 \\ v(t)_x^2 + v(t)_y^2 & v(t)_x & 1 \\ w(t)_x^2 + w(t)_y^2 & w(t)_x & 1 \end{vmatrix}.
$$

We define the **circle center** of $u(t)$, $v(t)$, and $w(t)$ at $t = 0$ as the point c given by the coordinates

$$
c_x = - \lim_{t \to 0} \frac{d}{2D}, \qquad c_y = - \lim_{t \to 0} \frac{e}{2D}.
$$

We allow a circle center to be located at infinity. When leaving out the time dependency, these are of course the ordinary formulas describing a circle center. The circle $C(u(t), v(t), w(t))$ is **oriented clockwise** at $t = 0$ iff $w(t)$ is on the right of $l_{uv}(t)$ at $t = 0$. If $w(t)$ is on the left of $l_{uv}(t)$ at $t = 0$, then $C(u(t), v(t), w(t))$ is **oriented counterclockwise**.

If $u(0) = v(0) = w(0) = (0,0)$, then we say that the circle defined by $u(t)$, $v(t)$ and $w(t)$ has **positive radius** at $t = 0$ if and only if

$$
\text{maximum } (\ |c_x|\ ,\ |c_y|\ ) \quad > \quad 0. \tag{4.1}
$$

Example 4.8
Let again $u(t) = (0, -t)$, $v(t) = (-t, 0)$, and $w(t) = (t - t^2, -2t)$. Then $a = t^3$ and $d = e = 4t^3 - 2t^4 + t^5$. So $c = (-2, -2)$ and we can conclude that u, v and w define a circle of positive radius at $t = 0$. As $w(t)$ is on the left of $l_{uv}(t)$ at $t = 0$, the circle $C(u(t), v(t), w(t))$ is oriented counterclockwise at $t = 0$.

Example 4.9
Let $u(t) = (-t^3, 2t)$, $w(t) = (t^3, -2t)$, and $v(t) = (-t^4, 3t^2)$. Then $C(u, v, w)$ is oriented clockwise at $t = 0$, while the circle center c of $C(u, v, w)$ is situated at infinity.

4.2.4   Cocircularity.

Let $u(t)$, $v(t)$, and $w(t)$ be distinct polynomial sites. Assume that at $t = 0$ the sites $u(t)$, $v(t)$, and $w(t)$ are not collinear and that the circle $C(u(t), v(t), w(t))$ is oriented clockwise. As long as the sites do not coincide, we can analyze if a fourth polynomial site $q(t)$ is inside or outside of the circle defined by $u(t)$, $v(t)$, and $w(t)$. Consider the polynomial $I(t) \in \mathbb{R}[t]$ defined by

$$
I(t) \quad = \quad
\begin{vmatrix}
u(t)_x & u(t)_y & u(t)_x^2 + u(t)_y^2 & 1 \\
v(t)_x & v(t)_y & v(t)_x^2 + v(t)_y^2 & 1 \\
w(t)_x & w(t)_y & w(t)_x^2 + w(t)_y^2 & 1 \\
q(t)_x & q(t)_y & q(t)_x^2 + q(t)_y^2 & 1
\end{vmatrix}.
$$

We call the four sites **cocircular** at $t = 0$ if $I(t)$ is the null polynomial. Let otherwise $\mathrm{rs}(I(t))$ denote the ruling sign of $I(t)$. If $\mathrm{rs}(I(t)) = 1$, we say that $q(t)$ is **outside** of the polynomial circle $c_{uvw}(t)$ at $t = 0$, and if $\mathrm{rs}(D(t)) = -1$, we say that $q(t)$ is **inside** the circle. A set of polynomial sites $S(t)$ is in **general position** at $t = 0$, iff no three sites are collinear at $t = 0$ and no four sites are cocircular at $t = 0$.

Example 4.10
Let $u(t)$, $v(t)$, and $w(t)$ be as in Example 4.8. Let $q(t) = (0, 0)$. We check whether $q(t)$ is inside or outside of the clockwise oriented circle $C(u(t), w(t), v(t))$ at $t = 0$. As $I(t) = 4t^4 + O(t^5)$, we conclude that $q(t)$ is outside of $C(u(t), w(t), v(t))$ at $t = 0$.

Remark 4.11
For small negative t, the circle $C(u(t), w(t), v(t))$ is oriented counterclockwise. So the orientation swaps at $t = 0$. The site $q(t)$ is inside the clockwise oriented circle $C(u(t), v(t), w(t))$ for small negative t.

4.2.5   Ordering the sites.

The **lexicographic ordering** for polynomial sites is as follows. Let $u(t)$ and $v(t)$ be two polynomial sites. First consider the polynomials u_x and v_x that give the x-component. If $u_x \neq v_x$, order $u(t)$ and $v(t)$ according to the coefficients of the term of lowest degree of u_x and v_x that are distinct. If $u_x = v_x$, then compare the coefficients of lowest degree that are distinct of u_y and v_y. We denote this ordering by $O_<$.

Example 4.12
Let $u(t) = (2t^2, t)$ and $v(t) = (t, t)$. The first order coefficient of u_x equals 0 while the first order coefficient of v_x equals 1. As this is the lowest order coefficient of u_x and v_x that is distinct, it follows that $u(t) < v(t)$ with respect to $O_<$.

4.3 The type of a set of polynomial sites.

Let $S(t) = \{p_1(t), \ldots, p_n(t)\}$ be a list of distinct polynomial sites that is in general position at $t = 0$. A clockwise polynomial circle $c_{uvw}(t)$ with $u(t)$, $v(t)$, and $w(t)$ in $S(t)$ is a **Voronoi circle** at $t = 0$ iff there are no polynomial sites from $S(t)$ inside $c_{uvw}(t)$ at $t = 0$. Represent a Voronoi circle $c(t)$ by the ordered list of labels of the polynomial sites $u(t)$, $v(t)$, and $w(t)$ that define $c(t)$. The order of the labels corresponds to the cyclic, clockwise order of the defining sites on $c(t)$ at $t = 0$, compare with Section 4.2.3. The set of all these lists is the **type** of $S(t)$ at $t = 0$.
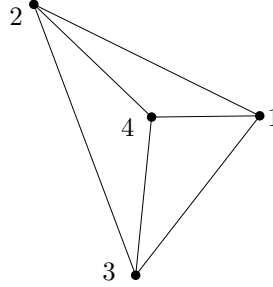
Figure 4.1: The Delaunay triangulation of the sites of Example 4.13 at $t = 0.1$.

Example 4.13
Let $S(t)$ be the set of polynomial sites given by

$$
\begin{aligned}
q_1 &= (2t,\ 2t^3 + t^4), \\
q_2 &= (-2t - t^3,\ 2t), \\
q_3 &= (-2t^2 - 2t^4,\ -3t + 2t^2 - t^3 + t^4), \\
q_4 &= (t^2 - 2t^3 + t^5,\ -t^4).
\end{aligned}
$$

The relative position of the sites at $t = 0.1$ is shown in Figure 4.1. The set $S(t)$ defines at $t = 0$ the clockwise oriented circles $134, 142, 132$ and 243, where we list only the labels. The polynomial site q_4 is inside the circle 132 at $t = 0$, while the other circles are empty at $t = 0$. Therefore the type of $S(t)$ is given by $\{142, 134, 243\}$.

Remark 4.14
Note that this definition of type again represents the situation for small positive t. This is because the type is defined in terms of the 'inside circle relation', compare Section 4.2.4.

4.3.1 Abstract Delaunay graph.

The notion of type enables us to define an **abstract Delaunay graph** $aD(S(t))$ of $S(t)$ at $t = 0$. In fact, we use Lemma 2.7 as a definition for $aD(S(t))$. The **vertices**

of $aD(S(t))$ at $t = 0$ are the labels occurring in the type. Two labels are connected by an **edge** if both occur in the same Voronoi circle at $t = 0$. Note that the closed paths of length three in $aD(S(0))$ correspond with the Voronoi circles at $t = 0$. The **multiplicity** of an edge is the number of distinct Voronoi circles that contain both the vertices incident to the edge.

Example 4.15

Consider the type at $t = 0$ of the set of polynomial sites from Example 4.13. It defines a abstract Delaunay graph $aD(S(t))$ with vertex set $\{1, 2, 3, 4\}$ and edge set $\{12, 13, 14, 23, 24, 34\}$. The multiplicities of the edges 12, 23, and 13 equal one, those of the other edges equal two. Compare this to the Delaunay triangulation shown in Figure 4.1.

Property 4.16

Let $p_a(t)$ and $p_b(t)$ be two distinct sites of $S(t)$.

   (i)   If $p_a(t)p_b(t)$ forms an edge of the convex hull $CH(S(t))$ for small enough positive t, then the multiplicity of the edge ab in $aD(S(0))$ equals one at $t = 0$.

   (ii)   If $p_a(t)p_b(t)$ forms an edge of the Delaunay triangulation $D(S(t))$ but not of $CH(S(t))$ for small enough positive t, then the multiplicity of the edge ab in $aD(S(0))$ equals two at $t = 0$.

Proof. Combine the definition of type and Lemma 2.3. ∎

4.3.2   Combinatorial convex hull.

The convex hull of a set of distinct points in the plane can be defined as an intersection of half-planes, see Section 2.1. But if a set of sites shrinks to one point, the convex hull of the sites also shrinks to one point. However, we can define a combinatorial convex hull of a set of polynomial sites at $t = 0$ by making use of half-planes.

Let $S(t)$ be a set of distinct sites in general position. It is not necessary that all sites coincide in $(0, 0)$ at $t = 0$. Some i is a **vertex** of the **combinatorial convex hull** $cCH(S(t))$ of $S(t)$ at $t = 0$ if there exists a polynomial site $p_j(t) \neq p_i(t)$ such that all sites $p_k(t)$ with $k \neq i, j$ are on the right of the polynomial line $l_{ij}(t)$ at $t = 0$. We call such a line a **bounding line**. Two vertices i and j are connected by a directed **edge**, notation $i \to j$, iff $l_{ij}(t)$ is a bounding line of $cCH(S(t))$ at $t = 0$.

Property 4.17

Let $S(t)$ be a set of distinct polynomial sites $S(t)$ in general position. C_0 denotes the combinatorial convex hull $cCH(S(t))$ at $t = 0$. Let $a, b \in C_0$ and $p_c(t) \in S(t)$.

   (i) C_0 is an abstract directed circuit graph.

   (ii)   The edges of C_0 are exactly the edges of multiplicity 1 of the abstract Delaunay graph $aD(S(t))$ at $t = 0$.

   (iii)   The direction of an edge ab of C_0 equals $a \to b$ iff the Voronoi circle containing both a and b is oriented like abc.

Proof. We prove the claims separately.

(i) A circuit graph is a connected graph that is regular of degree two. For t positive, small enough, the boundary of $CH(S(t))$ is an oriented polygon where the vertices have the same labels as the vertices of $cCH(S(t))$ at $t = 0$. The polygon is oriented so that all points of $S(t)$ not lying on an edge $p_i(t)p_j(t)$ of $CH(S(t))$ are on the right of the directed line defined by $p_i(t)$ and $p_j(t)$ that passes first through $p_i(t)$. This orientation and the connectedness are inherited when t vanishes.

(ii) This follows from Property 4.16.

(iii) If abc is the clockwise orientation of the Voronoi circle defined by $p_a(t)$, $p_b(t)$, and $p_c(t)$, then $p_c(t)(t)$ is on the right of $l_{ab}(t)$ at $t = 0$. ∎

Example 4.18
Consider the ordered set $S(t) = \{u(t), v(t), w(t)\}$ of polynomial sites introduced in Example 4.6. As $w(t)$ is on the left of $l_{uv}(t)$ at $t = 0$, the combinatorial convex hull $cCH(S(t))$ of $S(t)$ at $t = 0$ is given by 132.

Example 4.19
Let $S(t) = \{q_1(t), q_2(t), q_3(t), q_4(t)\}$ as in Example 4.13. Then $cCH(S(t))$ at $t = 0$ equals 132.

4.4 The Voronoi diagram of a set of points and angles between the points.

In this section we define the Voronoi diagram of a set of points and angles between the points. This enables us to introduce a Voronoi diagram for a set of polynomial sites. Moreover, we connect the notions of polynomial lines and polynomial circles in the context of Voronoi diagrams.

4.4.1 Definition.

Suppose $S = \{p_1, \ldots, p_n\}$ is a set of n not-necessarily distinct points in the plane. To every pair of points (p_i, p_j) we add an angle α_{ij} such that the following rule holds: if two points p_i and p_j are distinct then there is a unique line though p_i and p_j that makes some angle $\alpha_{ij} \in \mathbb{R}/2\pi\mathbb{Z}$ with the x-axis, directed from $-\infty$ to ∞; if p_i and p_j do coincide then we allow every value in $\mathbb{R}/2\pi\mathbb{Z}$ for α_{ij}.

Let γ_n be a set of n points $p_1(\gamma_n), \ldots, p_n(\gamma_n)$ and $\binom{n}{2}$ angles $\alpha_{12}, \ldots, \alpha_{(n-1)n}$ that obey aboves rule. Fix two points $p_i = p_i(\gamma_n)$ and $p_j = p_j(\gamma_n)$. The **bisection point** $b(p_i, p_j)$ is the point $\frac{1}{2}(p_i + p_j)$. If $p_i \neq p_j$, the bisection point is just the middle of the line segment $p_i p_j$. If $p_i = p_j$ then $b(p_i, p_j)$ coincides with the double point $p_i = p_j$. The **perpendicular bisector** $B(p_i, p_j)$ is the line through $b(p_i, p_j)$ perpendicular to the angle $\alpha_{ij} = \alpha_{ij}(\gamma_n)$. Let $\mathbf{n}$ be any non-zero vector, pointing in the direction α_{ij}. The **Voronoi half-plane** $vh(p_i, p_j)$ is the half-plane defined by

$$\mathbf{n} \cdot (x - b_x, y - b_y) \leq 0. \tag{4.2}$$

The **Voronoi cell** $V(p_i)$ is defined as

$$V(p_i) \quad = \quad \bigcap_{j \neq i} vh(p_i, p_j).$$

A point x is on the **Voronoi edge** $e(p_i, p_j)$ iff it is on the intersection of the Voronoi cells $V(p_i)$ and $V(p_j)$, that is

$$x \in e(p_i, p_j) \quad \Leftrightarrow \quad x \in V(p_i) \cap V(p_j).$$

The **Voronoi diagram** is the family of subsets of $\mathbb{R}^2$ consisting of the Voronoi cells $V(p_i)$ and all of their intersections. The **shape** or **boundary** of the Voronoi diagram is the union of the boundaries of the Voronoi cells.

Remark 4.20
We will always use this definition in a geometric context which imposes restrictions on the angles α_{ij}.

Remark 4.21
We show how to get Equation 4.2. The line given by $\mathbf{n} \cdot (x, y) = 0$ defines the line through the origin that is perpendicular to $\mathbf{n}$. We have to translate this line over the bisection point in order to get the bisector $B(p_i, p_j)$. As $\mathbf{n} \cdot \mathbf{n} > 0$, the Voronoi half-plane $vh(p_i, p_j)$ is the half-plane bounded by the line $B(p_i, p_j)$ in the direction of the tail of $\mathbf{n}$.

Remark 4.22
Taking for $\mathbf{n}$ the vector $(\cos \alpha_{ij}, \sin \alpha_{ij})$ of length 1 in the direction α_{ij} gives the inequality $(y - b_y) \sin \alpha_{ij} \leq (b_x - x) \cos \alpha_{ij}$ for the Voronoi half-plane $vh(p_i, p_j)$.

4.4.2   The Voronoi diagram of a set of polynomial sites.

Let $S(t) = \{p_1(t), \ldots, p_n(t)\}$ be a set of polynomial sites that is in general position at $t = 0$. The angle $\alpha_{ij}(0)$ for any two sites $p_i(t)$ and $p_j(t)$ is just the direction ϕ_{ij} as defined in Section 4.2. We define the Voronoi diagram of the set of polynomial sites at $t = 0$ as the Voronoi diagram of the points $(p_1(0), \ldots, p_n(0))$ and the angles $\alpha_{12}, \ldots, \alpha_{(n-1)n}$.

Remark 4.23
At this stage, we do not define Voronoi vertices: if a Voronoi vertex is defined as an intersection of three Voronoi half-planes, it can become a complete line, compare Example 4.26.

Example 4.24
Let $S(t)$ be the set of polynomial sites, introduced in Example 4.13. In Table 4.1 we list the Voronoi half-planes, the directions of the bisectors that bound the half-planes, and the inequalities defining the half-planes. This results in the Voronoi diagram $V(S(0))$, depicted in Figure 4.2. The Voronoi regions $V(q_1), V(q_2)$ and

$V(q_3)$ all have positive area, while $V(q_4) = \{(0,0)\}$. This shows that the shape of the Voronoi diagram of q_1, q_2, q_3, and q_4 equals the shape of the diagram of q_1, q_2, and q_3, with q_4 omitted.

half-plane	direction	inequality
$vh_{1;2}$	$\pi - \arctan\frac{1}{2}$	$2x \geq y$
$vh_{1;3}$	$\arctan\frac{3}{2} - \pi$	$-\frac{2}{3}x \leq y$
$vh_{1;4}$	π	$x \geq 0$
$vh_{2;3}$	$-\arctan\frac{5}{2}$	$\frac{2}{5}x \leq y$
$vh_{2;4}$	$-\frac{\pi}{4}$	$x \leq y$
$vh_{3;4}$	$\frac{\pi}{2}$	$y \leq 0$

Table 4.1: The half-planes, the directions of the lines bounding the half-planes, and the inequalities of the half-planes defined by $q_1(t), q_2(t), q_3(t)$ and $q_4(t)$ at $t = 0$.
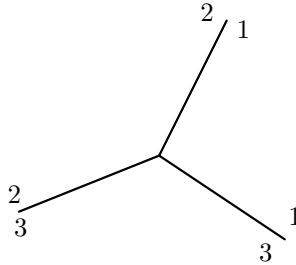
Figure 4.2: The Voronoi diagram of the points $q_1(t), q_2(t), q_3(t)$ and $q_4(t)$ at $t = 0$.

Remark 4.25
Given the particular sites in Example 4.24, it is easy to check that the picture of the Voronoi diagram for small negative values of t is close to the image under the point reflection in $(0,0)$ of the picture in Figure 4.2.

Example 4.26
Let $S(t)$ be the set of polynomial sites of Example 4.6 and Example 4.8, that is, $u(t) = (0, -t)$, $v(t) = (-t, 0)$, and $w(t) = (t - t^2, -2t)$. Then vh_{uv} is given by $y \leq x$, the half-plane $vh_{u,w}$ by $y \geq x$, and $vh_{v,w}$ by $y \geq x$ as well. Therefore, $V(u)$ is just the line $y = x$, while $V(v)$ is given by $y \geq x$, and $V(w)$ by $y \leq x$, all at $t = 0$.

4.4.3 Polynomial bisector.

Let $u(t)$ and $v(t)$ be two distinct polynomial sites. We have introduced the bisector of u and v at $t = 0$ as the line passing through the bisection point $b(u, v)$ and

perpendicular to the direction ϕ_{uv}. We can derive directly an equation $B_t(u, v)$ for the bisector depending on t as follows. We construct two polynomial sites $b(t)$ and $a(t)$ that lie on the ordinary bisector for every t. The point $b(t)$ is just the bisection point $\frac{1}{2}(u(t) + v(t))$. The other point $a(t)$ is the image of $u(t)$ under the $\frac{\pi}{2}$ rotation around $b(t)$, that is,

$$a(t) \quad = \quad \begin{pmatrix} 0 & -1 \\ 1 & 0 \end{pmatrix} \cdot (u - b)^T + b.$$

Finally, put $B_t(u, v) := l_{ba}(t)$. We call $B_t(u, v)$ the **polynomial bisector** of $u(t)$ and $v(t)$.

Lemma 4.27
Let $u(t)$ and $v(t)$ be two polynomial sites. Let $B(u, v)$ be the perpendicular bisector of $u(t)$ and $v(t)$ at $t = 0$. Then

$$B(u, v) \quad = \quad \lim_{t \downarrow 0} B_t(u, v).$$

Proof. By construction, the direction of $B_t(u, v)$ at $t = 0$ is perpendicular to ϕ_{uv}. As $B(u, v)$ and $\lim_{t \downarrow 0} B_t(u, v)$ both pass through the bisection point $b(0)$, the two lines coincide. ∎

Example 4.28
Let $S(t) = \{u(t), v(t), w(t)\}$ be as in Example 4.26. The polynomial bisector $B_t(u, v)$ is given by
$$B_t(u, v) = \{(x, y) \in \mathbb{R}^2 \mid y = x\},$$
while
$$B_t(u, w) = \{(x, y) \in \mathbb{R}^2 \mid y = -2t + t^2 - \frac{1}{2}t^3 + x - tx\}.$$

4.4.4   Half-planes and Voronoi circles.

Let $S(t)$ be a set of polynomial sites that is in general position at $t = 0$. In Section 4.4.1 we have introduced the Voronoi diagram $V(S(t))$ of $S(t)$ by means of half-planes, while in Section 4.3 we have defined the type of $S(t)$ at $t = 0$ in terms of Voronoi circles. The following lemma gives a connection between polynomial bisectors and circle centers.

Lemma 4.29
Suppose that $p_i(t)$, $p_j(t)$, and $p_k(t)$ are distinct non-collinear polynomial sites. Denote by c the circle center of $p_i(t)$, $p_j(t)$, and $p_k(t)$ at $t = 0$. Let $B_t(p_i, p_j)$ be the polynomial bisector of $p_i(t)$ and $p_j(t)$. Then

$$c \quad = \quad \lim_{t \to 0} \left(B_t(p_i, p_j) \cap B_t(p_i, p_k) \right).$$

Proof. For t positive and small enough, $p_i(t)$, $p_j(t)$, and $p_k(t)$ are distinct points in general position. For such points Lemma 2.4 states that the intersection of the bisectors of the points is the center of the circle defined by the points. But then it holds for $t = 0$ as well. ∎

Now we are able to define a Voronoi vertex so that a vertex is exactly one point in the plane, compare with Remark 4.23. Let $p_i(t)$, $p_j(t)$, and $p_k(t)$ be distinct non-collinear polynomial sites. Let $c = c_{ijk}(0)$ be the clockwise oriented polynomial circle through $p_i(t)$, $p_j(t)$, and $p_k(t)$ at $t = 0$. Let x be the circle center of $p_i(t)$, $p_j(t)$, and $p_k(t)$ at $t = 0$. Then x is a **Voronoi vertex** $v(p_i, p_j, p_k)$ at $t = 0$ if c is a Voronoi circle at $t = 0$.

Let $u(t)$, $v(t)$, and $w(t)$ be distinct polynomial sites that coincide in $(0, 0)$ at $t = 0$. Then the circle center of $u(t)$, $v(t)$, and $w(t)$ is not equal to $(0, 0)$ only for special configurations.

Lemma 4.30
Let $u(t)$, $v(t)$, and $w(t)$ be distinct polynomial sites that coincide in $(0, 0)$ at $t = 0$. If $\phi_{uv} \not\equiv \phi_{uw} \mod \pi$ or $\phi_{uv} \not\equiv \phi_{vw} \mod \pi$, then the circle center c of $u(t)$, $v(t)$, and $w(t)$ at $t = 0$ equals $(0, 0)$.

Proof. We may assume without loss of generality that $\phi_{uv} \not\equiv \phi_{uw} \mod \pi$. Lemma 4.29 states that $c = \lim_{t \to 0}(B_t(u, v) \cap B_t(u, w))$. From Lemma 4.27 it follows that $c \in B(u, v) \cap B(u, w)$ at $t = 0$. But then c is the unique intersection point $(0, 0)$ of two non-parallel lines $B(u, v)$ and $B(u, w)$. ∎

Example 4.31
Let $u(t) = (0, -t)$, $v(t) = (-t, 0)$, and $w(t) = (t - t^2, -2t)$. In Example 4.8 we have shown that u, v, and w define a circle with center $c = (-2, -2)$ at $t = 0$. We did so by evaluating the determinants a, d, and e introduced in Section 4.2.3. Alternatively, we can compute $c(t)$ as an intersection of two bisectors, say $B_t(u, v)$ and $B_t(u, w)$. This gives:

$$
\begin{aligned}
c(t) &= B_t(u, v) \cap B_t(u, w) \\
&= (x, x) \ \cap \ (x, -2t + t^2 - \frac{1}{2}t^3 + x - tx) \\
&= \frac{1}{2}(-4 + 2t - t^2, -4 + 2t - t^2).
\end{aligned}
$$

So $c = c(0) = (-2, -2)$ as expected. We have already computed the equations for the two bisectors in Example 4.28.

4.5 The positive area cells for one cluster.

In this section we assume we have a set S of polynomial sites that all coincide in the origin at $t = 0$. We show that in general some sites can be omitted without changing

the shape of the Voronoi diagram of S. We characterize those sites that determine this shape and present an efficient algorithm to compute the shape of the Voronoi diagram.

4.5.1   The direction hull and positive area cells.

A **zero cluster** at $t = 0$ is a set $S(t)$ of polynomial sites in general position such that $p_i(0) = (0, 0)$ for every site $p_i(t)$ in $S(t)$. We want to know the shape of the Voronoi diagram of a zero cluster. For this purpose it is enough to determine the boundary of the Voronoi cells of positive area at $t = 0$.

Assume that $S(t)$ is a zero cluster at $t = 0$. Fix some site $v(t)$ in the combinatorial convex hull $cCH(S(t))$ at $t = 0$. There is one incoming edge and one outgoing edge in $cCH(S(t))$ at $v(t)$ at $t = 0$. Suppose the incoming edge comes from $u(t)$, while the outgoing edges goes to $w(t)$. Site $v(t)$ is called a **corner site** of $S(t)$ at $t = 0$ if the direction of the incoming edge is distinct from the direction of the outgoing edge, that is, if $\phi_{uv} \neq \phi_{vw}$. The corner sites of $S(t)$ at $t = 0$ are by definition the vertices of the **direction hull** $DH(S(t))$ at $t = 0$. Two vertices $u(t)$ and $v(t)$ are connected by a directed edge $\overrightarrow{uv}$ if there are no corner sites on the path from $u(t)$ to $v(t)$ in $cCH(S(t))$.

Example 4.32
Let $S(t) = \{q_1(t), \ldots, q_4(t)\}$ be as introduced in Example 4.13. From Example 4.18 we know that $cCH(S(t))$ equals 132. Compare Table 4.1. The directions $\phi_{13} = \arctan\frac{3}{2}$, $\phi_{32} = \pi - \arctan\frac{5}{2}$ and $\phi_{21} = -\arctan\frac{1}{2}$ are all distinct. It follows that $DH(S(t)) = cCH(S(t)) = 132$ at $t = 0$.

Example 4.33
Let $S(t) = \{q_1(t), q_2(t), q_3(t)\}$ with $q_1(t) = (-t, 0)$, $q_2(t) = (0, t^2)$, and $q_3(t) = (t, -t^2)$. Then $cCH(S(t)) = 123$, while $DH(S(t)) = 13$, as $\phi_{12} = \phi_{23} = 0$.

Lemma 4.34
Let $S(t) = \{p_1(t), \ldots, p_n(t)\}$ be a zero cluster at $t = 0$. Then any bisector $B(p_i, p_j)$ passes through $(0, 0)$ at $t = 0$.

Proof. The bisector $B(p_i, p_j)$ passes through the bisection point $b(p_i, p_j) = (0, 0)$ at $t = 0$. ∎

Lemma 4.35
Let $S(t) = \{p_1(t), \ldots, p_n(t)\}$ be a zero cluster at $t = 0$. Then $V(p_i(0))$ has positive area if and only if $p_i \in DH(S(0))$.

Proof. Assume that $p_i \in DH(S(0))$. As $p_i \in cCH(S(0))$, it follows that $p_i \in CH(S(t))$ for $t > 0$, small enough. That means that there exists t_0 such that for all $0 < t < t_0$ the Voronoi cell $V(p_i(t))$ is unbounded. Moreover, p_i is incident with two edges $e(p_{i-1}, p_i)$ and $e(p_i, p_{i+1})$, say, that are unbounded for all $0 < t < t_0$. But this

implies that these edges are unbounded at $t = 0$ as well. The sites p_{i-1} and p_{i+1} are the direct predecessor and direct successor of p_i on $cCH(S(0))$. As $p_i \in DH(S(0))$, the directions $\phi_{i-1;i}$ and $\phi_{i;i+1}$ are distinct at $t = 0$. But this implies that $V(p_i(0))$ has two unbounded edges of distinct direction on its boundary and by the convexity of $V(p_i(0))$ this implies that $V(p_i(0))$ has positive area.

For the other direction, assume that $V(p_i(0))$ has positive area at $t = 0$. It follows from Lemma 4.34 that $V(p_i(0))$ is unbounded, and therefore has two unbounded edges on its boundary of distinct direction. This implies that $p_i \in DH(S(t))$ at $t = 0$. ∎

The Voronoi diagram $V(S(0))$ of a zero cluster at $t = 0$ looks as follows:

1. If $p_i(t) \notin DH(S(t))$ at $t = 0$, then area$(V(S(t))) = 0$ by Lemma 4.35.
2. If $p_i(t) \in DH(S(t))$ and if $p_{i-1}(t)$ and $p_{i+1}(t)$ are its direct predecessor and its direct successor at $t = 0$ in $DH(S(t))$, then

$$V(p_i(0)) \quad = \quad vh_0(p_i, p_{i-1}) \cap vh_0(p_i, p_{i+1}).$$

Corollary 4.36
The shape of the Voronoi diagram $\delta V(S(0))$ of a zero cluster $S(t)$ equals the shape of the Voronoi diagram of $DH(S(0))$.

We conclude that for computing the shape of the Voronoi diagram $\delta V(S(0))$ of a zero cluster, it is enough to consider sites on the direction hull $DH(S(0)) \subset S(t)$ only.

4.5.2 Determining the direction hull at $t = 0$.

In Section 4.2 we have defined the combinatorial convex hull $cCH(S(t))$ of a set of polynomial sites by imitating the characterization of the ordinary convex hull as an intersection of half-planes. Exploiting this similarity we show how to compute $cCH(S(t))$ by an adapted version of the convex hull algorithm as presented in [BKOS], page 6.

The original algorithm is an incremental algorithm: first it sorts the n points in the input and next it handles the points one by one. The original algorithm sorts the input points lexicographically. This results in a sequence of points that is ordered from left to right and then from bottom to top. The algorithm determines the convex hull in two steps. In the first step the **upper hull** is determined. The upper hull is basically that part of the convex hull that is running from the leftmost point to the rightmost point of the sorted points. It constructs the upper hull by adding one point at a time and checking if the sequence of points that will be the upper hull in the end keeps going right. The lower hull is defined and constructed in a similar way.

Our ordering $O_<$ mimics the lexicographic ordering. Just think of substituting a very small positive value of t in the set of polynomial sites and sorting the resulting points lexicographically. An example is displayed in Figure 4.4 where the position of some polynomial sites at $t = 0.59$ is indicated by the labels of the sites. In a similar fashion we define right turns for polynomial sites: we say that three sites $u(t)$, $v(t)$, and $w(t)$ ordered by $O_<$ make a **right turn** at $t = 0$, if $w(t)$ is on the right of $l_{uv}(t)$ at $t = 0$.

Algorithm 4.37
Combinatorial convex hull for polynomial sites.

Input: set $S(t)$ of n polynomial sites in general position.
Output: list L containing the vertices of $cCH(S(0))$ in clockwise order.
  1: Sort the sites by $O_<$, resulting in a sequence $p_1(t), \ldots, p_n(t)$.
  2: Create list $L_{\text{upper}} = \{p_1, p_2\}$.
  3: **for** every $i \in \{3, \ldots, n\}$ **do**
  4:     Append p_i to L_{upper}.
  5:     **while** L_{upper} contains more than two sites **and** the last three sites in L_{upper} do not make a right turn, **do**
  6:         Delete the middle of the last three sites from L_{upper}.
  7: Construct L_{lower} in a similar way and append the result to L_{upper}. Call the resulting list L;.
  8: **return** L.

The running time of the algorithm is $O(n \log n)$, cf. [BKOS]. Let $S(t)$ be a zero cluster again. Given its combinatorial convex hull $cCH(S(t))$ at $t = 0$, we compute in $O(n)$ time the direction hull $DH(S(t))$ at $t = 0$.

Algorithm 4.38
Direction hull.

Input: combinatorial convex hull $cCH(S(0))$ of a zero cluster $S(t)$.
Output: direction hull $DH(S(t))$ at $t = 0$.
  1: Compute the direction ϕ_{uv} for every edge uv in $cCH(S(t))$ at $t = 0$.
  2: **if** two consecutive edges uv and vw have the same direction, that is, $\phi_{uv} = \phi_{vw}$, **then**
  3:     Delete w and its incident edges.
  4:     Create a new edge uw.

4.6   Degenerate Voronoi cells and edges.

Let $S(t)$ be a zero cluster at $t = 0$. We have seen before that only sites in the direction hull $DH(S(0))$ generate a Voronoi cell of positive area. It is possible however that for a site $p_i \in S(t) \setminus DH(S(0))$ there exists an edge $e(p_i, p_j)$ that does not collapse on $(0,0)$ at $t = 0$. In this section we consider sites $p_i(t) \in S(t)$ such that there exists,

at $t = 0$, an edge $e(p_i, p_j)$ with $x \in e(p_i, p_j)$, $x \neq (0,0)$. We first give an explicit example of an edge $e(p_i, p_j)$ where even $(0,0) \notin e(p_i, p_j)$, while $p_i \notin DH(S(0))$. Next we present an algorithm that determines all edges $e(p_i, p_j)$ that contain some $x \in \mathbb{R}^2$ with $x \neq (0,0)$ for a zero cluster $S(t)$ at $t = 0$.
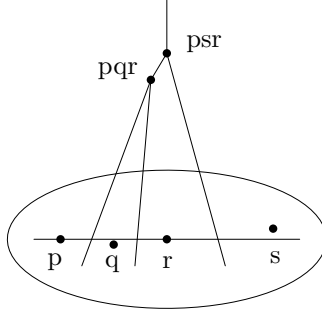

Figure 4.3: Edge of zero length outside $(0,0)$.

Example 4.39
Let $S(t) = (p(t), q(t), r(t), s(t))$, where $p(t) = (-2t, 0)$, $q(t) = (-t, -\frac{1}{4}t^2)$, $r(t) = (0,0)$, and $s(t) = (2t, 2t^2)$. The direction hull at $t = 0$ consists of the two sites $p(t)$ and $q(t)$, while $\phi_{pq} = 0$. Therefore the shape of the Voronoi diagram $\delta V(S(0))$ is just a vertical line through the origin. There are two Voronoi cells of positive area at $t = 0$: $V(p)$, whose cell is the left half-plane, and $V(s)$, whose cell is the right half-plane.

The type of $V(S(t))$ however is prq, psr. A schematic picture of the situation is given in Figure 4.3. From the type it follows that combinatorially, $V(S(t))$ consists of two vertices or circle centers, prq and psr that are connected by an edge $e(p, r)$. Besides, there are unbounded edges $e(p, q)$ an $e(q, r)$, incident to the circle center prq and edges $e(r, s)$ and $e(p, s)$, incident to psr. Both circle centers are situated at the point $(0, 2)$. This implies that the length of $e(p, r)$ at $t = 0$ equals zero, while the four other edges involved, have infinite length.

Let $S(t)$ be a zero cluster at $t = 0$. An edge $e(p_i, p_j)$ with $p_i, p_j \in S(t)$ is an **outside edge** at $t = 0$ if there exists $x \in e(p_i, p_j)$ such that $x \neq (0,0)$. Here we allow x to be any point of the form $x = (a, b)$, $x = (\pm\infty, b)$, $x = (a, \pm\infty)$ or $x = (\pm\infty, \pm\infty)$, where $a, b \in \mathbb{R}$. Allowing these possibilities is motivated by Example 4.8, which demonstrates that circle centers defined by polynomial sites can be at infinity.

Algorithm 4.40 determines all outside edges of a set of polynomial sites in general position at $t = 0$.

Algorithm 4.40
Determining outside edges and their positions.

Input: a zero cluster $S(t)$.
Output: all outside edges with their endpoints at $t = 0$.
  1: Determine the type T of $S(t)$ at $t = 0$.
  2: Any edge uv of multiplicity 1 in the abstract Delaunay graph $aD(S(0))$ corresponds to an unbounded edge $e(u, v)$ in the Voronoi diagram $V(S(t))$. This edge $e(u, v)$ starts at the circle center of the unique circle listed in T that has both u and v on its boundary. The direction of $e(u, v)$ is perpendicular to ϕ_{uv}. Edge $e(u, v)$ is oriented so that it makes an angle of $\frac{\pi}{2}$ with ϕ_{uv};
  3: Determine those circles in T that have positive radius;
  4: **for** a and b two labels occurring in some circle of positive radius **do**
  5:     (We show how to 'draw' the edge ab).
  6:     Check if we have not drawn ab before in step 2 as an unbounded edge.
  7:     **if** the combination of the labels a and b occurs twice in the list of the circles of positive radius **then**
  8:         there are two circle centers distinct from $(0, 0)$. We connect the two circle centers by an edge ab;
  9:     **else if** the combination of the labels occurs only once **then**
 10:         we connect the corresponding circle center c_{ab} to the origin.

Determining the shape of the Voronoi diagram is relatively easy, compare Section 4.5. We have seen in this section, however, that the combinatorial structure on the boundary itself can get rather complicated.

4.7   Example: 20 polynomial sites.

In this section we analyze a slightly bigger example, illustrating the techniques and theory developed in the former sections. We consider a set $S(t)$ of 20 polynomial sites. We determine the shape of the Voronoi diagram $V(S(t))$ at $t = 0$. Next we focus on the outside edges of $V(S(t))$ at $t = 0$. We visualize the polynomial sites and compare the outcome of the computation to the visualization. First we introduce the polynomial sites. $S(t)$ is a set of 20 distinct sites $(p_1(t), \ldots, p_{20}(t))$ such that $p_i(t) = (0, 0)$ for $i = 1, \ldots, 20$:

p_1	$(0, t^5)$,	p_{11}	$(-2t^2 - 2t^4, -3t + 2t^2 - t^3 + t^4)$,
p_2	$(0, 2t + t^4 + 2t^5)$,	p_{12}	$(-2t - t^4, 3t^2 + 3t^3 - t^5)$,
p_3	$(2t, 2t^3 + t^4)$,	p_{13}	$(-2t^2 - t^4, -2t^2 + 3t^3)$,
p_4	$(t^2, 2t + 2t^2 - t^3)$,	p_{14}	$(-t + 3t^2 - 2t^3 + 3t^4, t + 3t^2 - 3t^5)$,
p_5	$(-2t^4, -t^5)$,	p_{15}	$(-t - 2t^5, -3t^3 + 2t^5)$,
p_6	$(3t^5, t^2 + 2t^3 + 3t^5)$,	p_{16}	$(t^2 - 2t^3 + t^5, -t^4)$,
p_7	$(2t + 3t^2 - 2t^3, 2t - 2t^2 - t^3)$,	p_{17}	$(3t^3 + 2t^5, -t^4)$,
p_8	$(-2t - t^3, 2t)$,	p_{18}	$(3t^3 + 3t^4 + 2t^5, 2t - 2t^3 - t^4)$,
p_9	$(-2t + t^3, -2t - t^3)$,	p_{19}	$(t^2 + t^3 + 3t^5, 0)$,
p_{10}	$(t + 2t^2 + 2t^3, -t + 3t^3)$,	p_{20}	$(3t^2 + 2t^3 + 3t^5, t^2 + 3t^3 + 2t^4)$.

We visualize $S(t)$ by considering any $p_i(t) \in S(t)$ as a plane curve, represented by a parametrization $(p_{i,x}(t), p_{i,y}(t))$. In Figure 4.4 these twenty curves are plotted for $t \in [0, 1]$. The position of a curve at $t = 0.59$ is marked by its label.
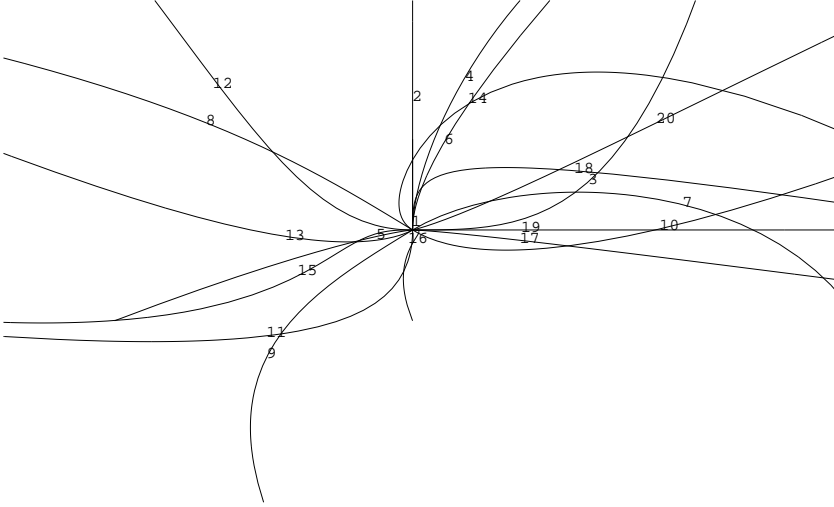

Figure 4.4: The polynomial sites for $t \in [0, 1]$.

4.7.1   The positive area diagram.

Recall that the type of $S(t)$ is defined a the set of all Voronoi circles at $t = 0$. We have computed it using brute force. That is, for every $\binom{n}{3}$ unordered triples of polynomial sites $p_i(t)$, $p_j(t)$ and $p_k(t)$ we first determine the orientation at $t = 0$ of the circle C passing though $p_i(t)$, $p_j(t)$ and $p_k(t)$. Next we check if any of the $n - 3$ remaining sites of $S(t)$ is contained in C. If not, we conclude that C is a Voronoi circle and add the labels i, j and k ordered with respect to the orientation of C to the type in the making. It turns out that the type of $S(t)$ is given by:

((1, 5, 6), (1, 17, 5), (1, 6, 17), (2, 8, 4), (2, 4, 18), (2, 14, 8), (2, 18, 14), (3, 20, 7), (3, 11, 10), (3, 10, 20), (4, 7, 18), (5, 13, 6), (5, 17, 13), (6, 13, 15), (6, 15, 14), (6, 14, 20), (6, 16, 17), (6, 19, 16), (6, 20, 19), (7, 20, 18), (8, 12, 9), (8, 14, 12), (9, 13, 11), (9, 12, 15), (9, 15, 13), (10, 11, 13), (10, 13, 20), (12, 14, 15), (13, 17, 16), (13, 16, 19), (13, 19, 20), (14, 18, 20)).

Counting multiplicities of the edges shows that all edges have multiplicity 2 except for the edges

$$(4, 8), (3, 7), (3, 11), (4, 7), (8, 9), (9, 11).$$

As site p_7 is on the right of $l_{4,8}$ at $t = 0$ the combinatorial convex hull $cCH(S(0))$ is given by $(8, 4, 7, 3, 11, 9)$. The directions of the edges of $cCH(S(0))$ are $\phi_{8;4} = 0$, $\phi_{4;7} = 0$, $\phi_{7;3} = -\frac{\pi}{2}$, $\phi_{3;11} = -\arctan(\frac{2}{3}) - \frac{\pi}{2}$, $\phi_{11;9} = \frac{\pi}{2} + \arctan 2$, and $\phi_{9;8} = \frac{\pi}{2}$. The directions $\phi_{8;4}$ and $\phi_{4;7}$ are equal, so site p_4 is not a corner site. We conclude that the direction hull $DH(S(0))$ is given by $(8, 7, 3, 11, 9)$. This outcome can almost be 'guessed' from Figure 4.4 by considering the convex hull of the points $p_1(t)$ to $p_{20}(t)$ for small t. Knowing the direction hull and the directions of the edges of the direction hull, we know in fact the shape of the Voronoi diagram $\delta V(S(0))$. It is depicted on the left in Figure 4.5.

4.7.2 Combinatorics of the edges outside $(0, 0)$.

The only Voronoi circle that has a circle center outside of $(0, 0)$ at $t = 0$ is the clockwise oriented circle $(8, 12, 9)$. Its center is at infinity. This means that the unbounded edge $e(8, 9)$ starts at the Voronoi vertex at infinity, while two edges $e(8, 12)$ and $e(9, 12)$ run between vertices situated in $(0, 0)$ and this vertex at infinity. We have seen before that $p_4 \in cCH(S(0))$ with p_8 its direct predecessor and p_7 its direct successor in $cCH(S(0))$. As there are no further circle centers situated outside the origin, there are two unbounded edges $e(4, 8)$ and $e(4, 7)$ that, starting in $(0, 0)$, both run upwards, but never meet. A schematic picture of the combinatorics of the edges outside $(0, 0)$ is given on the right in Figure 4.5.
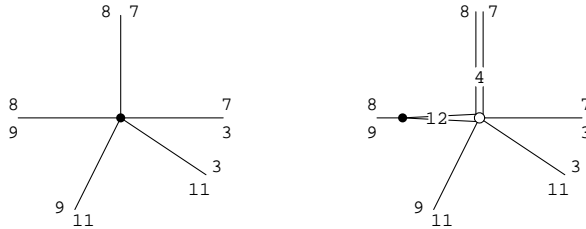
Figure 4.5: The positive area diagram at $t = 0$ on the left. The combinatorics outside $(0, 0)$ included on the right.

4.8 The shape of a Voronoi diagram at $t = 0$.

In Section 4.5 we have given a method that determines the shape of the Voronoi diagram of a zero cluster at $t = 0$. That is, we assumed that all sites coincide in the origin at $t = 0$. In this section we apply this method in order to determine the shape of a Voronoi diagram at $t = 0$ for an arbitrary set of polynomial sites in general position.

Let $S(t)$ be a set of polynomial sites of size n that is in general position at $t = 0$. The **cluster locations** $l(0) = \{l_1(0), \ldots, l_m(0)\}$ of $S(t)$ at $t = 0$ are the distinct positions of the sites in $S(t)$ at $t = 0$. An **l_j-cluster**, for $l_j \in \mathbb{R}^2$ is a collection of polynomial sites that coincides at l_j at $t = 0$. Write $S(t) = \cup_{j=1}^m S_j(t)$, where $S_j(t) \subset S(t)$ is the set of sites in $S(t)$ such that $p_{j_i}(0) = l_j(0)$ for all $p_{j_i} \in S_j(t)$. That is, we divide $S(t)$ with respect to the l_j-clusters at $t = 0$.

Lemma 4.41
The shape of the Voronoi diagram $\delta V(S(t))$ at $t = 0$ of $S(t)$ is given by

$$\delta V(S(0)) \quad = \quad \bigcup_{j=1,\ldots,m} \left(V(l_j(0)) \cap \delta V(S_j(0)) \right).$$

Proof. First of all, suppose that $|S_j(0)| = 1$, for all $j = 1, \ldots, m$. In this case the lemma just states that the Voronoi diagram of distinct points coincides with the subdivision of the plane into Voronoi cells, see Section 2.2. Next consider an arbitrary point x in the interior of, say, $V(l_j)(0)$. Then x is, by definition, closer to l_j than to any other location l_k for $k \neq j$. The lemma follows from Corollary 4.36 adapted for an l_j-cluster $S_j(t)$. $\blacksquare$
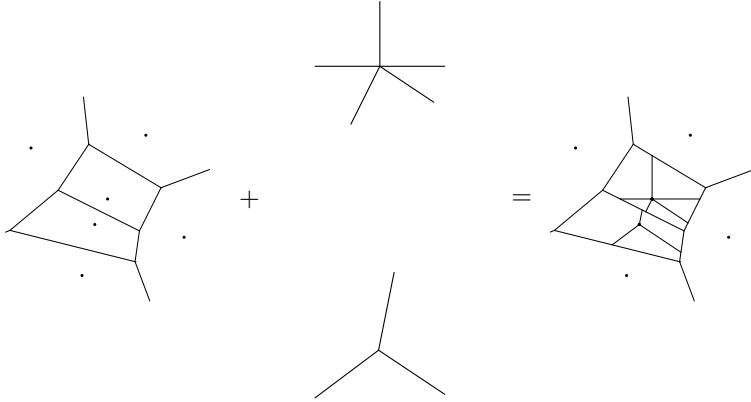

Figure 4.6: Plugging diagrams.

Example 4.42
Suppose we are given the following sites:

$$S(t) \quad = \quad ((-6, 4), (-2, -6), (-1, -2 - 3t), (0, -3t), (3, 5), (6, -3),$$
$$(-1 - 3t, -2 + t), (-2t, -2t), (-2t, 2t), (2t, 0), (2t, 2t), (-1 + 2t, -2)).$$

The cluster locations at $t = 0$ are given by

$$l(0) \quad = \quad ((-6, 4), (-2, -6), (-1, -2), (0, 0), (3, 5), (6, -3)).$$

The Voronoi diagram $V(l(0))$ of the cluster locations is presented on the left in Figure 4.6. There are two clusters consisting of more than one point. The shape of the Voronoi diagram of the zero cluster, given by

$$S_1(t) \quad = \quad ((0, -3t), (-2t, -2t), (-2t, 2t), (2t, 0), (2t, 2t)),$$

is presented in the top middle of Figure 4.6, while the shape of the Voronoi diagram of the $(-1, -2)$-cluster

$$S_2(t) \quad = \quad ((-1, -2 - 3t), (-1 - 3t, -2 + t), (-1 + 2t, -2)),$$

is shown in the bottom middle. According to Lemma 4.41, we can plug these two cluster diagrams in the cluster locations diagram in order to get the shape of the Voronoi diagram of $S(t)$ at $t = 0$. This final diagram is depicted on the right in Figure 4.6.

4.9   Generalizations and conclusion.

4.9.1   Dropping general position.

Throughout this chapter we have assumed that sets of polynomial sites are in general position. General position is not needed for the methods presented to work. Dropping general position just means that a lot of extra cases have to be checked, which distracts from the main line. Note that the notion of type as introduced in Section 2.3 is defined for point sets that are not in general position as well. As we can also compute convex hulls for point sets that are not in general position, there are no big obstructions for extending the methods to sets of polynomial sites in arbitrary position.

Recall from Section 4.2 that general position for polynomial sites is defined in terms of cocircularity and collinearity polynomials: if some set $S(t)$ is not in general position at $t = 0$, then there is at least one cocircularity polynomial $I(t)$ or collinearity polynomial $D(t)$ that is equal to the null polynomial. This implies that $S(t)$ is not in general position for any value of t.

4.9.2   Generalization to higher order Voronoi diagrams.

In the k-th order Voronoi diagram, the plane is partitioned according to the k closest sites, see Chapter 3. Algorithm 3.5 computes the k-th order Voronoi diagram of a set S of distinct points in general position, using

- circles through three points of S,

- points from S inside these circles,

- directions of lines between points of S.

We have shown in this chapter that these concepts can be generalized to sets $S(t)$ of polynomial sites. Therefore, Algorithm 3.5 can also be generalized to sets of polynomial sites in general position. This will give us a combinatorial k-th order Voronoi diagram.
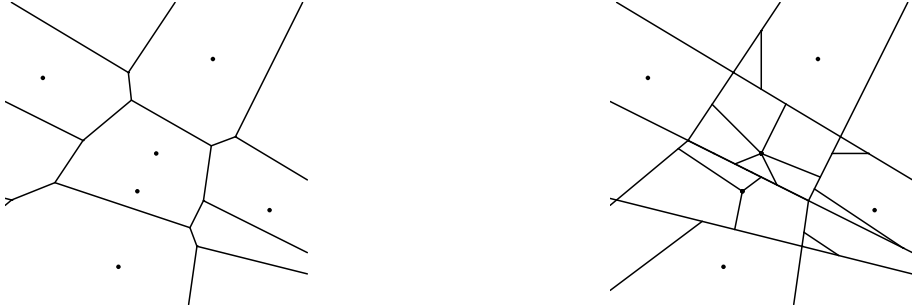

Figure 4.7: No plugging of second order diagrams.

It is also clear that we cannot directly generalize Lemma 4.41 for obtaining the shape of a k-th order Voronoi diagrams. That is because the two steps approach, dealing with cluster locations and clusters apart, is not allowed anymore for $k > 1$.

Example 4.43
Let $S(t)$ be as in Example 4.7. In Figure 4.7 we show on the left the second order Voronoi diagrams of the cluster locations $l(0)$ that we have found in Example 4.42. On the right, the second order Voronoi diagram for $S(t)$, with $t = 0.001$ is shown.

4.9.3 Polynomial arithmetic.

So far, we did not pay any attention to how to compute efficiently with polynomial sites: higher order terms can often be skipped without changing the type or the position of the Voronoi vertices and edges. But at this point we have no rule available that tells us on forehand when it is allowed to skip higher order terms.

Example 4.44
Let $S(t)$ be as introduced in Example 4.13. Suppose that we change q_4 in Examples 4.13 and 4.24 from $q_4 = (t^2 - 2t^3 + t^5, -t^4)$ into $q_4 = (t^2, -t^4)$. Then the type of $S(t)$ at $t = 0$ and the shape of the Voronoi diagram of $S(t)$ at $t = 0$ remains the same.

This is one reason for considering certain properties of sites or point sets, rather than the sites themselves. We will do so in the following chapters.

4.9.4   Conclusion

The polynomial sites model enables us to introduce limit pictures of Voronoi diagrams by means of the shape of a Voronoi diagram. Moreover, we have seen that this model can be used to extend the notion of 'type' to sets of points that sometimes coincide. The type gives us the complete combinatorics of a limit situation.

The methods presented in this chapter however do only visualize the shapes of those cells that have positive area at $t = 0$. This demonstrates that not all cells in the limit Voronoi diagram at $t = 0$ are treated in an equal way. The ingredient that is missing is the relation between shape and scale. Informally, think of dividing the polynomials defining the polynomial sites by powers of t until Voronoi cells that had zero area at $t = 0$ before dividing get positive area. That is, we want to zoom in at a cluster in order to find out the shape of a Voronoi cell of some arbitrary site $p_i(t)$. In order to solve this problem we will define *clickable* Voronoi diagrams in a following chapter. We do so by exploiting properties of point sets, like angles between two points or hooks between three points.

Chapter 5

Voronoi diagrams and angle compactifications.

Given a configuration c of n distinct points, one can determine the set a_n of angles of lines through any two points in c. We distinguish a_n, the set of angles up to 2π, and $\overline{a_n}$, the angles up to π. We analyze in both cases what sets of angles are possible. We show in which cases it is possible to reconstruct the Voronoi diagram $V(c)$, knowing the angles only. We compactify the configuration space of distinct points by taking the closure of the graph of the map that associates the angles to a configuration. We present a variety T_n as an algebraic alternative. We analyze the connection between boundary points of the compactification and singularities of T_n for small n and give geometric interpretations.

5.1 CDA_n: space of angles on n points.

In this section we introduce several spaces that will be important to us later on. We recall the notion of configuration space of n distinct labeled points in the plane. Both an introduction on and applications (in robotics!) of configuration spaces can be found in [AG]. Next we define two spaces by considering, for n distinct points in the plane, all angles between pairs of points. Here we distinguish angles mod π and angles mod 2π.

5.1.1 The angle of two points.

Given two distinct points p_i and p_j, we determine the angle that the line that passes through p_i and p_j makes with the positive x-axis. We distinguish the directed and undirected line.

Definition 5.1
See also Figure 5.1.
(i)   For any two distinct points p_i and p_j in the plane define the **directed angle**
$\alpha_{ij} \in \mathbb{R}/2\pi\mathbb{Z}$ as the argument of the point

$$(\cos\alpha_{ij}, \sin\alpha_{ij}) \quad = \quad (\frac{d_x}{\|d_x\|}, \frac{d_y}{\|d_y\|}),$$

where $d = (d_x, d_y) := p_j - p_i$. Note that α_{ij} is determined up to multiples of 2π.
(ii)   The **undirected angle** *$\overline{\alpha_{ij}}$ is defined as $\overline{\alpha_{ij}} = \overline{\alpha_{ji}} = \alpha_{ij} \mod \pi$. We often choose $\overline{\alpha_{ij}} \in (-\frac{\pi}{2}, \frac{\pi}{2}]$.*
(iii)   If $(p_j - p_i)_x \neq 0$, then the **slope** *a_{ij} is defined as $a_{ij} = \frac{(p_j - p_i)_y}{(p_j - p_i)_x}$. If $(p_j - p_i)_x = 0$, then $a_{ij} = \infty$. It holds that $a_{ij} \in (-\infty, \infty]$.*
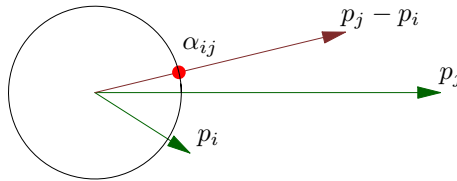

Figure 5.1: The directed angle α_{ij} between two points p_i and p_j.

Example 5.2
Let $p_i = (1,1)$ and $p_j = (-1,0)$. Then $d = p_j - p_i = (-2,-1)$, so $\frac{d_y}{d_x} = \frac{1}{2}$, but the angle $\alpha_{ij} = \arctan(\frac{1}{2}) + \pi$ as $d_x < 0$.

Remark 5.3
If $(p_j - p_i)_x \neq 0$, then $a_{ij} = \tan\overline{\alpha_{ij}}$ and $\overline{\alpha_{ij}} = \arctan a_{ij}$.

5.1.2   Configuration spaces of n distinct points.

Definition 5.4
The **configuration space** *$CONF_n(\mathbb{R}^2)$ of n points in $\mathbb{R}^2$ is the set*

$$CONF_n(\mathbb{R}^2) \quad := \quad \{(p_1, \ldots, p_n) \in (\mathbb{R}^2)^n \mid p_i \neq p_j \text{ if } i \neq j\}.$$

Two elements $p, q \in CONF_n(\mathbb{R}^2)$ are $\sim_{\{s,t\}}$-equivalent if they only differ by a scaling, s, combined with a translation, t. The **reduced configuration space** *is the quotient space* **conf**$_n = CONF_n/\sim_{\{s,t\}}$.

conf$_n$ is a smooth manifold. We determine its dimension. A **standard representative** for a class in **conf**$_n$ is constructed as follows. Translate the configuration in such a way that $p_1 = (0,0)$. Scale the configuration in such a way that p_2 is at

distance one from p_1. This shows that we need three parameters less than $2n$ to describe an element in **conf**$_n$.

Property 5.5
$dimension(\mathbf{conf}_n) = 2n - 3$.

Remark 5.6
Note that **conf**$_n$ is not compact: take $n = 3$, then the ratio $\frac{|p_3 - p_1|}{|p_2 - p_1|}$ is continuous but not bounded.

Remark 5.7
Let $\hat{c} = \{\hat{p}_1, \ldots, \hat{p}_n\}$ be the standard representative of a class $[c]$ in **conf**$_n$ and let $c = \{p_1, \ldots, p_n\}$ be an arbitrary element of $[c]$. Then $p_i =| p_2 - p_1 | \hat{p}_i + p_1$. If we write $T_{\mathbf{conf}_n}$ for the set of standard representatives of classes in **conf**$_n$, then $CONF_n = \{\hat{c}\mathbb{R}_{>0} + \mathbb{R}^2 \mid \hat{c} \in T_{\mathbf{conf}_n}\}$.

5.1.3 Compactification of the graph of the angle map.

For an element $c \in CONF_n$, write down for every pair of points $p_i, p_j \in c$, with $i \neq j$, the angle $\alpha_{ij} \in \mathbb{R}/2\pi Z$ or $\overline{\alpha}_{ij} \in \mathbb{R}/\pi\mathbb{Z}$. This gives $\binom{n}{2}$ angles, one for every unordered pair of labels i and j.

Definition 5.8
$DA_n := (\mathbb{R}/2\pi\mathbb{Z})^{\binom{n}{2}}$ is the space of directed angles; $UA_n := (\mathbb{R}/\pi\mathbb{Z})^{\binom{n}{2}}$ the space of undirected angles. The directed **angle map** *ψ_{DA_n} is the map*

$$\psi_{DA_n} : \quad \begin{array}{ccc} CONF_n & \to & DA_n, \\ (p_1, \ldots, p_n) & \mapsto & (\alpha_{ij})\ _{1 \leq i < j \leq n}. \end{array}$$

The undirected angle map ψ_{UA_n} is defined in a similar way.

Remark 5.9
As a direct product of circles DA_n and UA_n are smooth.

Remark 5.10
ψ_{DA_n} and ψ_{UA_n} are well-defined on **conf**$_n$: both mapping are constant on classes of **conf**$_n$.

Definition 5.11
The **graph** *of ψ_{DA_n} is the set $\{(c, \psi_{DA_n}(c)) \in (\mathbb{R}^2)^n \times DA_n \mid c \in CONF_n\}$. The* **compactification** *CDA_n of the graph of the angle map, is the closure of $graph(\psi_{DA_n})$ in $(\mathbb{R}^2)^n \times DA_n$. The compactification CUA_n is defined in a similar way.*

Remark 5.12
CDA_n is in fact not a compactification as it is not compact: $CONF_n$ is not bounded, compare Remark 5.6. The projection map from CDA_n to $(\mathbb{R}^2)^n$ is proper however.

Recall that a map is **proper** if it is continuous and if the preimage of every compact set is compact again.

5.2   From angles back to point configurations.

In this section we consider the mappings $\psi_{\mathrm{DA}_n} : \mathbf{conf}_n \to DA_n$ and $\psi_{\mathrm{UA}_n} : \mathbf{conf}_n \to UA_n$. We describe the fibers of both mappings by showing which configurations c can be reconstructed from knowing the angles $\psi_{\mathrm{DA}_n}(c)$ or $\psi_{\mathrm{UA}_n}(c)$ only.

5.2.1   Distinct points and angles in $\mathbb{R}/2\pi\mathbb{Z}$.

A configuration $c \in CONF_n$ is called **collinear** iff all points in c are collinear. A class of configurations $[c] \in \mathbf{conf}_n$ is collinear if the class elements are collinear. Define $CLCONF_n := \{c \in CONF_n \mid c \text{ collinear}\}$, and similarly $\mathbf{clconf}_n$.

Lemma 5.13
The map $\psi_{DA_n} : \mathbf{conf}_n \backslash \mathbf{clconf}_n \to DA_n$ is injective.

Proof. We have to show that for $[c], [d] \in \mathbf{conf}_n \backslash \mathbf{clconf}_n$ with $[c] \neq [d]$ it holds that $\psi_{\mathrm{DA}_n}([c]) \neq \psi_{\mathrm{DA}_n}([d])$. Let c and d be the standard representative of $[c]$, resp. $[d]$. If $[c] \neq [d]$ then also $c \neq d$. Let $p_i(c)$ be the i-th point of the configuration c and let $\alpha_{ij}(c) \in \mathbb{R}/2\pi\mathbb{Z}$ be the angle between $p_i(c)$ and $p_j(c)$. Note that for standard representatives $p_1(c) = p_1(d) = (0,0)$. We show that in any case there exists some labels u and v such that $\alpha_{uv}(c) \neq \alpha_{uv}(d)$.

Let $i \in \{2, \ldots, n\}$ be minimal such that $p_i(c) \neq p_i(d)$. If $i = 2$, then $p_2(c) \neq p_2(d)$, therefore $\alpha_{12}(c) \neq \alpha_{12}(d)$. Assume that $i > 2$. In this case $p_2(c) = p_2(d) = (\cos \alpha_{12}, \sin \alpha_{12})$ for some $\alpha_{12} \in (-\pi, \pi]$. Let m be the line through p_1 and $p_i(c)$. If $p_i(d) \notin m$, then $\alpha_{1i}(c) \neq \alpha_{1i}(d)$. Assume that $p_i(d) \in m$. If $p_2 \notin m$, then $\alpha_{2i}(c) \neq \alpha_{2i}(d)$.

We are left with the case that $p_1, p_2, p_i(c)$ and $p_i(d)$ are all collinear on line m. As $c, d \notin CLCONF_n$, there exists j such that $p_j(c) \notin m$. If $p_j(d) = p_j(c)$ then $\alpha_{ji}(c) \neq \alpha_{ji}(d)$. Let l be the line through p_1 and $p_j(c)$. If $p_j(d) \in l$, then $\alpha_{2j}(c) \neq \alpha_{2j}(d)$. Finally, if $p_j(d) \notin l$, then $\alpha_{1j}(c) \neq \alpha_{1j}(d)$. ∎

Remark 5.14
Suppose we are given an image point $a = \psi_{\mathrm{DA}_n}([c])$ for some $[c] \in \mathbf{conf}_n \backslash \mathbf{clconf}_n$. We construct the standard representative from the angles in a as follows. Put $p_1 = (0,0)$ and $p_2 = (\cos \alpha_{12}, \sin \alpha_{12})$. A point p_i is on the line l_{12} through p_1 and p_2 if and only if

$$\overline{\alpha_{12}} = \overline{\alpha_{1i}} = \overline{\alpha_{2i}} \quad \mathrm{mod} \ \pi. \tag{5.1}$$

As $[c] \in \mathbf{conf}_n \backslash \mathbf{clconf}_n$, we know that there exists p_i that is not on the line l_{12}. We find it by checking Equation 5.1. We construct p_i as the intersection of the lines

l_{1i} and l_{2i}. Here l_{1i} is the line that passes through p_1 and has direction α_{1i} and l_{2i} is the line that passes through p_2 with direction α_{2i}. Any other point p_j of the standard representative is constructed in a similar way: there is always a pair of vertices from the non-degenerated triangle $p_1 p_2 p_i$ such that the line through these two vertices does not contain p_j.

Let $c \in CLCONF_n$. Then all points $p_1, \ldots, p_n$ from c are on a common line l_c that makes some undirected angle $\overline{\alpha_c} \in (-\frac{\pi}{2}, \frac{\pi}{2}]$ with the positive x-axis. Order the labels of the points according to the order of the points on l_c as encountered from left to right, or from bottom to top, in case $\overline{\alpha_c} = \frac{\pi}{2}$. This defines an ordered n-tuple $\sigma(c)$. The n-tuple $\sigma([c])$ is defined as $\sigma(c)$, for some representative $c \in [c]$. Define an equivalence class $\sim_{\alpha,\sigma}$ on $\mathbf{clconf}_n$ as follows: $[c] \sim_{\alpha,\sigma} [d]$ if and only if both $\overline{\alpha_{[c]}} = \overline{\alpha_{[d]}}$, and $\sigma([c]) = \sigma([d])$.

Lemma 5.15
Consider $\psi_{DA_n} : CLCONF_n \to DA_n$.
  (i) *ψ_{DA_n} is constant on classes of $\sim_{\alpha,\sigma}$.*
  (ii) *The map $\psi_{DA_n} : \mathbf{clconf}_n / \sim_{\alpha,\sigma} \to DA_n$ is injective*

Proof. We prove the two claims.
  (i) Let $[c], [d] \in \mathbf{clconf}_n$ such that $[c] \sim_{\alpha,\sigma} [d]$. Let $p_i(c), p_i(d)$ and $p_j(c), p_j(d)$ denote the i-th and j-th points of some representatives c and d of the classes $[c]$ and $[d]$. Then $\overline{\alpha_{ij}(c)} = \overline{\alpha_{ij}(d)}$, as all four points are collinear. Moreover, $p_j(c)$ is on the right of $p_i(c)$ whenever $p_j(d)$ on the right of $p_i(d)$, as $\sigma(c) = \sigma(d)$. So, $\alpha_{ij}(c) = \alpha_{ij}(d)$.
  (ii) Suppose that $[c] \not\sim_{\alpha,\sigma} [d]$. Let $p_i(c), p_i(d), p_j(c)$ and $p_j(d)$ be as above. If $\overline{\alpha_c} \neq \overline{\alpha_d}$, then clearly $\psi_{DA_n}([c]) \neq \psi_{DA_n}([d])$. Assume $\overline{\alpha_c} = \overline{\alpha_d}$. Then $\sigma(c) \neq \sigma(d)$. Let i be minimal such that $k := \sigma(c)_i \neq \sigma(d)_i =: l$ Then $\alpha_{kl}(c) = \alpha_{kl}(d) + \pi$. Therefore $\psi_{DA_n}([c]) \neq \psi_{DA_n}([d])$. ∎

We use Lemma 5.13 and Lemma 5.15 to answer the following question. Is it possible, given some $a = \psi_{DA_n}(c)$, with $c \in CONF_n$, to determine the Voronoi diagram $V(c)$? Let the **reduced Voronoi diagram**, notation $\tilde{V}(c)$, of a point $c \in CONF_n$ be the Voronoi diagram $V(c)$ up to scaling and translation. A reduced configuration of points $[c]$ or a reduced Voronoi diagram $\tilde{V}(c)$ is **reconstructible** from a list of angles a iff $[c]$ resp. $\tilde{V}(c)$ is uniquely determined by a.

Property 5.16
$\tilde{V}(c)$ is independent of the choice of $c \in [c]$.

Notation: By $\tilde{V}([c])$, for $[c] \in \mathbf{conf}_n$, the reduced Voronoi diagram of some representative $c \in [c]$ is indicated. Note that if one can reconstruct the class $[c] \in \mathbf{conf}_n$ from $\psi_{DA_n}(c)$, for $c \in CONF_n$, then one can also construct the reduced Voronoi diagram $\tilde{V}([c])$.

Corollary 5.17
Let $a = \psi_{DA_n}([c])$, with $[c] \in \mathbf{conf}_n$.
   (i)   If $[c] \in \mathbf{conf}_n \setminus \mathbf{clconf}_n$, then $[c]$ is reconstructible.
   (ii) If $[c] \in \mathbf{clconf}_n$, then $[c]$ is not reconstructible, except for $n = 2$.

Proof. The first claim follows from Lemma 5.13 and Remark 5.14. The preimage $\psi_{\mathrm{DA}_n}^{-1}([c])$ consists of distinct classes of $\mathbf{conf}_n$, except for $n = 2$, consult Lemma 5.15. This proves the second claim.   ∎

Corollary 5.18
$\tilde{V}([c])$ is reconstructible if and only if either $[c] \in \mathbf{conf}_n \setminus \mathbf{clconf}_n$, or $[c] \in \mathbf{clconf}_n$ and $n = 2$ or $n = 3$.

Proof. From Corollary 5.17 it follows that $[c]$ is reconstructible in the cases mentioned except for $[c] \in \mathbf{clconf}_n$ in case $n = 3$. But in this case, $\tilde{V}([c])$ consists just of two parallel bisectors perpendicular to $\overline{\alpha_c}$. From $a_3 = \psi_{\mathrm{DA}_n}([c])$ we can determine the order of the three points on the line, which gives us the labels of the bisector. Changing the relative positions of the three points in $[c]$ has no influence on $\tilde{V}(c)$ as long as the order of the points is maintained. Suppose, on the other hand that $[c] \in \mathbf{clconf}_n$ for $n > 3$. It is easy to show that in this case mutually distinct classes of configurations in the fiber $\psi_{\mathrm{DA}_n}^{-1}([c])$ correspond with mutually distinct reduced Voronoi diagrams.   ∎

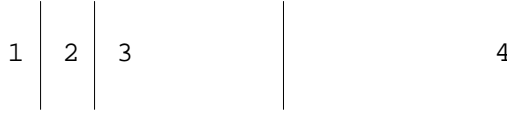$$1 \mid 2 \mid 3 \qquad\qquad\mid \qquad\qquad 4$$

Figure 5.2: The Voronoi diagram of four collinear points.

Example 5.19
Consider the element $d \in DA_4$ defined by $\alpha_{12} = \alpha_{13} = \alpha_{14} = \alpha_{23} = \alpha_{24} = 0$. Suppose that we try to construct a configuration S of labeled points having those angles. It is clear that any such configuration consists of four points on a common horizontal line. An example is given in Figure 5.2. Moreover, it is possible to reconstruct the order of the points on the line: from left to right we encounter the points p_1, p_2, p_3 and p_4 in that particular order. This shows however that from the information present in d we cannot determine the ratio $|p_1 p_2|/|p_1 p_3|$ of the lengths of the line segments $p_1 p_2$ and $p_1 p_3$: whatever this ratio is, the angles α_{12}, α_{13} and α_{23} do not change. The Voronoi diagram of p_1 to p_4 consists of the three vertical bisectors $B(p_1, p_2)$, $B(p_1, p_3)$ and $B(p_2, p_3)$. Again it is impossible to determine the ratio $|B(p_1, p_2) - B(p_2, p_3)|/|B(p_2, p_3) - B(p_3, p_4)|$ of the distances between the bisectors. This shows that it is impossible to associate a unique reduced Voronoi diagram to $d \in DA_4$.

5.2.2 Distinct points and angles in $\mathbb{R}/\pi\mathbb{Z}$.

Suppose we start with some $c \in CONF_n$. Assume we have determined $\overline{a} = \psi_{\mathrm{UA}_n}(c)$, that is, the set of all angles $\overline{\alpha_{ij}}$ mod π between pairs of points $(p_i, p_j) \in c$. We introduce another equivalence class on $\mathbf{conf}_n$. Let $[c], [d]$ in $\mathbf{conf}_n$. The classes $[c]$ and $[d]$ are **reflection equivalent**, notation $[c] \sim_R [d]$ if and only if the standard representative c of $[c]$ equals the standard representative d of $[d]$ up to a reflection in $p_1(c) = p_1(d) = (0, 0)$.

Lemma 5.20
The map $\psi_{UA_n} : (\mathbf{conf}_n \setminus \mathbf{clconf}_n)/\sim_R \to UA_n$ is injective

Proof. Proceed as in the proof of Lemma 5.13, but take those standard representatives that have $\alpha(c), \alpha(d) \in (-\frac{\pi}{2}, \frac{\pi}{2}]$. It is possible to put mod π bars on all α_{ij}'s that occur in the proof. ∎

If we take angles between points in $\mathbb{R}/\pi\mathbb{Z}$, all collinear configurations that have their points on a line with angle $\overline{\alpha} \in (-\frac{\pi}{2}, \frac{\pi}{2}]$ are mapped to the same $\overline{a} = (\overline{\alpha}, \ldots, \overline{\alpha})$ in UA_n. So it is impossible to reconstruct the original order of the points on the line.

Corollary 5.21
Let $\overline{a} = \psi_{UA_n}([c])$, for $[c] \in \mathbf{conf}_n$.
 (i) If $[c] \in \mathbf{conf}_n \setminus \mathbf{clconf}_n$, then $[c]$ is reconstructible up to a point reflection.
 (ii) If $[c] \in \mathbf{clconf}_n$ and $n = 2$, then $[c]$ is reconstructible up to a point reflection.
 (iii) If $[c] \in \mathbf{clconf}_n$ and $n = 3$, then $[c]$ is not reconstructible but the reduced Voronoi diagram $\tilde{V}([c])$ is reconstructible
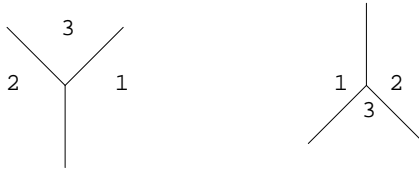 *(iv) If $[c] \in \mathbf{clconf}_n$ and $n > 3$, then $\tilde{V}([c])$ is not reconstructible.*

Figure 5.3: $V(c)$ reconstructed from angles mod π.

Example 5.22
Let $c = \{p_1, p_2, p_3\}$, with $p_1 = (2, 0)$, $p_2 = (0, 0)$ and $p_3 = (1, 1)$. The Voronoi diagram $V(c)$ is shown on the left in Figure 5.3. Then $\alpha_{12} = \pi$, $\alpha_{13} = \frac{3\pi}{4}$ and $\alpha_{23} = \frac{\pi}{4}$. So $\overline{\alpha_{12}} = 0$, while $\overline{\alpha_{13}} = \alpha_{13}$ and $\overline{\alpha_{23}} = \alpha_{23}$. We get a 'reconstructed' configuration c' consisting of $p_1' = (0, 0)$, $p_2' = (1, 0)$ and $p_3' = (-\frac{1}{2}, -\frac{1}{2})$. This configuration c' together with its Voronoi diagram $V(c')$ is shown on the right in Figure 5.3.

5.3   Angle models for small n.

In this section, we analyze the compactifications CDA_n and CUA_n for $n = 2$. Moreover, we give a complete description of the image $\psi_{DA_3}(CONF_3)$. For points on the boundary of $\psi_{DA_3}(CONF_3)$, we give a geometric interpretation in terms of coinciding points.

Remark 5.23
D. G. Kendal has introduced the 'The theory of shape' in a statistical context. As a specific example, the shapes of triangles are analyzed. To compare with this result, consult [Ke1] and [Ke2].

5.3.1   n=2.

In the directed case, we have the following diagram:

$$
\begin{array}{ccc}
CONF_2 & \subset & \mathbb{R}^2 \times \mathbb{R}^2 \\
\cap & & \cap \\
\mathrm{graph}(\psi_{DA_2}) \quad \subset \quad CDA_2 & \subset & \mathbb{R}^2 \times \mathbb{R}^2 \times \mathbb{R}/2\pi\mathbb{Z}.
\end{array}
$$

ψ_{DA_2} maps a configuration $c = (p_1, p_2) \in CONF_n$ to the directed angle α_{12}. For simplicity we assume that $p_1 = (0,0)$. As $c \in CONF_2$, this implies that $p_2 \in \mathbb{R}^2 \setminus \{(0,0)\}$. This space $\mathbb{R}^2 \setminus \{(0,0)\}$ is homeomorphic to a doubly open cylinder: imagine the omitted point $(0,0)$ as one side of the cylinder and infinity as the other side.

A classic construction is the following: The **blow-up** of $\mathbb{R}^2$ at $(0,0)$ is by definition the closed subset $X \subset \mathbb{R}^2 \times \mathbb{P}^1$ of all points $(x_1, x_2, y_1, y_2) \in \mathbb{R}^2 \times \mathbb{P}^1$ such that $x_1 y_2 = x_2 y_1$. The projection $\pi : X \to \mathbb{R}^2$ onto the first factor has the following properties, compare [Ha].

1. $\pi^{-1}(p_2)$ consists of a single point, if $p_2 \in R^2 \setminus \{(0,0)\}$.
2. $\pi^{-1}((0,0)) = \mathbb{P}^1$.
3. The points of $\pi^{-1}((0,0))$ are in 1-1 correspondence to the set of (undirected) lines through $(0,0)$.

We consider CDA_2, the closure of $\mathrm{graph}(\psi_{DA_2})$.

Lemma 5.24
CDA_2 is homeomorphic to a half-open cylinder times a plane.

Proof. (sketch). The plane comes from varying p_1, so assume $p_1 = (0,0)$. Then $p_2 \in \mathbb{R}^2 \setminus \{(0,0)\}$, provided that $(p_1, p_2) \in CONF_2$. Write $p_2 = r(\cos\alpha, \sin\alpha)$, with $r \in \mathbb{R}_{>0}$, and $\alpha \in \mathbb{R}/2\pi\mathbb{Z}$. Any configuration $((0,0), \alpha)$, is added exactly once in order to obtain the closure of $\mathrm{graph}(\psi_{DA_2})$, as $\lim_{r \to 0} r(\cos\alpha, \sin\alpha)$. The punctured plane $\mathbb{R}^2 \setminus \{(0,0)\}$, is homeomorphic to a doubly open cylinder. Adding all points

of the form $((0,0), \alpha_{12})$, with $\alpha_{12} \in \mathbb{R}/2\pi\mathbb{Z}$ means that we attach one full circle to that end of the open cylinder that corresponds to $p_2 = (0,0)$. ∎

Remark 5.25
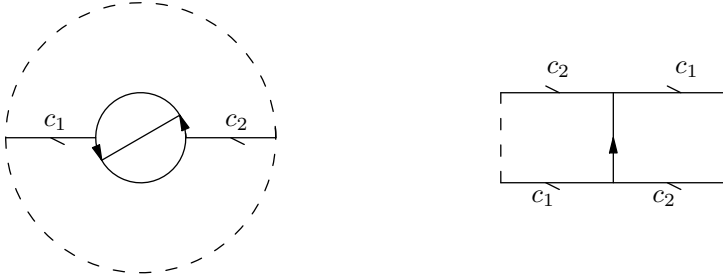Lemma 5.24 demonstrates that CDA_n can have a 'boundary'.

Figure 5.4: Antipodal identification.

In the undirected case, we consider CUA_2, the closure of $\text{graph}(\psi_{\text{UA}_2})$.

Lemma 5.26
CUA_2 is homeomorphic to a Möbius strip times a plane.

Proof. (sketch). Start as in the proof of Lemma 5.24. Write p_2 in polar coordinates, that is, $p_2 = r(\cos \alpha, \sin \alpha)$, with $r \in \mathbb{R}_{>0}$, and $\alpha \in \mathbb{R}/2\pi\mathbb{Z}$. Any undirected angle α_{12} is added twice, once for $p_2 = \lim_{r \to 0} r(\cos \alpha, \sin \alpha)$ and once for $p_2 = \lim_{r \to 0} r(\cos \alpha + \pi, \sin \alpha + \pi)$. This gives the antipodal identification as indicated on the left in Figure 5.4 by the little solid arrows. It is allowed to cut the space as long as it is eventually pasted back together in the same way as it was cut. We make two cuts, c_1 and c_2, through the side of the cylinder. This enables us to perform the antipodal paste, resulting in the rectangle on the right of Figure 5.4. Pasting back the cuts we have made, results in the Möbius strip, compare e.g. [Mu]. ∎

Remark 5.27
Note that the construction in the proof of Lemma 5.26 is exactly the blow-up of $\mathbb{R}^2$ at $(0,0)$ that we have discussed above.

5.3.2   n=3.

We consider the possible angles mod 2π between three distinct points p_1, p_2 and p_3 in the plane. That is, we determine the image $\psi_{\text{DA}_3}(CONF_3)$ in DA$_3$. Let l_{ij} denote the directed line that passes first through p_i and last through p_j. The triangle with

vertices p_1, p_2 and p_3 is **oriented clockwise** if p_3 is on the right of l_{12}. The triangle is oriented anti-clockwise if p_3 is on the left of l_{12}.

Lemma 5.28
Let $c = (p_1, p_2, p_3) \in CONF_3$. Let $\triangle$ denote the triangle with vertices p_1, p_2 and p_3. For $(\alpha_{12}, \alpha_{13}, \alpha_{23}) = \psi_{DA_3}(c)$ the following holds.
  (i)   If $\triangle$ oriented clockwise, then $0 < \alpha_{13} - \alpha_{23} < \alpha_{13} - \alpha_{21} < \pi \mod 2\pi$.
 (ii)   If $\triangle$ oriented anti-clockwise, then $0 < \alpha_{21} - \alpha_{23} < \alpha_{21} - \alpha_{13} < \pi \mod 2\pi$.
(iii)   If p_1, p_2 and p_3 collinear then

$$\alpha_{12} = \alpha_{13} = \alpha_{23} \ \lor \ \alpha_{12} = \alpha_{13} = \alpha_{32} \ \lor \ \alpha_{21} = \alpha_{13} = \alpha_{23}.$$

Moreover, for any image point $(\alpha_{12}, \alpha_{13}, \alpha_{23}) \in \psi_{DA_3}(CONF_3)$ either (i), (ii), or (iii) holds.
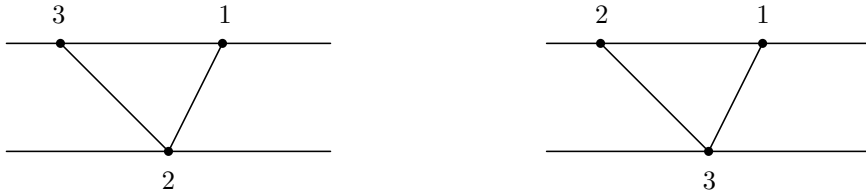

Figure 5.5: The clockwise and anti-clockwise case.

Proof. Note that the differences of angles as they occur in the statements in the lemma does not change if $\triangle$ is rotated.

(i)   Assume $\triangle$ is oriented clockwise. Rotate $\triangle$ such that $\alpha_{13} = \pi$, compare the triangle on the left in Figure 5.5. As p_1 is on the right of l_{23} it follows that $\alpha_{21} < \alpha_{23} < \pi$.

(ii)   Assume $\triangle$ is oriented anti-clockwise. Rotate $\triangle$ such that $\alpha_{12} = \pi$, compare the triangle on the right in Figure 5.5. As p_1 is on the right of l_{32} it follows that $\alpha_{31} < \alpha_{32} < \pi$. It follows that $\alpha_{12} - \alpha_{32} < \alpha_{12} - \alpha_{31} < \pi \mod 2\pi$, or equivalently, that $\alpha_{21} - \alpha_{23} < \alpha_{21} - \alpha_{13} < \pi \mod 2\pi$.

(iii)   Proof by inspection.

As any triangle on the vertices p_1, p_2 and p_3 is either oriented anti-clockwise, or oriented clockwise or degenerate, the lemma follows.   ∎

Boundary points of $\psi_{DA_3}(CONF_3)$ are characterized as follows.

Corollary 5.29
Let $a_3 = (\alpha_{12}, \alpha_{13}, \alpha_{23})$ be a boundary point of $\psi_{DA_3}(CONF_3)$.
  (i)   If $a_3 = \psi_{DA_3}(c)$ for $c \in CONF_3$, then $\overline{\alpha_{12}} = \overline{\alpha_{13}} = \overline{\alpha_{23}}$.
 (ii)   If $a_3 \notin \psi_{DA_3}(CONF_3)$, then $\alpha_{12} = \alpha_{13} \lor \alpha_{13} = \alpha_{23} \lor \alpha_{23} = \alpha_{12} + \pi$.
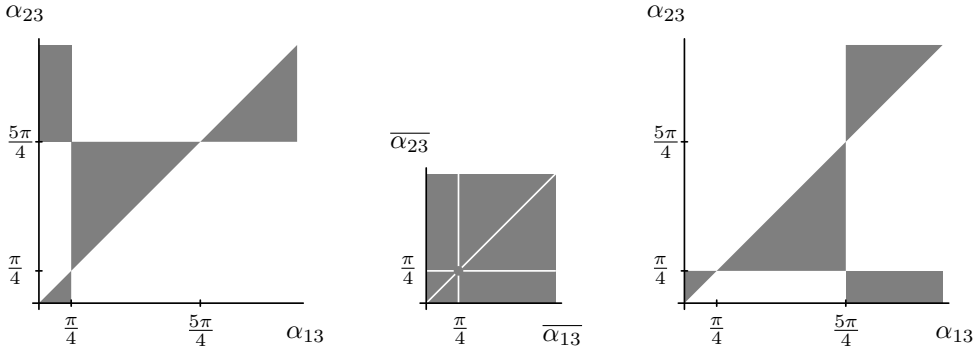
Figure 5.6: Possible values for α_{13}, $\overline{\alpha_{13}}$, α_{23} and $\overline{\alpha_{23}}$, in case $\alpha_{12} = \frac{\pi}{4}$ and $\alpha_{12} = \frac{5\pi}{4}$.

Example 5.30

Figure 5.6 shows the possible values of α_{13} and α_{23}, for $\alpha_{12} = \frac{\pi}{4}$, on the left, and, for $\alpha_{12} = \frac{3\pi}{4}$, on the right. Note that

(i) Configurations of points that are not collinear are mapped by ψ_{DA_3} to the interior of the triangles and rectangles in the figure.

(ii) Configurations that are collinear are mapped to the vertices of the big central triangle on the left and on the right.

(iii) Other points on the boundary of the triangles and rectangles do not correspond to configurations in **conf**$_3$.

Example 5.31

The picture in the middle of Figure 5.6 shows the possible values of $\overline{\alpha_{13}}$ and $\overline{\alpha_{23}}$ for $\overline{\alpha_{12}} = \frac{\pi}{4}$. The only configurations in UA_3 that are not image points of $\psi_{UA_n}(CONF_3)$ are the points where two angles mod π coincide but not all three.

Recall that **conf**$_3 \setminus$ **clconf**$_3$ consists of the configurations of three distinct, non-collinear points up to scalings and transformations.

Corollary 5.32

Let $a_3 = (x, y, z)$. Then $a_3 = \psi_{DA_3}([c])$ for some $[c] \in$ **conf**$_3 \setminus$ **clconf**$_3$ if and only if

$$
\begin{array}{lllll}
& 0 < x < \pi; & y < x; & y > z; & z > 0, \\
\vee & 0 < x < \pi; & y > x; & z < x + \pi; & y < z, \\
\vee & 0 < x < \pi; & y > 0; & y < x; & z > x + \pi; \quad z < 2\pi, \\
\vee & 0 < x < \pi; & z > \pi + x; & y > z; & y < 2\pi, \\
\vee & \pi < x < 2\pi; & y > 0; & y < z; & z < x - \pi, \\
\vee & \pi < x < 2\pi; & y > x; & z > 0; & y < 2\pi; \quad y < x - \pi, \\
\vee & \pi < x < 2\pi; & y > z; & z > x - \pi; & y < x, \\
\vee & \pi < x < 2\pi; & y > x; & y < z; & z < 2\pi.
\end{array}
$$

*The boundary of $\psi_{DA_3}([c])$ with $[c] \in$ **conf**$_3 \setminus$ **clconf**$_3$ is depicted in Figure 5.7.*
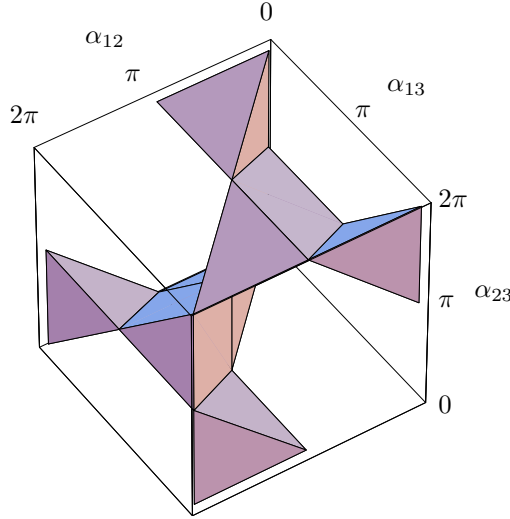
Figure 5.7: The boundary of $\psi_{\mathrm{DA}_3}([c])$ with $[c] \in \mathbf{conf}_3 \setminus \mathbf{clconf}_3$.

Remark 5.33

In Corollary 5.29 we have classified those points $a_3 \in DA_3$ that are on the boundary of $\psi_{\mathrm{DA}_3}(CONF_3)$ but not in $\psi_{\mathrm{DA}_3}(CONF_3)$ itself. These triples of angles can be interpreted as the triples of angles that correspond to configurations of three points, such that exactly two points coincide. Consider the angles between the points in the three configurations presented in Figure 5.8. In the leftmost configuration, $\alpha_{12} = \alpha_{13}$, in the configuration in the middle, $\alpha_{21} = \alpha_{23}$, while in the rightmost configuration, $\alpha_{31} = \alpha_{32}$. This interpretation holds, as long as the three points are not collinear, compare the first statement of Corollary 5.29.

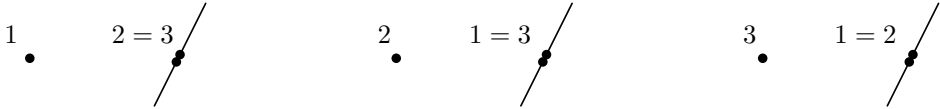Figure 5.8: Configurations for two coinciding points.

Example 5.34

Fix $p_1 = (0,0)$ and $p_2 = (1,1)$. This assures that $\alpha_{12} = \frac{\pi}{4}$. Suppose that the position of p_3 is given by $p_3(t) = p_2 + 1.1(\cos t, \sin t)$, for $t \in [0, 2\pi)$. So $\alpha_{23} = t$. Then $(\alpha_{13}(t), t)$ is a curve, that is defined for any t. It is depicted in Figure 5.9, on the left.

Example 5.35

Fix $p_1 = (0,0)$ and $p_2 = (1,1)$ again. Let $p_3(t) = \sqrt{2}(\cos t, \sin t)$. In this case, the curve $(\alpha_{13}(t), t)$ is built up out of straight line segments, see Figure 5.9, on the right. At $t = \frac{5\pi}{4}$, the point p_3 passes through p_1. At this t, the curve is not defined. This t coincides with a swap $\alpha_{13} = \alpha_{13} + \pi$.
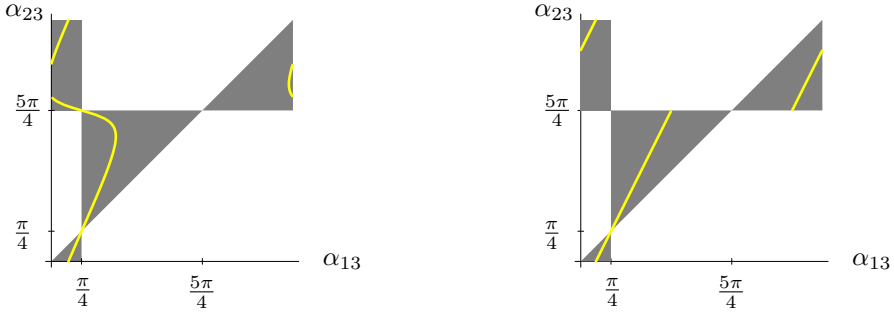

Figure 5.9: Configurations for moving third point.

There are some obvious geometric transformations that relate points in the image $\psi_{DA_3}(CONF_3)$. We use these relations for analyzing the structure of $\psi_{DA_3}(CONF_3)$. Here we consider DA_3 as a quotient of $\mathbb{R}^3$. That is, identify points $a = (a_x, a_y, a_z)$ and $b = (b_x, b_y, b_z)$ in $\mathbb{R}^3$ iff $a_x \equiv b_x \mod 2\pi$ etcetera.

Lemma 5.36

Let $(x, y, z) = \psi_{DA_3}(c)$, with $c = (p_1, p_2, p_3) \in CONF_3$. Let σ be an element of the symmetric group S_3. The consequence of a permutation σ of the labels of the points in c is as follows.

$\sigma \in S_3$	$\sigma(c) \in \psi_{DA_3}(CONF_3)$	geometric action in DA_3
()	$(x,\ y,\ z)$	
(12)	$(x + \pi,\ z,\ y)$	$T_{(\pi,0,0)} \circ S_{\alpha_{13}=\alpha_{23}}$
(13)	$(z + \pi,\ y + \pi,\ x + \pi)$	$T_{(\pi,\pi,\pi)} \circ S_{\alpha_{12}=\alpha_{23}}$
(23)	$(y,\ x,\ z + \pi)$	$T_{(0,0,\pi)} \circ S_{\alpha_{12}=\alpha_{13}}$
(123)	$(z,\ x + \pi,\ y + \pi)$	$R_{-\frac{2\pi}{3}} \circ T_{(0,\pi,\pi)}$
(132)	$(y + \pi,\ z + \pi,\ x)$	$R_{\frac{2\pi}{3}} \circ T_{(\pi,\pi,0)}$

A 'T' indicates a translation over a given vector, an 'S' a reflection in a given plane, while 'R' indicates a rotation with respect to the axis through $(0,0,0)$ and $(1,1,1)$ over a given angle.

Proof. A sketch of the six permutations of the labels of the components of p suffices to determine $\sigma(p)$. The geometric action that corresponds to applying the three order two elements on the labels is clear. The following formula, see [Go], gives the image r' of the rotation of a vector r through an angle ϕ about an axis $\hat{n}$.

$$r' \quad = \quad r\cos\phi + \hat{n}(\hat{n} \cdot r)(1 - \cos\phi) + (r \times \hat{n}\sin\phi).$$

In our case, $\hat{n}$ is the normalized vector $\frac{1}{3}\sqrt{3}(1,1,1)$, while $r = \{x, y, z\}$. Applying this formula for $\phi = -\frac{2\pi}{3}$ gives $r' = \{z, x, y\}$, while $\phi = \frac{2\pi}{3}$ leads to $r' = \{y, z, x\}$. This explains the action corresponding to the order three elements of S_3. ∎

Lemma 5.37
If $(x, y, z) \in \psi_{DA_3}(CONF_3)$, then also $(x + \rho, y + \rho, z + \rho) \in \psi_{DA_3}(CONF_3)$ for any $\rho \in [0, 2\pi)$.

Proof. A rotation of $\rho \in [0, 2\pi)$ of the baseline, that is the axis with respect to which angles are measured, corresponds to adding ρ to all angles α_{12}, α_{13} and α_{23}. ∎

Lemmata 5.36 and 5.37 suggest to consider the set of all possible angles between three distinct points up to the permutations and baseline rotations introduced in the lemmata. Define $\Phi^3_{p,r} := \psi_{DA_3}(CONF_3)/\sim_{\{p,r\}}$, the **fundamental image** of $\psi_{DA_3}(CONF_3)$, as the image $\psi_{DA_3}(CONF_3)$ up to permutations and rotations.

Corollary 5.38
$\psi_{DA_3}(CONF_3)$ up to baseline rotations is obtained by projecting $\psi_{DA_3}(CONF_3)$ on the plane $\alpha_{12} + \alpha_{13} + \alpha_{23} = 0$.

Proof. This follows directly from Lemma 5.37, as any vector (ρ, ρ, ρ) is orthogonal to the plane $\alpha_{12} + \alpha_{13} + \alpha_{23} = 0$. ∎

We can actually construct the projection π_r on the plane $P : \alpha_{12} + \alpha_{13} + \alpha_{23} = 0$ as follows. $u_1 = (1, -1, 0)$ and $u_2 = (\frac{1}{2}, \frac{1}{2}, -1)$ form an orthogonal basis of P. Let e_1 and e_2 be the corresponding unit length vectors. Then π_r is given by

$$\pi_r : \quad \mathbb{R}^3 \quad \rightarrow \quad \mathbb{R}^2,$$
$$c \quad \mapsto \quad (<c, e_1>, <c, e_2>).$$

$\pi_r(\psi_{DA_3}(CONF_3))$ is shown on the left in Figure 5.10.

Remark 5.39
π_r maps $(\pi, 0, 0)$ to $p = (\pi A, \pi B)$, maps $(0, \pi, 0)$ to $q = (-\pi A, \pi B)$ and maps $(0, 0, \pi)$ to $(0, 2\pi B)$, where $A = \frac{1}{2}\sqrt{2}$ and $B = \frac{1}{6}\sqrt{6}$. As a consequence, any $a_3 \in \psi_{DA_3}(CONF_3)$ has a representative mod 2π that is mapped by π_r in the area shown on the right in Figure 5.10.

Next lemma is the 'projected' version of Lemma 5.36.

Lemma 5.40
Let $(x, y, z) = \psi_{DA_3}((p_1, p_2, p_3))$, with $c = (p_1, p_2, p_3) \in CONF_3$. The orbit of $\pi_r(x, y, z))$ under the action of the symmetric group S_3 on the labels of p_1, p_2 and
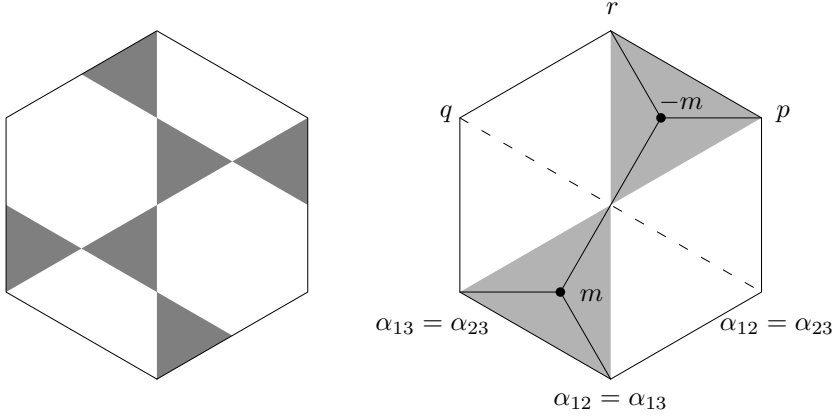
Figure 5.10: $\pi_r(\psi_{\text{DA}_3}(CONF_3))$ and six times $\Phi^3_{p,r}$.

p_3 is given in the following table.

$\sigma \in S_3$,	geometric action,	coordinates.	
()	−	$(A(x - y),$	$B(x + y - 2z))$
(12)	$T_{\delta p} + S_{\alpha_{13}=\alpha_{23}}$	$(A(\pi + x - z),$	$B(\pi + x - 2y + z))$
(13)	$S_{\alpha_{12}=\alpha_{23}}$	$(A(z - y),$	$B(z + y - 2x))$
(23)	$T_{\delta r} + S_{\alpha_{12}=\alpha_{13}}$	$(A(y - x),$	$B(x + y - 2z - 2\pi))$
(123)	$R_{\delta m, -\frac{2\pi}{3}}$	$(A(z - x - \pi),$	$B(x + z - 2y - \pi))$
(132)	$R_{\delta m, \frac{2\pi}{3}}$	$(A(y - z),$	$B(2\pi + y + z - 2x))$

Here p, q, r and A, B are as in Remark 5.39 and m is given by $m = (-\frac{\pi A}{3}, -\pi B)$. Moreover, $\delta = 1$, if the second coordinate of $\pi_r(x, y, x) < 0$ and $\delta = -1$, if the second coordinate of $\pi_r(x, y, x) > 0$.

Proof. We can easily compute the coordinates of the points in the orbit by projecting the orbit in $\psi_{\text{DA}_3}(CONF_3)$ that we found in Lemma 5.36. Concerning the geometric action: the reflection matrix S_a for a reflection of a point in the line $y = ax$ is given by

$$S_a = \frac{1}{1 + a^2} \begin{pmatrix} 1 - a^2 & 2a \\ 2a & a^2 - 1 \end{pmatrix}.$$

It is easy to check that the action of (12) boils down to a translation over p followed by a reflection in the line $\alpha_{13} = \alpha_{23}$. Similarly for the action of the other two involutions. The rotation matrix R_α for a rotation of a point around the origin is given by

$$R_\alpha = \begin{pmatrix} \cos\alpha & -\sin\alpha \\ \sin\alpha & \cos\alpha \end{pmatrix}.$$

A rotation of a vector v around an arbitrary center m is given by $R_\alpha(v - m) + m$. This allows us to check the action of (123) and (132).   ∎

Corollary 5.41
$\Phi^3_{p,r}$ *is given by the triangle in the picture on the right of Figure 5.10 with vertices* $(0,0)$, $-m$ *and* p.

Proof. Every element of the orbit of S_3 acting on a $\pi_r(x,y,z)$ for some $(x,y,z) = \psi_{DA_3}(c)$, with $c \in CONF_3$ lives 'at the same place' in its own triangle in the picture on the right of Figure 5.10: the three order 2 elements map $\pi_r(x,y,z)$ on one of the three gray triangles on the other site of the dotted line $\alpha_{12} = \alpha_{23}$. The two order three elements rotate $\pi_r(x,y,z)$ clockwise or anti-clockwise into the two adjacent gray triangles.   ∎

Corollary 5.42
Let P *be the plane orthogonal to the vector* $(1,1,1)$. *Then the 2-dimensional wallpaper group* p6m *is acting on* $P \cap \psi_{DA_3}(CONF_3)$.

Proof. There are order 6, order 3 and order 2 rotations, and 6 axes of reflection. This characterizes the 17-th wallpaper group, see for example [CM].   ∎

5.4   The triangle variety $\mathbf{T_n}$.

We want to answer the question:

  are CUA_n and CDA_n smooth manifolds?

Moreover, we are interested in their algebraic counterparts. In this section we describe an algebraic variety that is very similar to CUA_n. We know that $CONF_n$ is contained in CUA_n: by definition, CUA_n equals the closure of the graph of the undirected angle map:

$$CONF_n \ \subset \ CUA_n \ \subset \ (\mathbb{R}^2)^n \times (\mathbb{R}/\pi\mathbb{Z})^{\binom{n}{2}}.$$

Therefore, CUA_n contains a '$CONF_n$ part' that is smooth. The remaining points of CUA_n lie above the **diagonal** $\Delta \subset (\mathbb{R}^2)^n$ consisting of configurations with at least two coinciding points p_i and p_j. We make an algebraic description for $\mathbb{R}/\pi\mathbb{Z} = \mathbb{P}^1$ by taking coordinates $(a_{ij} : 1)$ and $(1 : b_{ij})$, where

$$a_{ij} = \tan\overline{\alpha}_{ij}; \qquad b_{ij} = \frac{1}{\tan\overline{\alpha}_{ij}}.$$

For simplicity, we consider only the case where $b_{ij} \neq 0$ on each $\mathbb{P}^1$, so we work on the $(a_{ij} : 1)$-chart. We have transformed ψ_{UA_n} in a rational map ψ_{slope} given by

$$\psi_{\text{slope}}((x_0,y_0),\ldots,(x_{n-1},y_{n-1})) \ = \ \{(\frac{y_j - y_i}{x_j - x_i})\}_{0 \leq i < j \leq n-1},$$

where $((x_0, y_0), \ldots, (x_{n-1}, y_{n-1})) \in CONF_n$. Without loss of generality we assume throughout this section that $x_0 = y_0 = 0$. That is, we consider configurations up to translation. The dimension of $CONF_n(\mathbb{R}^2)$ up to translations equals $2n - 2$. The slope a_{0i}, for $i \in \{1, \ldots, n-1\}$ is denoted short as a_i. The triangle T_{ij} is the triangle with vertices (x_0, y_0), (x_i, y_i), and (x_j, y_j). The following lemma shows that there exists a relation between the x-coordinates of the vertices of T_{ij} and the slopes of the lines bounding T_{ij}. Let

$$t_{ij} \quad = \quad a_i x_i - a_j x_j - a_{ij} x_i + a_{ij} x_j.$$

Lemma 5.43
$t_{ij} = 0$ *on the* $(a_{ij} : 1)$-*chart of* $CONF_n$.

Proof. It holds that $y_i = a_i x_i$, $y_j = a_j x_j$, and $y_i - y_j = a_{ij}(x_i - x_j)$. Substitute the former two equations in the last equation. ∎

Corollary 5.44
On the $(a_{ij} : 1)$-*chart we have that* $CUA_n \subset \{t_{ij} = 0\}$ *for* $1 \le i < j \le n-1$.

A question is if equality holds. That is, if the closed algebraic set $\{t_{ij} = 0\}_{1 \le i < j \le n-1}$ is contained in CUA_n. The answer is no. We prove this later on by means of the six-slopes formula:
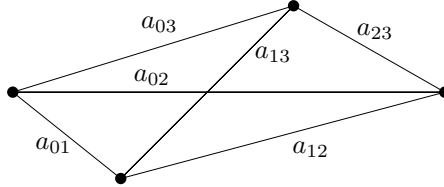
Figure 5.11: For four distinct points the six-slopes formula holds.

Lemma 5.45 (six-slopes formula)
Let p_0, p_1, p_2 *and* p_3 *be distinct points in the plane. Then* $\Delta = \Delta_{0123} = 0$, *where* Δ *is given by*

$$\Delta \quad = \quad (a_1 - a_{12})(a_2 - a_{23})(a_3 - a_{13}) - (a_1 - a_{13})(a_2 - a_{12})(a_3 - a_{23}). \quad (5.2)$$

Proof. Assume that $p_0 = (0,0)$ and $p_1 = (1, a_1)$. We compute coordinates for the points p_2 and p_3. Let l_{ij} be the line through the points p_i and p_j. The lines l_{02} and l_{03} are given by

$$l_{02} : y_2 \quad = \quad a_2 x, \qquad l_{03} : y_3 \quad = \quad a_3 x,$$

and l_{12} and l_{13} by

$$l_{12} : y - a_1 \quad = \quad a_{12}(x - 1), \qquad l_{13} : y - a_1 \quad = \quad a_{13}(x - 1).$$

We compute the intersections $(x_2, y_2) = l_{02} \cap l_{12}$, and $(x_3, y_3) = l_{03} \cap l_{13}$:

$$
\begin{aligned}
x_2 &= \frac{a_1 - a_{12}}{a_2 - a_{12}} & x_3 &= \frac{a_1 - a_{13}}{a_3 - a_{13}} \\
y_2 &= a_2 x_2 & y_3 &= a_3 x_3
\end{aligned}
$$

After some formula manipulation the expression follows as $a_{23} = \frac{y_3 - y_2}{x_3 - x_2}$.   ∎

Remark 5.46
Some remarks on Equation 5.2.

   (i)   Interchanging indices $1 \leftrightarrow 2$, etcetera, changes the appearance of the expression for Δ_{0123}, but does not change the expression itself.

   (ii)   By Δ_{ijkl} we denote Δ_{0123} with 0, 1, 2 and 3 replaced by i, j, k and l.

   (iii)   If no three points of p_0, p_1, p_2 and p_3 are collinear, then we can express a_{23} as follows in terms of a_1, a_2, a_3, a_{12} and a_{13}:

$$
a_{23} = \frac{a_3(a_1 - a_{13})(a_2 - a_{12}) - a_2(a_1 - a_{12})(a_3 - a_{13})}{(a_1 - a_{13})(a_2 - a_{12}) - (a_1 - a_{12})(a_3 - a_{13})}. \tag{5.3}
$$

Corollary 5.47
$\Delta_{ijkl} = 0$ *on* CUA_n.

Proof.   This follows from Lemma 5.45 and the definition of CUA_n.   ∎

Instead of just looking at the zeros of $t_{ij} = 0$, we add the condition that all Δ_{ijkl} equal zero as well. This leads to the following definition.

Definition 5.48
*The **triangle variety** T_n is the set of common zeroes of the polynomials t_{ij} for $1 \leq i < j \leq (n-1)$ and Δ_{ijkl} for $0 \leq i < j < k < l \leq (n-1)$. Any variable, of the form a_{ij} or x_i, takes value in $\mathbb{R}$.*

Example 5.49
The zero set of a collection of polynomials $f_1 \ldots, f_n$ is indicated by $V(f_1, \ldots, f_n)$. So $T_4 = V(t_{12}, t_{13}, t_{23}, \Delta_{123})$.

Note that the ideal of the triangle variety T_n contains: one polynomial t_{ij} for every triangle with vertices p_0, p_i and p_j; one polynomial Δ_{ijkl} for every quadrilateral with vertices p_i, p_j, p_k and p_l. We could consider explicitly triangles with vertices p_i, p_j and p_k by including:

$$
t_{ijk} = a_{ik}(x_i - x_k) - a_{ij}(x_i - x_j) - a_{jk}(x_j - x_k).
$$

The following lemma shows that this is not necessary however.

Lemma 5.50
$t_{ijk} = t_{ij} - t_{ik} + t_{jk}$.

Proof. This follows directly from the following equations:

$$t_{ij} = a_i x_i - a_j x_j - a_{ij} x_i + a_{ij} x_j,$$
$$t_{ik} = a_i x_i - a_k x_k - a_{ik} x_i + a_{ik} x_k,$$
$$t_{jk} = a_j x_j - a_k x_k - a_{jk} x_j + a_{jk} x_k.$$ ■

5.4.1   Singularities of T_n for small n.

In this section we determine singularities of the triangle variety T_n for $n = 3$ and $n = 4$. For this purpose recall the definition of **singularity**.

Definition 5.51
*See [Ha]. Let $Y \subset A^n$ be an affine variety, and let $f_1, \ldots, f_t \in A = k[x_1, \ldots, x_n]$ be a set of generators for the ideal of Y. Then Y is **nonsingular at a point** $P \in Y$ if the rank of the Jacobian matrix $((\partial f_i / \partial x_j)(P))$ is $n - r$, where r is the dimension of Y. If Y is nonsingular at every point, then Y is **nonsingular**.*
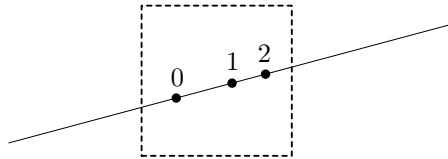
5.4.2   n=3.

Figure 5.12: Three coinciding points with coinciding directions.

Lemma 5.52
An element $c = (x_0, x_1, x_2, a_1, a_2, a_{12}) \in T_3$ is singular iff all points and all slopes coincide. That is:

$$x_0 = x_1 = x_2, \qquad and \qquad a_1 = a_2 = a_{12}.$$

The type of this singularity is A_∞.

Proof. $T_3 = V(t_{12})$, with $t_{12} = a_1 x_1 - a_2 x_2 - a_{12} x_1 + a_{12} x_2$. T_3 is singular if the rank of the Jacobian of t_3 is smaller than $5 - 4 = 1$, that is if all partial derivatives of t_{12} vanish.

variable	x_1	x_2	a_1	a_2	a_{12},
partial derivative	$a_1 - a_{12}$	$a_{12} - a_2$	x_1	$-x_2$	$x_2 - x_1$.

Solving this system gives the solutions $x_1 = x_2 = 0 \wedge a_1 = a_2 = a_{12}$. For the type of the singularity: note that $t_{12} = (a_1 - a_{12})x_1 + (a_{12} - a_2)x_2$. From this it follows

that the singular set is given by $a_i = a_j = a_{ij}$, and that the singularity is of type A_∞, cf. [Si]. ∎

Remark 5.53

Geometrically, the singularities of T_3 correspond to degenerated configurations where both the three points coincide and the directions between the points coincide, see Figure 5.12.

5.4.3   n=4.

Lemma 5.54

Define

$$
\begin{aligned}
A_1 &= (a_2 - a_{12})(a_3 - a_{23}) - (a_2 - a_{23})(a_3 - a_{13}), \\
A_2 &= (a_1 - a_{12})(a_3 - a_{13}) - (a_1 - a_{13})(a_3 - a_{23}), \\
A_3 &= (a_2 - a_{23})(a_1 - a_{12}) - (a_2 - a_{12})(a_1 - a_{13}), \\
A_{12} &= (a_1 - a_{13})(a_3 - a_{23}) - (a_2 - a_{23})(a_3 - a_{13}), \\
A_{13} &= (a_2 - a_{12})(a_3 - a_{23}) - (a_1 - a_{12})(a_2 - a_{23}), \\
A_{23} &= (a_1 - a_{13})(a_2 - a_{12}) - (a_1 - a_{12})(a_3 - a_{13}).
\end{aligned}
$$

(i)   *If $A_1 \neq 0$, then*

$$
x_2 = x_1 \frac{(a_{12} - a_{13})(a_{23} - a_3)}{A_1}; \qquad x_3 = x_1 \frac{(a_{12} - a_{13})(a_{23} - a_2)}{A_1}.
$$

If $A_2 \neq 0$, then

$$
x_1 = x_2 \frac{(a_{12} - a_{23})(a_{13} - a_3)}{A_2}; \qquad x_3 = x_2 \frac{(a_{12} - a_{23})(a_{13} - a_1)}{A_2}.
$$

If $A_3 \neq 0$, then

$$
x_2 = x_3 \frac{(a_{23} - a_{13})(a_{12} - a_1)}{A_3}; \qquad x_1 = x_3 \frac{(a_{23} - a_{13})(a_{12} - a_2)}{A_3}.
$$

(ii) $\frac{\partial \Delta}{\partial a_{ij}} = A_{ij}$.

Proof. As $t_{23} = 0$ on T_n, it follows that $(a_{23} - a_3)x_3 = (a_{23} - a_2)x_2$. As $t_{12} - t_{13} = 0$, we arrive at

$$
(a_{12} - a_2)x_2 - (a_{13} - a_3)x_3 = a_{12}x_1 - a_{13}x_1.
$$

Add $(a_{23} - a_3)$ times this last equation to f_{23} and substitute $(a_{23} - a_2)x_2$ for $(a_{23} - a_3)x_3$. This gives that $A_1 x_2 = (a_{12} - a_{13})(a_{23} - a_3)x_1$, resulting in the formula for x_2. The formula for x_3 is obtained by adding $(a_{23} - a_2)(f_{12} - f_{13})$ to f_{23} and

substituting $(a_{23} - a_3)x_3$ for $(a_{23} - a_2)x_2$. Substitute the expression for x_2 in f_{12}, multiply by A_1 and reorder:

$$x_1 a_1 A_1 + x_1 (a_{12} - a_2)(a_{12} - a_{13})(a_{23} - a_3) = x_1 a_{12} A_1,$$
$$x_1 \Delta = 0.$$

The last equation holds in two cases. In the first case, $x_1 = 0$. But from the expressions for x_2 and x_3 it follows that then $x_2 = 0$ and $x_3 = 0$ as well, while no conditions are set on the slopes. In the other case $\Delta = 0$, while for x_2 and x_3 the two formulas in the Lemma hold. The equations in case of $A_2 \neq 0$ and $A_3 \neq 0$ follow by relabeling. This proves the first claim. The second claim follows by inspection. ∎

Corollary 5.55
$CUA_4 \neq V(t_{12}, t_{13}, t_{23})$.

Proof. This follows from the proof of Lemma 5.54: The variety $V(t_{12}, t_{13}, t_{23})$ contains $0 = x_1 = x_2 = x_3$ as a component, *without* the condition that $\Delta_{0123} = 0$. ∎

Remark 5.56
Corollary 5.55 and its proof explain why we have added the Δ_{ijkl}'s in the definition of triangle variety T_n, cf. Definition 5.48.

Lemma 5.57
A configuration $c \in T_4$ is singular iff, up to relabeling, both $x_0 = x_1 = x_2$ and $a_1 = a_2 = a_{12}$.

Proof. Consider the Jacobian J_4 of T_4 and apply Definition 5.51. The Jacobian of T_4 where the nine variables are in the order x_1, x_2, x_3, a_1, a_2, a_3, a_{12}, a_{13}, a_{23} is given by:

$$\begin{pmatrix} a_1 - a_{12} & a_{12} - a_2 & 0 & x_1 & -x_2 & 0 & x_2 - x_1 & 0 & 0 \\ a_1 - a_{13} & 0 & a_{13} - a_3 & x_1 & 0 & -x_3 & 0 & x_3 - x_1 & 0 \\ 0 & a_2 - a_{23} & a_{23} - a_3 & 0 & x_2 & -x_3 & 0 & 0 & x_3 - x_2 \\ 0 & 0 & 0 & -A_1 & -A_2 & -A_3 & \pm A_{12} & \pm A_{13} & \pm A_{23} \end{pmatrix}.$$

The dimension of T_4 equals $2 \cdot 4 - 2 = 6$. Therefore, a configuration is singular iff the rank of its Jacobian is equal to or smaller than 2. Denote by $m(i, j, k)$ the submatrix of J_4 consisting of columns i, j and k where the fourth row is deleted. We distinguish several cases, by considering the number of distinct clusters of coinciding points in c.

(i) [≥ 3 **clusters**] We may assume that $x_1 \neq 0$, $x_2 \neq 0$, $x_3 \neq 0$ and $x_1 \neq x_2$. Consider $m(5, 6, 7)$:

$$m(5, 6, 7) = \begin{pmatrix} -x_2 & 0 & x_2 - x_1 \\ 0 & -x_3 & 0 \\ x_2 & -x_3 & 0 \end{pmatrix}.$$

The determinant of $m(5, 6, 7)$ equals $x_2 x_3 (x_2 - x_1) \neq 0$. This implies non-singularity.

(ii) [2 **clusters: (2,2)**] We may assume that $x_1 = 0$ and that $x_2 = x_3 \neq 0$. In this case the determinant of $m(5, 6, 7)$ equals $(x_2)^3$, which implies non-singularity .

(iii) [2 **clusters: (3,1)**] See also Figure 5.13. Assume that for $c \in T_4$ it holds that $x_0 = x_1 = x_2$; that $a_1 = a_2 = a_{12}$ and that $x_3 \neq x_0$. As a consequence $a_3 = a_{13} = a_{23}$. It follows that the first and last row J_4 vanishes. Therefore, c is singular. If we only assume that $x_0 = x_1 = x_2$ and that $x_3 \neq x_0$, then the determinants $\det(m(1, 6, 8)) = (x_3)^2(a_1 - a_{12})$ and $\det(m(2, 6, 8)) = (x_3)^2(a_{12} - a_2)$ show that the condition $a_1 = a_2 = a_{12}$ is necessary for a singularity.

(iv) [1 **cluster**] It holds that $x_0 = x_1 = x_2 = x_3 = 0$. Consider J_4. First assume that the last row of J_4 equals zero. As $\Delta = 0$ on T_4 this means that we are looking for solutions of the system of equations

$$A_1 \;=\; A_2 \;=\; A_3 \;=\; A_{12} \;=\; A_{13} \;=\; A_{23} \;=\; \Delta \;=\; 0.$$

Applying Mathematica's `Reduce` function results in 10 reductions. Each of these 10 reductions contains equations of the form $a_1 = a_2 = a_{12}$. We are left with the case that some $A_{ij} \neq 0$. If $\mathrm{rank}(J_4) \leq 2$, then the determinants of all 2×2 submatrices of $m(1, 2, 3)$ vanish. This gives a system of nine equations that can be reduced to the six equations of the form $a_1 = a_2 = a_3 = a_{12} = a_{13}$, that is, five slopes are equal. Again, each of these equations contains a condition of the form $a_1 = a_2 = a_{12}$. ∎

Figure 5.13: Typical singular configuration: three coinciding, collinear points with a fourth point.

Remark 5.58

The singularities of T_4 are closely related to the singularities of T_3. The singularity in the (3,1) case is of type A_∞ just as for T_3. But if all points coincide a more complicated singularity occurs as several A_∞ singularities 'meet': one can move any of the four points away in such a way that the three remaining points are as in the configuration of Lemma 5.52.

It is still an open question whether $CUA_4 = T_4$. Maybe we need to add some relations or inequalities to T_4 to obtain equality?

Chapter 6

Continuity of the Voronoi map.

In Chapter 4 we have introduced the compactification CDA_n of the graph of the angle map, applied to n distinct point in the plane. By means of the extended definition of Voronoi diagram, as introduced in Chapter 3, we are able to consider the Voronoi diagram $V(\gamma_n)$ of a data set $\gamma_n \in CDA_n$. The main result of this chapter is Theorem 6.11. It states, up to a compactness condition, that two data sets γ_n and η_n in CDA_n that are Euclidean close, have Voronoi diagrams that are Hausdorff close. That is, the Voronoi diagram generated by a set of not necessarily distinct points and the angles between those points does not change dramatically if we perturb both the points and the angles only slightly.

6.1 Introduction.

In Chapters 3 and 4 we have extended the notion of Voronoi diagram to configurations of points together with the angles between the points. This allows us to consider Voronoi diagrams of point sets that include coinciding points. More precisely, in Section 5.1.3, we have introduced a compactification CDA_n, as the closure of the graph of the angle map

$$\psi_{\mathrm{DA}_n} : CONF_n \quad \rightarrow \quad DA_n.$$

The angle map ψ_{DA_n} maps a set c of n distinct points in the plane to the angles in $\mathbb{R}/2\pi\mathbb{Z}$ between the points in c.

In this chapter we call the elements $\gamma_n \in CDA_n$, consisting of n points in $\mathbb{R}^2$ and $\binom{n}{2}$ angles in $\mathbb{R}/2\pi\mathbb{Z}$, data sets. With any data set $\gamma_n \in CDA_n$, we associate a Voronoi diagram $V(\gamma_n)$ in Section 6.2.

One can wonder whether the data sets are a robust way of storing Voronoi diagrams.

That is, we consider the following question: if we perturb a data set $\gamma_n \in CDA_n$ slightly, how does the corresponding Voronoi diagram $V(\gamma_n)$ change? By perturbing a data set $\gamma_n \in CDA_n$ we mean that both the points components and the angle components of γ_n are allowed to be perturbed slightly, as long as the perturbed data set $\tilde{\gamma}_n$ is again in CDA_n. A first result is given in Theorem 6.1, that is a kind of one point continuity theorem. It states that a point x that was on the one-skeleton of a Voronoi diagram $V(\gamma_n)$ before perturbing, cannot be too far from the one skeleton of the Voronoi diagram of the perturbed data set.

Before we are able to give a more general continuity result, we first need a suitable metric on the set of Voronoi diagrams. A metric that is often used to compare pictures, is the so-called Hausdorff metric. Two subsets A and B of $\mathbb{R}^2$ are close to each other in the Hausdorff metric, iff the maximal Euclidean distance from any point $b \in B$ to the set A is small and vice versa. For a precise definition, see Section 6.4.

In order to prove a continuity theorem with respect to the Hausdorff metric, we have to add some restrictions to our underlying point configurations. We add four so-called camera points, points that are very far away around our configuration. Now we restrict the configurations we are interested in to a relatively small bounded subset of the plane. If we only change the configurations within this subset, the camera points guarantee us that the Voronoi diagrams of the configurations are not changing outside a second, larger bounded subset of the plane. But then we are ready for proving the main result of this chapter: Theorem 6.11 states that, up to the compactness condition, two data sets that are Euclidean close, have Voronoi diagrams that are Hausdorff close. Note that it is essential that the continuity theorem holds on the whole of the chosen compact subset of CDA_n: that is, the points added to the graph of ψ_{DA_n} by taking the closure are essential as there availability is used in the proof of Theorem 6.11.

6.2   Preliminaries.

Throughout this chapter we compare data sets $\gamma_n, \eta_n \in CDA_n$. Write

$$\gamma_n \;\; = \;\; (p_1(\gamma_n), \ldots, p_n(\gamma_n), \alpha_{12}(\gamma_n), \ldots, \alpha_{(n-1)n}(\gamma_n)),$$

and similarly η_n. We say that η_n is within **distance** δ of γ_n, notation $d(\gamma_n, \eta_n) < \delta$, iff

$$\max_{1 \le k \le n} \|p_k(\gamma_n) - p_k(\eta_n)\| < \delta \quad \wedge \quad \max_{1 \le i < j \le n} \|\alpha_{ij}(\gamma_n) - \alpha_{ij}(\eta_n)\| < \delta.$$

Here, $\|.\|$ denotes the ordinary Euclidean distance on $\mathbb{R}^2$ and $\mathbb{R}/2\pi\mathbb{Z}$.

From Section 4.4 we recall the definition of Voronoi diagram in terms of not necessarily non-coinciding points in the plane and directed angles between those points. This enables us to define for any $\gamma_n \in CDA_n$ a Voronoi diagram $V(\gamma_n)$. In Section 2.2 we

have seen that the Voronoi cell of a generator p_i can be written as the intersection of all Voronoi half-planes $vh(p_i, p_j)$. We use this characterization to introduce the Voronoi cell of a point $p_i(\gamma_n)$.

Fix two points $p_i = p_i(\gamma_n)$ and $p_j = p_j(\gamma_n)$. The **bisection point** $b(p_i, p_j)$ is the point $\frac{1}{2}(p_i + p_j)$. If $p_i \neq p_j$, the bisection point is just the middle of the line segment $p_i p_j$. If $p_i = p_j$ then $b(p_i, p_j)$ coincides with the double point $p_i = p_j$. The **perpendicular bisector** $B(p_i, p_j)$ is the line through $b(p_i, p_j)$ perpendicular to the angle $\alpha_{ij} = \alpha_{ij}(\gamma_n)$. Let $\mathbf{n}$ be any non-zero vector, pointing in the direction α_{ij}. The **Voronoi half-plane** $vh(p_i, p_j)$ is the half-plane defined by

$$\mathbf{n} \cdot (x - b_x, y - b_y) \quad \leq \quad 0.$$

The **Voronoi cell** $V(p_i)$ is defined as

$$V(p_i) \quad = \quad \bigcap_{j \neq i} vh(p_i, p_j).$$

A point x is on the **Voronoi edge** $e(p_i, p_j)$ iff it is on the intersection of the Voronoi cells $V(p_i)$ and $V(p_j)$, that is

$$x \in e(p_i, p_j) \quad \Leftrightarrow \quad x \in V(p_i) \cap V(p_j).$$

The **Voronoi diagram** is the family of subsets of $\mathbb{R}^2$ consisting of the Voronoi cells $V(p_i)$ and all of their intersections. The **one-skeleton** of the Voronoi diagram is the union of the boundaries of the Voronoi cells. Note that the notion of one-skeleton equals the notion of shape of a Voronoi diagram, introduced in Section 4.4.1.

6.3 One point continuity.

In this section we prove the following theorem.

Theorem 6.1
Let $\gamma_n \in CDA_n$ be a set of data representing n generators in $\mathbb{R}^2$ and $\binom{n}{2}$ angles in $\mathbb{R}/2\pi\mathbb{Z}$ between these generators. Suppose that x is on the one-skeleton of the corresponding Voronoi diagram $V(\gamma_n)$. Then for every $\epsilon > 0$ there exists $\delta > 0$, such that when we perturb γ_n by not more than δ, the one-skeleton of any perturbed diagram is within distance ϵ of x.

In order to prove this theorem, we perform the following steps:

1. We decrease ϵ a finite number of times: for every pair of generators (p, q) whose bisector $B(p, q)$ does not pass through x we decrease ϵ, if necessary, in such a way that

$$d(x, B(p, q)) \quad > \quad 2\epsilon.$$

2.   For every pair of generators (p, q) we show how to choose δ_{pq}. If $x \in B(p, q)$ before perturbing then after perturbing by δ_{pq},

$$B(p, q) \cap B_\epsilon(x) \quad \neq \quad \emptyset.$$

If $x \notin B(p, q)$ before perturbing then after perturbing by δ_{pq},

$$B(p, q) \cap B_\epsilon(x) \quad = \quad \emptyset.$$

Of course this last statement can only hold if we adjust ϵ as indicated above.
3.   Set $\delta := \min_{p,q} \delta_{pq}$.

These steps gives us enough control on the bisectors to complete the proof. We first show that the bisection point of two generators p and q can not get more perturbed than the generators themselves.

Lemma 6.2
Let p and q be two points in the plane. Let $b(p, q) = (p+q)/2$. If $\max(\, \|\bar{p} - p\|, \, \|\bar{q} - q\| \,) < \delta$, then

$$\|b(\bar{p}, \bar{q}) - b(p, q)\| \quad < \quad \delta.$$

Proof. $\|b(\bar{p}, \bar{q}) - b(p, q)\| = \|\frac{1}{2}(\bar{p} + \bar{q}) - \frac{1}{2}(p + q)\| = \|\frac{1}{2}(\bar{p} - p) + \frac{1}{2}(\bar{q} - q)\| \leq \frac{1}{2}\|\bar{p} - p\| + \frac{1}{2}\|\bar{q} - q\| < \delta.$ ∎

We apply Lemma 6.2 in choosing δ_{pq} such that a bisector $B(p, q)$ that passes through x before perturbation still passes through $B_\epsilon(x)$ after perturbation.

Lemma 6.3
Let p, q and α_{pq} be data from $\gamma_n \in CDA_n$ such that $x \in B(p, q)$. Write $r = \|x - b(p, q)\|$. Let

$$\delta_{pq} \quad = \quad \min(\frac{\epsilon}{1 + r}, 1).$$

If $\max(\, \|\bar{p} - p\|, \, \|\bar{q} - q\|, \, \|\bar{\alpha}_{pq} - \alpha_{pq}\|) < \delta_{pq}$ then the bisector $B(\bar{p}, \bar{q})$ passes through $B_\epsilon(x)$.

Proof. We treat the perturbation of the bisector angle α_{pq} and the bisection point $b(p, q)$ separately and add up the maximal effect. Let $l_{\bar{\alpha}_{pq}}$ be the image of a rotation over $\pm\delta_{pq}$ around $b(p, q)$ of the line $B(p, q)$. Then x is at distance $r \sin \delta_{pq}$ of $l_{\bar{\alpha}_{pq}}$. Moreover, from Lemma 6.2 it follows that $\|b(\bar{p}, \bar{q}) - b(p, q)\| < \delta_{pq}$. Let $d = \|x - B(\bar{p}, \bar{q})\|$. Adding up the two effects gives that $d < \delta_{pq} + r \sin \delta_{pq}$. We want d to be smaller than ϵ. As δ_{pq} is a majorant for $\sin \delta_{pq}$, we are safe if we ensure, as claimed, that $\delta_{pq} < \epsilon/(1 + r)$. ∎

The next lemma gives a value of δ that ensures that a bisector that misses x before perturbation, stays away far enough from x after perturbation.

Lemma 6.4

Let p, q and α_{pq} be data from $\gamma_n \in CDA_n$. Let $x \in \mathbb{R}^2$ be such that

$$\|x - B(p, q)\| \quad > \quad 2\epsilon.$$

Write $r = \|x - b(p, q)\|$. The angle between the bisector $B(p, q)$ and the line through $b(p, q)$ and x is denoted by $\gamma \in (0, \frac{\pi}{2}]$. Let

$$\delta_{pq} \quad = \quad \frac{\gamma r - 2\epsilon}{r + 2}.$$

If $\max(\|\bar{p} - p\|, \|\bar{q} - q\|, \|\bar{\alpha}_{pq} - \alpha_{pq}\|) < \delta_{pq}$ then $\|x - B(\bar{p}, \bar{q})\| > \epsilon$.

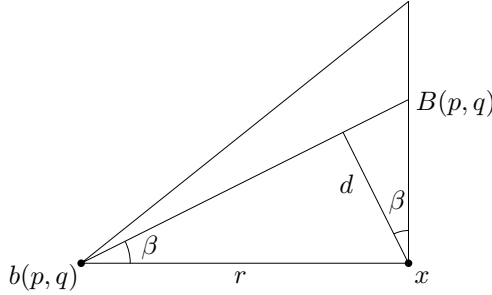Figure 6.1: d is the distance from the bisector B to x.

Proof. First we show that indeed $\delta_{pq} > 0$. As $2\epsilon < r \sin \gamma < r\gamma$ it follows that $\gamma r - 2\epsilon > 0$. We treat the perturbation of the bisector angle α_{pq} and the bisection point $b(p, q)$ separately and add up the maximal effect. Let $l_{\bar{\alpha}_{pq}}$ be the image of a rotation over $\pm \delta_{pq}$ around $b(p, q)$ of the line $B(p, q)$. The distance d of x to $l_{\bar{\alpha}_{pq}}$ s given by $r \sin \beta$. Here $\beta := \gamma - \delta_{pq}$, see also Figure 6.1. Moreover, from Lemma 6.2 it follows that $\|b(\bar{p}, \bar{q}) - b(p, q)\| < \delta_{pq}$ This implies that the composite minimal distance, that is the distance of x to $B(\bar{p}, \bar{q})$ could become as small as $d_1 := r \sin(\gamma - \delta_{pq}) - \delta pq$. We want this distance d_1 to stay bigger than ϵ. As $\frac{1}{2}(\gamma - \delta_{pq})$ is a minorant of $\sin(\gamma - \delta_{pq})$ we are safe if we ensure, as claimed, that

$$\delta_{pq} \quad < \quad \frac{\gamma r - 2\epsilon}{r + 2}. \qquad \blacksquare$$

The following corollary is obvious but useful.

Corollary 6.5

Let x, p, q, α_{pq} and δ_{pq} be as in Lemma 6.4. Suppose that (p, q, α_{pq}) is perturbed by a vector of length at most δ_{pq}. For every point $y \in B_\epsilon(x)$ it holds that

$$y \in vh(p, q) \text{ before perturbation} \quad \Leftrightarrow \quad y \in vh(p, q) \text{ after perturbation},$$

where $vh(p, q)$ denotes the Voronoi half-plane of generators p and q containing p.

We are ready to prove Theorem 6.1.

Proof of Theorem 6.1. Let x be on the 1-skeleton of $V(\gamma_n)$ before perturbation. Let $\epsilon > 0$. Adjust ϵ a finite number of times: for every pair of generators (p, q) whose bisector $B(p, q)$ does not pass through x we set

$$\epsilon \quad = \quad \min(\epsilon, \frac{1}{3}d(x, B(p, q))).$$

This ensures that for every such pair (p, q) it holds that $d(x, B(p, q)) > 2\epsilon$.

Next determine a δ_{pq} for every pair of generators in such a way that i) if $x \in B(p, q)$, then the condition in Lemma 6.3 is fulfilled; ii) if $x \notin B(p, q)$, then the condition of Lemma 6.4 is fulfilled. Let δ be the minimum of all these δ_{pq}, that is, $\delta := \min_{(p,q)} \delta_{pq}$. Define

$$P \quad := \quad \{p \in \gamma_n \mid V(p) \cap B_\epsilon(x) \neq \emptyset, \text{ before perturbation}\}.$$

Consequently, P has at least two elements. Say $P = \{p_1, \ldots, p_m\}$, for some $m \geq 2$. Before perturbation it holds that

$$B_\epsilon(x) \quad = \quad \bigcup_{i=1}^{m}(V(p_i) \cap B_\epsilon(x)).$$

Suppose that, after perturbation, $B_\epsilon(x) \subset V(s)$, for some generator s. We show that this leads to a contradiction. First note that $s \in P$ leads to a contradiction immediately: we can apply Lemma 6.3. This implies that after perturbation some bisector $b(s, p_i)$ passes through $B_\epsilon(x)$. We are left with the case that $s \notin P$. Fix a point $y \in B_\epsilon(x)$ such that y is not on any bisector before or after perturbation. Then

$$y \in V(p_1) \quad \text{before perturbation, say,}$$
$$y \in V(s) \quad \text{after perturbation.}$$

We concentrate on the bisector $B(p_1, s)$ now. If $x \notin B(p_1, s)$ before perturbation, we apply Corollary 6.5: any point in $B_\epsilon(x)$ stays in the same half-plane $vh(p_1, s)$. As a consequence, $y \in vh(p_1, s)$ before and after perturbation. This is in contradiction with our assumption that $y \in V(s)$ after perturbation. So $x \in B(p_1, s)$ before perturbation. This implies that

$$B(p_1, s) \cap B_\epsilon(x) \neq \emptyset,$$

after perturbation: a contradiction with our assumption as well.   ∎

6.4   The distance between two Voronoi diagrams.

6.4.1   Hausdorff distance.

If we want to compare two Voronoi diagrams, a suitable notion of distance is the Hausdorff distance: two sets A and B are within **Hausdorff distance** r iff r is the

smallest number such that any point of A is within distance r from some point of B and vice versa. Let us give this definition more formally. Suppose we have a metric space (X, d). For $A \subset X$ and $r > 0$ we define the open neighborhood $N_r(A)$ as the set

$$N_r(A) \quad := \quad \{\, y \mid d(x, y) < r, \text{ for some } x \in A\}.$$

Think of $N_r(A)$ as the territorial border of A.

Definition 6.6
Let (X, d) be a metric space. The **Hausdorff distance** *$h(A < B)$ between two subsets $A, B \subset X$ is defined as $h(A, B) := \inf\{r : A \subset N_r(B) \text{ and } B \subset N_r(A)\}$.*

The Hausdorff distance h defines a metric on the set of nonempty compact subsets of (X, d), see [Ca]. Note that

$$h(A, B) < r \quad \Leftrightarrow \quad A \subset N_r(B) \;\wedge\; B \subset N_r(A).$$

6.4.2 A compactness condition.

In this section we put a compactness condition on the configuration space of data sets. It consists of two ingredients. Suppose that $\{p_1, \ldots, p_n\}$ denotes the underlying point set of some data set $\gamma_n \in CDA_n$. First we restrict the domain of $\{p_1, \ldots, p_n\}$ to a closed disk $\mathcal{U}$. Moreover, we add four camera points c_1, c_2, c_3 and c_4 far away outside $\mathcal{U}$. Lemma 6.8 shows that we can choose $\mathcal{U}$ and c_1, c_2, c_3 and c_4 in such a way that it is guaranteed that the Voronoi diagram of γ_n, extended with c_1, c_2, c_3 and c_4, changes inside some compact subset of the plane only, provided that we perturb $\{p_1, \ldots, p_n\}$ within $\mathcal{U}$.

For $\mathcal{U}$ we choose the unit disk, that is $\mathcal{U} := \{x \in \mathbb{R}^2 \mid \|x\| \leq 1\}$.

Definition 6.7
Let $\gamma_n \in CDA_n$ be a set of data representing n generators $\{p_1, \ldots, p_n\}$ in $\mathcal{U}$ and $\binom{n}{2}$ angles in $\mathbb{R}/2\pi\mathbb{Z}$ between those generators. Let furthermore

$$\begin{aligned} c_1 &= (-N, 0), & c_2 &= (0, N), \\ c_3 &= (N, 0), & c_4 &= (0, -N). \end{aligned}$$

for some $N \gg 1$ be the so-called **camera points**. *The* **Voronoi diagram with camera points** *$V_N(\gamma_n)$ is the Voronoi diagram of the data set $\overline{\gamma}_n$, which consists of the generators $\{p_1, \ldots, p_n\} \cup \{c_1, \ldots, c_4\}$ and the $\binom{n+4}{2}$ angles between those generators.*

Lemma 6.8
Let $N > 2 + 2\sqrt{2}$ and let $B_N^C := \{x \in \mathbb{R}^2 \mid d(x, 0) > N\}$. Then $V_N(\gamma_n) \cap B_N^C$ does not change, provided that γ_n is perturbed inside $\mathcal{U}$.

Proof. Let $z = R(\cos\phi, \sin\phi)$ be an arbitrary point in B_N^C. It is enough to show that z is always closer to at least one camera point than to $\mathcal{U}$. Using the symmetry we can assume, without loss of generality, that $0 < \phi \leq \frac{\pi}{4}$. So it is enough to show that $d(z, c_3) < d(z, \mathcal{U})$ or, equivalently, that $d(z, \mathcal{U})^2 - d(z, c_3)^2 > 0$. Now,

$$
\begin{aligned}
d(z, c_3)^2 &= R^2 \sin^2\phi + (N - R\cos\phi)^2, \\
&= R^2 + N^2 - 2NR\cos\phi,
\end{aligned}
$$

is maximal when $\phi = \frac{\pi}{4}$. From now on assume that

$$
d(z, c_3)^2 = R^2 + N^2 - \sqrt{2}NR.
$$

As $d(z, \mathcal{U}) = R - 1$, we have to show that

$$
d(z, \mathcal{U})^2 - d(z, c_3)^2 = (R^2 - 2R + 1) - (R^2 + N^2 - \sqrt{2}NR) > 0.
$$

Substituting $R = N + X$, where $X > 0$, gives that

$$
d(z, c_3)^2 - d(z, \mathcal{U})^2 = N((\sqrt{2} - 1)N - 2) + (\sqrt{2}N - 2)X + 1.
$$

Now, $(\sqrt{2} - 1)N - 2 > 0$, whenever $N > 2 + 2\sqrt{2}$, while $(\sqrt{2}N - 2) > 0$ whenever $N > \sqrt{2}$. This proves the lemma. ∎

6.5   Continuity of the Voronoi map.

6.5.1   The Voronoi map.

In our original configuration space, generators live in $\mathbb{R}^2$. But under the compactness condition above, generators all live on the unit disk $\mathcal{U}$ and we have four additional camera points, c_1, c_2, c_3 and c_4. That is, we have a restricted configuration space

$$
CDA_n^{\mathcal{U}} := \{c_1, \ldots, c_4; p_1, \ldots, p_n; \alpha_{12}, \ldots, \alpha_{(n+3)(n+4)}\}, \quad p_i \in \mathcal{U}; \ \alpha_{ij} \in \mathbb{R}/2\pi\mathbb{Z}.
$$

Let $V(n) \subset P(\mathbb{R}^2)$ be the set of one-skeletons of Voronoi diagrams, defined by data sets $\gamma_n \in CDA_n^{\mathcal{U}}$. Denote by d be the Euclidean metric on $CDA_n^{\mathcal{U}}$ and by h the Hausdorff metric on $P(\mathbb{R}^2)$. We show that the map f_V,

$$
\begin{aligned}
f_V: \quad (CDA_n^{\mathcal{U}}, d) &\rightarrow (V(n), h), \\
\gamma_n &\mapsto V(\gamma_n),
\end{aligned}
$$

that maps a data set γ_n to its Voronoi diagram, is continuous. By definition, this means that we have to show that

$$
\forall \gamma_n \in CDA_n^{\mathcal{U}}, \ \forall \epsilon > 0, \ \exists \delta > 0, \ \forall \eta_n \in CDA_n^{\mathcal{U}}
$$
$$
d(\gamma_n, \eta_n) < \delta \quad \Rightarrow \quad h(V(\gamma_n), V(\eta_n)) < \epsilon. \tag{6.1}
$$

In Theorem 6.1 we have proved that

$$\forall(\gamma_n, x \in V(\gamma_n)),\ \forall \epsilon > 0,\ \exists \delta > 0 :\ d(\gamma_n, \eta_n) \leq \delta \ \Rightarrow\ d(x, V(\eta_n)) \leq \epsilon.$$

In this formula, δ really depends on both the particular position of x on $V(\gamma_n)$ and the particular diagram $V(\gamma_n)$. The uniform version of this claim is given by

$$\forall \epsilon > 0, \quad \exists \delta > 0, \quad \forall(\gamma_n, x \in V(\gamma_n)) :$$
$$d(\gamma_n, \eta_n) \leq \delta \quad \Rightarrow \quad d(x, V(\eta_n)) \leq \epsilon. \qquad (6.2)$$

Remark 6.9
It is clear that (6.2) does not hold if we regard the one-skeleton of Voronoi diagrams that correspond with data sets that do not contain the camera points. Suppose for example that our data consist of two points p and q that are close to each other. If we fix p, move q slightly, thereby changing α_{pq} slightly as well, some point that was far away on the bisector $B(p, q)$ before moving q, is on a big distance from $B(p, q)$ after disturbance.

6.5.2 $\{(\gamma_n, x) \mid x \in V(\gamma_n))\}$ is closed in $CDA_n \times \mathbb{R}^2$.

In this section we show that the set $\{(\gamma_n, x) \mid x \in V(\gamma_n)\}$ is closed in $CDA_n \times \mathbb{R}^2$. Or, equivalently, that the complement $\{(\gamma_n, x) \mid x \notin V(\gamma_n)\}$ is open. But this means exactly that we have to prove the following:

$$\forall \gamma_n,\ x \notin V(\gamma_n),\ \exists \epsilon > 0,\ \exists \delta > 0 :\ d(\gamma_n, \eta_n)\ <\ \delta \ \Rightarrow\ d(x, V(\eta_n))\ >\ \epsilon.$$

We do so in the following lemma.

Lemma 6.10
Let γ_n be a data set representing n generators in the plane and $\binom{n}{2}$ angles between those generators. Suppose that x is in the interior of Voronoi cell $V(p)$, for some generator $p \in \gamma_n$. Then there exists $\epsilon > 0$ and $\delta > 0$ such that the following holds: if we perturb γ_n by not more then δ, the one-skeleton of any perturbed diagram is at distance at least ϵ of x.

Proof. [Determine ϵ.] Start with some $\epsilon > 0$. For every pair of generators (p, q) whose bisector $B(p, q)$ does not pass through x we set

$$\epsilon \ = \ \min(\epsilon, \tfrac{1}{3} d(x, B(p, q))).$$

This ensures that $d(x, B(p, q))\ >\ 2\epsilon$ for every such pair (p, q).

[Determine $\delta(\epsilon)$.] As a consequence, we can apply Lemma 6.4 for every pair of generators (p, q) whose bisector $B(p, q)$ does not pass through x. The lemma gives us δ_{pq} such that any perturbation of the data by δ_{pq} implies that $d(x, B(p, q))\ >\ \epsilon$ after perturbation. Let $\delta := \min_{(p,q)} \delta_{pq}$ be the minimum of all these δ_{pq}.

[**Show that this δ works.**] Suppose that the claim of the lemma is not true. This means that after perturbation there are generators q_1 and q_2 such that both

$$B_\epsilon(x) \cap V(q_1) \neq \emptyset, \qquad \text{and} \qquad B_\epsilon(x) \cap V(q_2) \neq \emptyset,$$

hold. It follows that, after perturbation, $B(q_1, q_2) \cap B_\epsilon(x) \neq \emptyset$. Because of our choice of δ and ϵ this implies though that $x \in B(q_1, q_2)$ before perturbation. As $x \in V(p)$, before perturbation, we conclude that $q_1 \neq p$ and $q_2 \neq p$. But then there exists $y \in B_\epsilon(x)$ such that

$$y \in h(p, q_1),$$

before perturbation, and

$$y \in h(q_1, p),$$

after perturbation. This in contradiction with Corollary 6.5 however. ∎

6.5.3   Proof of the continuity.

In this section we prove the following theorem:

Theorem 6.11
Let $\gamma_n \in CDA_n^{\mathcal{U}}$. Then the Voronoi diagram $V(\eta_n)$ of any data set $\eta_n \in CDA_n^{\mathcal{U}}$ that is Euclidean-close to γ_n, is Hausdorff-close to the Voronoi diagram $V(\gamma_n)$:

$$\forall \epsilon > 0, \; \exists \delta > 0, \; : \; d(\gamma_n, \eta_n) \leq \delta \;\; \Rightarrow \;\; h(V(\gamma_n), V(\eta_n)) \leq \epsilon$$

Proof. The proof is divided into a number of steps.

Step 1.   It is enough to prove the following assertion.

$$\forall \epsilon > 0, \quad \exists \delta > 0, \quad \forall \gamma_n \in \mathcal{U}, \quad \forall x \in V(\gamma_n), \quad \forall \eta_n \in \mathcal{U}:$$
$$d(\gamma_n, \eta_n) \leq \delta \quad \Rightarrow \quad d(x, V(\eta_n)) \leq \epsilon. \qquad (6.3)$$

In (6.3) the implication holds for all choices of x on $V(\gamma_n)$. This implies that in fact

$$d(\gamma_n, \eta_n) \leq \delta \quad \Rightarrow \quad d(x, V(\eta_n)) \leq \epsilon \qquad \forall x.$$

This together with the fact that we can interchange γ_n and η_n defines the Hausdorff distance and therefore implies the claim of the theorem.

Step 2.   Construct a convergent sequence.
Suppose that Assertion 6.3 does not hold. That means that the negation must be true, where we replace $\forall \delta$ by $\forall m$:

$$\exists \epsilon > 0 : \; \forall m \in \mathbb{N}, \; \exists (\gamma_n, x \in V(\gamma_n)), \; \exists \eta_n :$$
$$(d(\gamma_n, \eta_n) \leq \frac{1}{m} \quad \wedge \quad d(x, V(\eta_n)) > \epsilon). \qquad (6.4)$$

Fix such ϵ and call it ϵ_0. We can find for every $m \in \mathbb{N}$ a triple t_m

$$t_m \quad := \quad (\gamma_n^m, \ x^m \in V(\gamma_n^m), \ \eta_n^m), \tag{6.5}$$

such that Assertion 6.4 is true.

Step 3. $\mathbf{x^m \in B_N}$, $\forall \mathbf{m}$.
Recall that B_N denotes the disk $B_N = \{x \in \mathbb{R}^2 \mid d(x,0) \leq N\}$. Suppose that $x^m \notin B_N$ for some $x^m \in V(\gamma_n^m)$. Then Lemma 6.8 tells us that $x^m \in V(\eta_n)$, for all $\eta_n \in CDA_n^{\mathcal{U}}$. So Assertion 6.4 can never be true.

Step 4. Remarks on compactness.
γ_n and η_n both live in the compact set

$$\mathcal{U}^n \times \{c_1, c_2, c_3, c_4\} \times (\mathbb{R}/2\pi\mathbb{Z})^{\binom{n+4}{2}}.$$

We have proved in Lemma 6.10 that the set $\{(\gamma_n, x) \mid x \in V(\gamma_n)\}$ is closed. This means that we get a sequence (t_m) of triples of the form (6.5) that live on a compact set. So, (t_m) has some convergent subsequence $t_m(k)$ that converges to, say, $(\tilde{\gamma}_n, \tilde{x}, \tilde{\eta}_n)$. Note that $\tilde{x} \in V(\tilde{\gamma}_n)$.

Step 5. A contradiction by combining Assertion 6.4 and Theorem 6.1.
Because of convergence, $V(\tilde{\gamma}_n) = V(\tilde{\eta}_n)$, so $\tilde{x} \in V(\tilde{\eta}_n)$. Apply Theorem 6.1 with

- $\tilde{x} \in V(\tilde{\eta}_n)$,

- $\epsilon = \frac{1}{3}\epsilon_0$.

The theorem gives us a δ_0 such that

$$d(\tilde{\eta}_n, \theta_n) \ < \ \delta_0 \quad \Rightarrow \quad d(V(\theta_n), \tilde{x}) \ < \ \tfrac{1}{3}\epsilon_0. \tag{6.6}$$

Choose m so big that the following condition hold:

$$d(\ (\gamma_n^m, x^m, \eta_n^m), (\tilde{\gamma}_n, \tilde{x}, \tilde{\eta}_n) \ ) \quad < \quad \min(\delta_0, \tfrac{1}{3}\epsilon_0). \tag{6.7}$$

We show that this leads to a contradiction on $d(x^m, V(\eta_n^m))$.
   (i)   The sequence t_m is constructed in such a way from Assertion 6.4 that

$$d(x^m, V(\eta_n^m)) \quad > \quad \epsilon_0. \tag{6.8}$$

  (ii)   We have chosen m so big, (6.7), that

$$d(x^m, \tilde{x}) \quad < \quad \tfrac{1}{3}\epsilon_0. \tag{6.9}$$

 (iii)   But m is also big enough such that $d(\tilde{\eta}_n, \eta_n^m) \ < \ \delta_0$. Therefore we conclude from (6.6), with $\theta_n := \eta_n^m$, that

$$d(V(\eta_n^m), \tilde{x}) \quad < \quad \tfrac{1}{3}\epsilon_0. \tag{6.10}$$

Now (6.9) combined with (6.10) gives a contradiction with (6.8).

This proves the theorem.   ∎

Chapter 7

Clickable Voronoi diagrams and hook compactifications.

We define a compactification space XAH_n of the configuration space of n distinct points in the plane, by considering data elements of pairs of points and triples of points. For every pair of points we write down the angle mod π between the two points, and for every ordered triple (p_i, p_j, p_k) of points, we specify a hook h_{ij}^{ik}. This hook expresses how to construct the point p_k given p_i and p_j. Now XAH_n is defined as the closure of the image space of all angles and hooks on n distinct points. We show that configurations that are added by taking the closure have a natural nested structure, easily revealed by analyzing the hooks. The main result of this chapter is an explicit construction establishing XAH_n as the graph of a function. This construction shows that XAH_n is a smooth manifold. If we replace the angles mod π by angles mod 2π we get a compactification space $XEDAH_n$. This space is isomorphic to the manifold with corners $FM_2(n)$, introduced by Kontsevich-Soibelman. On $XEDAH_n$ we define clickable Voronoi diagrams.

7.1 Fulton-MacPherson related models.

In this chapter we describe a compactification XAH_n of the configuration space of n distinct points in the plane. The basic idea of the compactification consists of considering the geometry of all pairs and all triples of distinct points. In section 7.2 we give an overview of the contents of this chapter: it describes in an informal way the construction and some properties of this compactification XAH_n. And it explains how clickable Voronoi diagrams are related to XAH_n. Sections 7.3 to 7.10 contain the mathematical constructions referred to in Section 7.2, while Section 7.11 is devoted to concluding remarks. We start however in this section by recalling the famous compactification due to Fulton an MacPherson, and by presenting a related compactification as described by Kontsevich and Soibelman. These two

compactifications have some important features that we mimic and extend in our compactification XAH_n.

7.1.1   The Fulton-MacPherson compactification.

The following compactification is defined in terms of a nonsingular algebraic variety. The authors note however, cf. [FM], page 188/189, that the same constructions work for complex manifolds, as well as for real manifolds. So, let X be a nonsingular algebraic variety, and let

$$CONF_n(X) \quad = \quad \{(p_1, \ldots, p_n) \in X^n \mid p_i \neq p_j \text{ if } i \neq j\},$$

be the configuration space of n distinct labeled points in X, cf. Definition 5.4. For a subset S of the set of labels $\{1, \ldots, n\}$, the small diagonal Δ_S is given by

$$\Delta_S \quad = \quad \{(p_1, \ldots, p_n) \in CONF_n(X) \mid p_{i_1} = \cdots = p_{i_m} \text{ for any } i_j \in S\}.$$

For any such S with at least two points, let $\mathrm{Bl}_\Delta(X^S)$ be the blow-up of X^S along Δ_S. For the definition of blow-up, consult [Ha]. There is a natural embedding

$$CONF_n(X) \quad \subset \quad X^n \times \prod_{|S| \geq 2} \mathrm{Bl}_\Delta(X^S).$$

The **Fulton-MacPherson compactification** $X[n]$ is defined as the closure of $CONF_n(X)$ in this product. We list some properties that are stated respectively as Theorems 1, 2 and 3 in [FM]. The definition of divisor can be found in [Ha].

1. $X[n]$ is nonsingular.
2.   For $n \geq 2$, $X[n]$ is the closure of $CONF_n(X)$ in the product of the $\mathrm{Bl}_\Delta(X^S)$ for $S \subset \{1, \ldots, n\}$ of cardinality 2 and 3.
3.   For each $S \subset \{1, \ldots, n\}$ with at least two elements, there is a nonsingular divisor $D(S) \subset X[n]$ such that
     (i)   The union of these divisors is $X[n] \backslash CONF_n(X)$.
     (ii)   An intersection of divisors $D(S_1) \cap \cdots \cap D(S_r)$ is nonempty iff the sets S_k are **nested** in the sense that each pair S_i and S_j is either disjoint or one is contained in the other.

Important for us is the 'first geometric description' of $X[n]$, as presented in Section 1 of [FM]. A configuration in $X[n]$ is called **degenerate**, if not all points in the configuration are distinct. Any such configuration c is described by a set of data given the locations of the points, and if two or more points coincide at say x, then a **screen** is specified for the set $S \subset \{1, \ldots, n\}$ of labels of the coinciding points. The data elements describing a screen for S at x consist of a labeled set of points x_a in the tangent space T_x of x, such that not all points in x_a are equal. This process is repeated for x_a until all points in the configuration c are separated in some screen. Think of repeatedly zooming in at clusters of points until all points are separated, cf. Figure 7.9. The divisor $D(S)$ of $X[n]$, mentioned in the property above consists of all configurations c in $X[n]$ that have a screen that contains exactly the points x_a for a in S.

7.1.2   The Fulton-MacPherson operad.

In [Ko] and [KS] the **Fulton-MacPherson operad** FM_d is discussed. A definition of operad can be found in [Ko]. As we consider only point configurations in $\mathbb{R}^2$, we set $d = 2$ in the sequel. The operad $FM_2 = \{FM_2(n)\}_{\geq 0}$ is defined as follows, cf. [KS]:

1. $FM_2(0) := \emptyset$.
2. $FM_2(1) :=$ point.
3. $FM_2(2) := \mathbf{conf}_2 = S^1$.
4.   For $n \geq 3$, the space $FM_2(n)$ is a manifold with corners, its interior is $\mathbf{conf}_n$, and all boundary strata are certain products of copies of $\mathbf{conf}_{n'}$ for $n' < n$.

A **manifold with corners** is a topological space that is locally homeomorphic with $\mathbb{R}^n_{\geq 0}$. The space $FM_2(n)$, $n \geq 2$ is defined explicitly as follows.

Definition 7.1
For $n \geq 2$, the manifold with corners $FM_2(n)$ is the closure of the image of $\mathbf{conf}_n$ in the compact manifold $(S^1)^{\binom{n}{2}} \times [0, +\infty]^{6\binom{n}{3}}$ under the map

$$[(p_1, \ldots, p_n)] \quad \mapsto \quad ((\alpha_{ij})_{1 \leq i < j \leq n}, \beta_{ij}^{ik}),$$

where i, j, and k are pairwise distinct indices, $\alpha_{ij} \in \mathbb{R}/2\pi\mathbb{Z}$, and $\beta_{ij}^{ik} = \frac{|p_i - p_k|}{|p_i - p_j|}$.

That is, Kontsevich and Soibelman define the space FM_2 in terms of data elements for pairs and triples of points in any reduced configuration $c \in \mathbf{conf}_n$: for any pair of points they write down the directed angle between the two points, while for every ordered triple (p_i, p_j, p_k) of points they specify the ratio β_{ij}^{ik} of the line segments $p_i p_k$ and $p_i p_j$.

7.1.3   Combining the models.

From the Fulton-MacPherson compactification we borrow the screen model, while from Kontsevich-Soibelman we borrow the angles and ratios. We extend, however, the ratios to hooks, by marking both the ratio β_{ij}^{ik} of the line segment $p_i p_k$ and $p_i p_j$ and the angle α_{ij}^{ik} between the line segments. In this way every hook has two representatives. One with a positive ratio β_{ij}^{ik} and one with a negative 'ratio' β_{ij}^{ik}. In the latter case we just add π to the hook angle α_{ij}^{ik}. These two distinct representatives are identified by an equivalence relation $\sim_k$. This will be important for getting a smooth model. Another adjustment that we make for obtaining smoothness is that we write down the angle between two distinct points up to multiples of π instead of up to 2π. To summarize, we get a map

$$\psi_{AH_n} : \mathbf{conf}_n(\mathbb{R}^2) \quad \to \quad AH_n := (\mathbb{R}/\pi\mathbb{Z})^{\binom{n}{2}} \times (([-\infty, \infty] \times \mathbb{R}/2\pi\mathbb{Z})/\sim_k)^{6\binom{n}{3}},$$

and define XAH_n as the closure of the image of $\mathbf{conf}_n$ in AH_n. The data elements and spaces introduced so far are discussed in detail in Section 7.3. In section 7.4 we

show that we can associate with any $x \in XAH_n$ a nested set of subsets of $\{1, \ldots, n\}$. This is done by analyzing the ratios. It turns out that for degenerate configurations certain ratios equal zero. If β_{ij}^{ik} is close to zero, then the length of the line segment $p_i p_k$ is very small compared to the length of the line segment $p_i p_j$. We then say that p_i and p_k coincide with respect to p_j.

Combinations of compactifications of configuration spaces and combinatorics receive a lot of attention in recent years. Elegant examples can be found in [De1] and [De2].

7.2   Informal introduction.

In this section we introduce most of the terminology that we use in the rest of the chapter, in a more intuitive setting.

7.2.1   Screens, clusters and nests.

Suppose we are looking at a plane containing $n \geq 2$ **sites**. By sites we mean points, but in order to be able to use points in other contexts, we prefer the word sites. When we see all n sites at first glance we are happy, but when we seem to see fewer sites we tend to look more closely. That is, we zoom in at a site in order to see if it is really one site, or in fact consists of a number of sites. At the same time we will lose sight of other sites. We repeat this procedure until we have found all n sites.

Imagine that the plane is in fact a computer **screen**. If some sites coincide, that is, if they form a **cluster**, we click on the cluster. Another screen pops up that contains exactly the sites in the cluster. If we click on a site and nothing happens, we know that at the level we are looking at, this site does not coincide with another site. So every non-trivial cluster corresponds to a screen. By continuing to click we always find all n sites. Label the sites with labels from 1 to n and write down the labels that are visible in every screen. This produces a **nest**, a nested set of subsets of $\{1, \ldots, n\}$, i.e. the clusters. If no sites coincide the nest consists of the set $\{1, \ldots, n\}$ only.

The **top screen** is the first screen we see. It contains all sites, but maybe not all sites are separated. We organize things in such a way that every screen contains at least 2 non-coinciding sites. That is, in every screen at least two sites are separated. We are not interested where in the plane a screen focuses. But we do want to know the exact relative position of the sites. We conclude that we consider site sets up to **scaling** and **translation**.

7.2.2   Pinpointing sites.

We want to describe such a family of screens filled by sites. A naive approach is by listing the screens together with the coordinates of the sites that occur in each screen. This may describe the situation well when the sites do not move, but assume

that two sites p_i and p_j that did coincide first in some screen start moving apart. This could change the relative positions of the sites in all screens were both p_i and p_j occur, but it is not at all clear how a change in coordinates in one screen should influence coordinates in other screens.
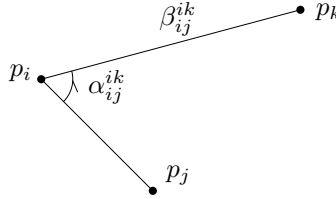

Figure 7.1: The hook $h_{ij}^{ik} = (\beta_{ij}^{ik}, \alpha_{ij}^{ik})$ hinged at p_i from p_j to p_k. The little arrow indicates the positive direction.

Instead of marking coordinates of the sites involved, we mark the **angle** α_{ij} between any two sites p_i and p_j and the **hook** h_{ij}^{ik} between any ordered triple (p_i, p_j, p_k) of sites. A hook h_{ij}^{ik} consists of an angle α_{ij}^{ik} and a ratio β_{ij}^{ik}. Consider Figure 7.1. Suppose that the sites p_i and p_j, thus the leg $\overline{p_i p_j}$ have been constructed. If we rotate p_j by angle α_{ij}^{ik} with respect to center of rotation p_i and multiply the image of the rotation by β_{ij}^{ik}, we get p_k.

Using these hooks and angles we can fill a screen with sites. Suppose that for a set of distinct sites $p_1, \ldots, p_n$ we know all hooks and angles between the sites. We show how to fill a screen with the sites. We put p_1 in the origin, as we do not care about translation. As we do not care about scaling either, we put p_2 at distance 1 of p_1. We use the angle α_{12} to assure that the line through p_1 and p_2 has the right direction, that is, we set $p_2 = (\cos \alpha_{12}, \sin \alpha_{12})$. All other sites p_i, for $i \in 3, \ldots, n$, can be constructed as in Figure 7.1 by a hook h_{12}^{1i}.

7.2.3 Degenerate configurations.

Let $CONF_n$ be the configuration space of n distinct sites in the plane and let ψ_{AH_n} be the map that maps an element $c \in CONF_n$ to the $\binom{n}{2}$ angles and the $6\binom{n}{3}$ hooks between the sites. In fact we embed the image space in a slightly bigger space AH_n, allowing also negative ratios. The space that we are really interested in is the closure of the image of $CONF_n$ in AH_n. We call this space XAH_n. Most points $x \in XAH_n$ can be realized as image points of a configuration $c \in CONF_n$, that is $x = \psi_{AH_n}(c)$. We call a point $x \in XAH_n$ **degenerate** if $x \in \overline{\psi_{AH_n}(CONF_n)} \backslash \psi_{AH_n}(CONF_n)$. It turns out that the degenerate points are exactly those points $x \in XAH_n$ such that at least one ratio coordinate $\beta_{ij}^{ik}(x) = 0$.

We go back to the nests and screens. By analyzing the set of all $\beta_{ij}^{ik}(x)$ in some point $x \in XAH_n$, we can associate a nest $C(x)$ with x. If no $\beta_{ij}^{ik}(x) = 0$, we think of x as

the image of a configuration where all sites are distinct, and in this case we associate the nest $\{\{1, \ldots, n\}\}$ with x. And with this nest we associate exactly one screen where all n sites occur and are distinct. In the other case at least one $\beta_{ij}^{ik}(x) = 0$. As we can introduce $\beta_{ij}^{ik} = \frac{|p_i - p_k|}{|p_i - p_j|}$ for distinct sites, we think of $\beta_{ij}^{ik}(x) = 0$ as if p_i is very close to p_k as seen from p_j. But this means exactly that p_i and p_k form a cluster with respect to p_j. In fact, one can prove that the set $\mathcal{C}(x)$ consisting basically of all sets $C_{ij} = \{k \mid \beta_{ij}^{ik} \neq 0\} \cup \{i, j\}$ defines a nest on $\{1, \ldots, n\}$. So $\mathcal{C}(x)$ is the nest that corresponds to $x \in XAH_n$. For every cluster in $\mathcal{C}(x)$ with at least two elements we define a screen as a copy of the plane.

7.2.4　Factorizing XAH_n.

Fix some $x \in XAH_n$. By analyzing the C_{ij} as explained above, we associate a family of screens with x denoted by **x-screens**. Our next goal is to fill the x-screens. The main idea of working with screens is as follows: the site set $p_1, \ldots, p_n$ that we think of as corresponding to some degenerate configuration $q \in XAH_n$, should be separated completely, somewhere in the hierarchy of x-screens. This puts a requirement on those points $q \in XAH_n$ that we can use to fill the x-screens with: the point q should not be more nested than x itself, in the following sense: if $\beta_{ij}^{ik}(x) \neq 0, \infty$, then also $\beta_{ij}^{ik}(q) \neq 0, \infty$. Another way to put this: we are not allowed to move down in the stratification with respect to the coincidence of sites. We do not need all $\binom{n}{2} + 6\binom{n}{3}$ data elements

$$(\alpha_{ij}(q))_{1 \leq i < j \leq n}, h_{ij}^{ik}(q)), \qquad i, j, k, \text{ pairwise distinct indices,}$$

for filling the x-screens with sites $p_1(q), \ldots, p_n(q)$, given some suitable $q \in XAH_n$. We just need enough data elements to pinpoint each site once. By exploiting the nested structure of x, we can avoid bad choices in picking the data elements. We do not want to be confronted with legs of length $0 \cdot \infty$ for example. These prerequisites result in a factor $\mathbf{Dom}_n(x)$ of data elements of XAH_n that are both suited and enough to fill the x-screens, given some suitable $q \in XAH_n$. Note that the choice of the data elements depends on x, although we use of course the data elements of q itself in order to fill the x-screens with sites $p_1(q), \ldots, p_n(q)$.

7.2.5　The hooked tree.

Again by using the nested structure of our fixed $x \in XAH_n$, we can define a partial order on the labels $1, \ldots, n$. This partial order tells in which order exactly we have to add the q-sites $p_1(q), \ldots, p_n(q)$ in the x-screens. It turns out that with every label $i \in 1, \ldots, n$ we can associate an **x-tag** $l_x(p_i)$. Such an x-tag is a pointer to one coordinate of $\mathbf{Dom}_n(x) \subset XAH_n$. As any such coordinate is either an angle or a hook, we conclude that every label i corresponds to a geometric construction (construct p_i as the end of a line segment of a given angle, or construct p_i as the end point of a given hook) that tells how to construct p_i.
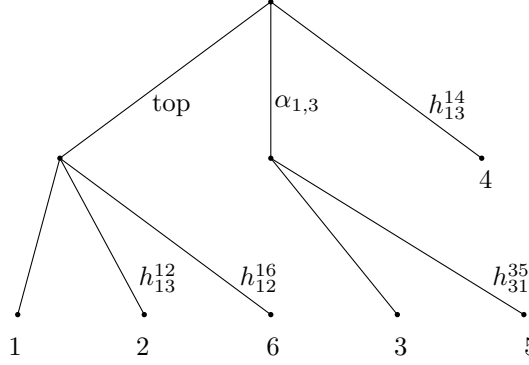
Figure 7.2: The hooked tree for the nest $< \{1, 2, 6\}, \{3, 5\} >$.

We store the set of x-clusters in a tree. The vertices of the tree are exactly the x-clusters. Two x-clusters are connected by an edge if one cluster is maximal in the other. Some edges are labeled by x-tags. This is done in such a way that if going up in the tree from leaf i, the first x-tag encountered points exactly to that hook or angle that is used to construct p_i in the set of x-screens. This tree is called the **hooked tree**.

7.2.6 Filling screens.

We discuss the use of the partial order a bit further. Our setup is such that in each x-screen separation occurs. Fix some x-screen S. As mentioned above, any x-screen S corresponds to some x-cluster C_S. Assume that all x-screens T, such that the cluster C_T contains C_S, have already been filled. We say that such screens T are **above** S. The x-screen S should exactly contain the sites with labels in the x-cluster C_S after filling. Moreover, the sites corresponding to the maximal subclusters of S are separated in the x-screen S. Let C_1 be the maximal subcluster of S with smallest minimal label i and let C_2 be the maximal subcluster with second smallest minimal label. The first site we put in S is the site p_i, that we place at the origin. The second site to construct is the site p_j, that we place at distance 1 of p_i. The angle that the line segment $p_i p_j$ makes with the positive axis is the so-called **screen orientation** $\mathcal{O}_S$ of S. It is defined recursively in terms of the screens above S. Note that by now we have constructed one leg $p_i p_j$ in S. All other sites in S can be constructed using hooks.

Suppose, for instance, that we want to construct all sites in some maximal subcluster $C_k \neq C_1, C_2$, where k is the minimal label of C_k and therefore $k > i, j$. We construct p_k by means of a hook h_{ij}^{ik}. One can think of this hook as a **hook on scale**, as p_i, p_j and p_k are separated at the same level. Note that k is automatically minimal in the maximal subcluster of C_k that has smallest minimal label. Let $m \in C_k$, with

$m > k$, be minimal in the second maximal subcluster of C_k. We construct p_m using h_{ki}^{km}. This is a different type of hook as p_k and p_m are separated one step deeper in the nest structure. Think of this type of hook as a **explosion hook**: for x itself $|\beta_{ki}^{km}(x)| = 0$, as p_k and p_m 'coincide with respect to p_i'. If we take an arbitrary point $q \in \mathbf{Dom}_n$, then $|\beta_{ki}^{km}(q)| \geq 0$, and if $|\beta_{ki}^{km}(q)| > 0$ we could say that an explosion occurs, as suddenly p_k and p_m do not coincide anymore with respect to p_i.

7.2.7 XAH_n is locally the graph of a function.

One purpose of this setup is to minimize the dimension of the factor $\mathbf{Dom}_n(x)$, that is, we want to use as few data elements of XAH_n for filling the x-screens as possible. That we cannot do better is shown by Lemma 7.31 that proves that the dimension of the factor $\mathbf{Dom}_n(x)$ equals the dimension of the reduced configuration space $\mathbf{conf}_n$. Given a set of filled x-screens, we can just read off angles and hooks from the screens. Theorem 7.58 proves that filling screens using data elements is consistent with reading off data elements, in the sense that we get back the data elements that we started with. Note that besides the data elements in the $\mathbf{Dom}_n(x)$ factor, we can also read off the data elements in the complementary factor $\mathbf{Rng}_n(x)$ of $\mathbf{Dom}_n(x)$ in the space of all angles and hooks on n points, AH_n. This shows that XAH_n can be written as the graph of some function $\mathbf{read} : \mathbf{Dom}_n(x) \to \mathbf{Rng}_n(x)$. As a consequence, we can prove in Theorem 7.61 that XAH_n is a smooth manifold. In fact there are some extra requirements on the structure presented to obtain smoothness that we did not discuss here. Details can be found in Sections 7.3 to 7.9.

7.2.8   Connection with Kontsevich-Soibelman.

In [KS], see also Section 7.1.2, Kontsevich and Soibelman describe a manifold with corners $FM_2(n)$ that is closely related to our smooth manifold XAH_n. The exact relation is given in Theorem 7.65 that describes a map $f : FM_2(n) \to XAH_n$ together with the fibers of f. Due to this close relation we can use the construction of the filled x-screens for points $x \in FM_2(n)$ as well. This is important in the following application. For an overview of the compactifications introduced so far, consult Table 7.1.

7.2.9   Adding Voronoi diagrams in the x-screens.

We apply the construction of filled x-screens to the analysis of Voronoi diagrams of points sets that may include coinciding points. We proceed by associating a Voronoi diagram to any point $x \in FM_2(n)$. First, consider some non-degenerate point $x \in FM_2(n)$. Then by definition, as in the XAH_n case, x can be expressed as image of some configuration $c \in CONF_n$. As no $\beta_{ij}^{ik}(x) = 0$ for a non-degenerate $x \in FM_2(n)$, there is exactly one x-screen associated with x, the top screen, that contains all sites $p_1(x), \ldots, p_n(x)$ in such a way that all sites are distinct. The

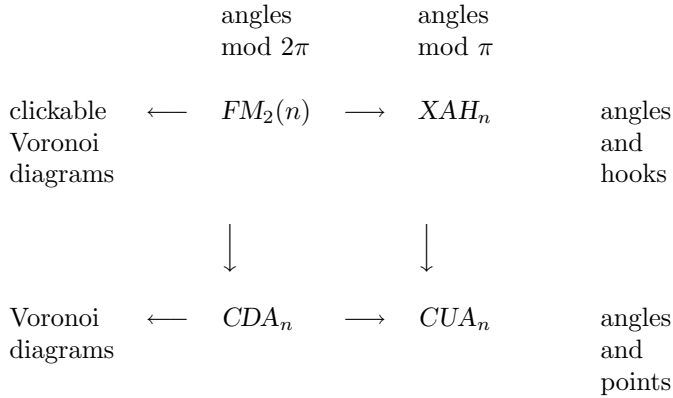|	angles mod 2π	angles mod π	
clickable Voronoi diagrams	$\longleftarrow$ $FM_2(n)$ $\longrightarrow$	XAH_n	angles and hooks
	$\downarrow$	$\downarrow$	
Voronoi diagrams	$\longleftarrow$ CDA_n $\longrightarrow$	CUA_n	angles and points

Table 7.1: Overview of compactifications.

Voronoi diagram $V_{FM}(x)$ associated to x in this case is the Voronoi diagram of the n sites in the top screen.

Next assume that x is a degenerate element of $FM_2(n)$. Suppose that we have filled the x-screens with the x-sites $p_1(x), \ldots, p_n(x)$ as described above. In this case, there is more then one x-screen, but it is guaranteed that in any x-screen S exactly those clusters are separated that are maximal subclusters of the cluster C_S. We define a Voronoi diagram $V_{FM}(x)$ in terms of the x-filled x-screens in two steps. In the first step we add the classic Voronoi diagram of the maximal subclusters of C_S to any x-screen S. This is called the initialization step. In the so-called completion step we recursively add the completed diagrams of all screens below S to S for all x-screens S. This is done as follows. A non-trivial cluster is a cluster that consists of at least two sites. Any non-trivial maximal cluster M of S corresponds to an x-screen S_M that is directly below S. We paste the completed Voronoi diagram $V_{FM}(S_M)$ of S_M into the Voronoi cell of M in the initialized Voronoi diagram $V(S)$.

This gives us a **clickable** Voronoi diagram $V_{FM}(x)$ for any $x \in FM_2$. By clicking on a non-trivial maximal cluster, if present, a screen appears. This screen contains the sites in the cluster and the Voronoi diagram of the sites. Recall the polynomial sites from Chapter 4. By computing ratios and angles we can associate an element $x_S \in FM_2$ to a set $S(t)$ of polynomial sites. Then the completed Voronoi diagram $V_{FM}(T)$ of the top screen T for x_S matches the limit Voronoi diagram of $S(t)$ at $t = 0$.

7.3   Angles and hooks.

We start this section by recalling and introducing data elements defined on pairs and triples of distinct points in $\mathbb{R}^2$. These data elements form the basis of the

compactification of a suitable quotient of the configuration space of n distinct points in the plane that we define later on in this section.

7.3.1　Data elements of pairs and triples of points.

Given two distinct points p_i and p_j, we can determine the angle between the line through p_i and p_j and the positive x-axis. We have done this in Definition 5.1. There we have introduced the directed angle $\alpha_{ij} \in \mathbb{R}/2\pi\mathbb{Z}$ and the undirected angle $\overline{\alpha_{ij}} \in \mathbb{R}/\pi\mathbb{Z}$. We store information on the geometry of three distinct points in hooks, see Figure 7.3.
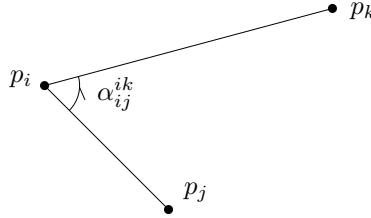
Figure 7.3: The angle α_{ij}^{ik} from p_j to p_k hinged at p_i. The small arrow indicates the positive direction.

Definition 7.2
Let p_i, p_j, and p_k be three distinct points in the plane. The **angle** α_{ij}^{ik} *from p_j to p_k hinged at p_i is given by $\alpha_{ij}^{ik} := \alpha_{ik} - \alpha_{ij} \mod 2\pi$. The* **ratio** β_{ij}^{ik} *from p_j to p_k hinged at p_i is given by*

$$\beta_{ij}^{ik} \quad := \quad \frac{|p_i - p_k|}{|p_i - p_j|}, \qquad \beta_{ij}^{ik} \in (0, \infty).$$

The **hook** h_{ij}^{ik} *from p_j to p_k hinged at p_i equals the ratio together with the angle: $h_{ij}^{ik} := (\beta_{ij}^{ik}, \alpha_{ij}^{ik})$. The point p_i is the* **hinge point** *of the hook h_{ij}^{ik} while the line segments $p_i p_j$ and $p_i p_k$ form its* **legs** *.*

Note that one triple of distinct points gives six hooks.

Remark 7.3
An alternative is to consider hooks in the complex plane. Let p_i, p_j, and p_k be distinct points in $\mathbb{C}$. Note that $\alpha_{ij} = (p_i - p_j)/|p_i - p_j|$. It is easy to check that, with $I = \sqrt{-1}$, it holds that

$$\frac{p_i - p_k}{p_i - p_j} \quad = \quad \beta_{ij}^{ik}\, e^{I \alpha_{ij}^{ik}}\,.$$

7.3.2 Geometric interpretation of the hook h_{ij}^{ik}.

Notation 7.4
Let p and q be points in the plane and $\alpha \in [-\pi, \pi)$ an angle. By $\mathbf{rot}_{\alpha,p}(q)$ denote the image of q under the anti-clockwise rotation around p by angle α. We abbreviate $\mathbf{rot}_{\alpha,(0,0)}$ by $\mathbf{rot}_{\alpha}$.

Suppose we are given two distinct points p_i and p_j, together with a hook h_{ij}^{ik}. The hook h_{ij}^{ik} can be seen as a prescription that tells how to construct the point p_k. Using α_{ij}^{ik}, we first construct p_j', the image of the rotation $\mathbf{rot}_{\alpha_{ij}^{ik},p_i}$, applied to p_j:

$$p_j' \quad = \quad \mathbf{rot}_{\alpha_{ij}^{ik},p_i}(p_j).$$

The half-line that starts in p_i and passes through p_j' contains p_k. The ratio β_{ij}^{ik} fixes the distance from p_k to p_i, thereby fixing p_k itself:

$$p_k \quad = \quad \beta_{ij}^{ik}(p_j' - p_i) + p_i.$$

Summary: we interpret a hook h_{ij}^{ik} as a point rotation followed by a vector multiplication. As a result the leg $p_i p_j$ is transformed into the leg $p_i p_k$.

7.3.3 Negative ratios.
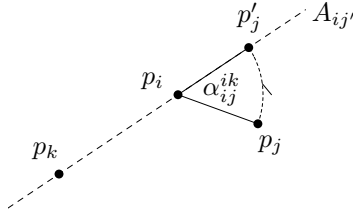
Figure 7.4: The local coordinate axis $A_{ij'}$.

In this section we give sense to 'negative ratios', as illustrated by Figure 7.4. Think of the line through the points p_i and p_j' as a local coordinate axis $A_{ij'}$. The origin on this axis is p_i and the point with coordinate 1 is p_j'. The position of p_k on this axis is given by the coordinate β_{ij}^{ik}. In this setting, any value of β_{ij}^{ik} in the interval $(-\infty, \infty)$ is meaningful: it just indicates the point with coordinate β_{ij}^{ik} on the $A_{ij'}$-axis. Suppose we allow the full interval $(-\infty, \infty)$ for values of β_{ij}^{ik}. Then there are two different ways to construct a point p_k by a hook h_{ij}^{ik}, given the points p_i and p_j. The hooks $(\beta_{ij}^{ik}, \alpha_{ij}^{ik})$ and $(-\beta_{ij}^{ik}, \alpha_{ij}^{ik} + \pi)$ both result in the same point p_k. If identifying $-\infty$ with ∞, we have by now described a map

$$\begin{array}{rccl} \phi_{ijk}: & CONF_3(\mathbb{R}^2) & \to & \mathbb{P}^1 \times \mathbb{R}/2\pi\mathbb{Z} \\ & (p_i, p_j, p_k) & \mapsto & (\beta_{ij}^{ik}, \alpha_{ij}^{ik}), \end{array}$$

under the identification

$$(\beta_{ij}^{ik}, \alpha_{ij}^{ik}) \quad \sim_k \quad (-\beta_{ij}^{ik}, \alpha_{ij}^{ik} + \pi). \tag{7.1}$$

Recall that $CONF_3(\mathbb{R}^2)$ denotes the configuration space of three distinct points in the plane. $\mathbb{P}^1$ denotes the **projective line**. It can be defined as S^1 with antipodal points identified. A point on the projective line can be seen as the coordinate q of a third point on an axis with respect to two fixed points $0 \neq 1$. A homeomorphism from the circle to the line $\mathbb{R} \cup \{\infty\}$ given by **stereographic projection** is shown in Figure 7.5. A line through P intersects the circle in another point, Q, and hits the x-axis in a point R. When P and Q coincide, this line is horizontal, so P is mapped to $R = \infty$, cf. also [R].
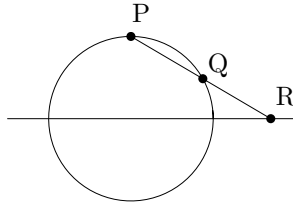
Figure 7.5: Stereographic projection yields a homeomorphism between the circle S^1 and the projective line $\mathbb{RP}^1 = \mathbb{R} \cup \infty$.

7.3.4   Klein bottle K_{ij}^{ik}.
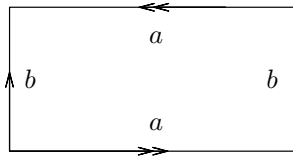
Figure 7.6: The Klein bottle is obtained by identifying sides a and b according to the arrows.

The **Klein bottle** is the quotient space obtained from a rectangle by identifying opposite sides, see Figure 7.6; see also [Mu]. In Figure 7.7 we have depicted another rectangle, but this time we add a description of the axes. For the horizontal axis we take the projective line $\mathbb{P}^1$. The vertical axis is $\mathbb{R}/2\pi\mathbb{Z}$. Recall the identification $(\beta_{ij}^{ik}, \alpha_{ij}^{ik}) \sim_k (-\beta_{ij}^{ik}, \alpha_{ij}^{ik} + \pi)$ introduced in 7.1.

Lemma 7.5
The quotient space $\mathbb{P}^1 \times \mathbb{R}/2\pi\mathbb{Z} \ / \ \sim_k$ defines a Klein bottle.

Proof. Consider Figure 7.7. Any class in $\mathbb{P}^1 \times \mathbb{R}/2\pi\mathbb{Z}/\sim_k$ has a representative in $[0,\infty] \times [0,2\pi]$. On $[0,\infty] \times [0,2\pi]$, there are three identifications.

  (i) The periodicity of directed angles in $\mathbb{R}/2\pi\mathbb{Z}$ is indicated by $\gg$.

 (ii) The identification $(0,\alpha_{ij}^{ik}) \sim_k (0,\alpha_{ij}^{ik} + \pi)$ is indicated by $\triangle$.

(iii) If $(0,\alpha_{ij}^{ik}) \sim_k (0,\alpha_{ij}^{ik} + \pi)$ holds on the compact set $\mathbb{P}^1 \times \mathbb{R}/2\pi\mathbb{Z}/\sim_k$, then also $(\infty,\alpha_{ij}^{ik}) \sim_k (\infty,\alpha_{ij}^{ik} + \pi)$, as any $\beta_{ij}^{ik} = 0$ corresponds to $\beta_{ik}^{ij} = \infty$. This gives the third identification, indicated in Figure 7.7 by $\wedge$.

For identifying the quotient space we are allowed to cut along $\alpha_{ij}^{ik} = \pi$, if we eventually paste back again along the same cut. This cut is indicated by $\propto$. We do cut and paste the bottom half on the top half, applying $\triangle$ and $\wedge$. This results in the cylinder shown on the right of Figure 7.7. On the top of the cylinder, $\gg$ and $\propto$ are directed clockwise, while on the bottom they are directed counterclockwise. This shows that we are in the situation of Figure 7.6. ∎
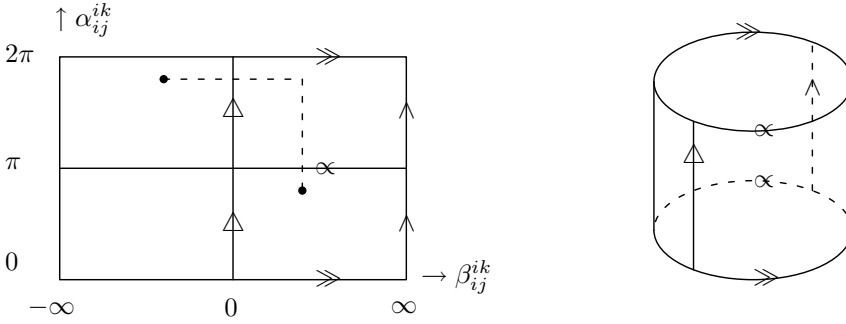
Figure 7.7: The identification $(\beta_{ij}^{ik}, \alpha_{ij}^{ik}) \sim_k (-\beta_{ij}^{ik}, \alpha_{ij}^{ik} + \pi)$.

What is essential for us is that the Klein bottle is a smooth manifold. Note that with every ordered triple (i,j,k) we have associated a Klein bottle K_{ij}^{ik} as the target space of ϕ_{ijk}. We can write ϕ_{ijk} as a composition: $\phi_{ijk} = c_{ijk} \circ h_{ijk}$. The map h_{ijk} maps an ordered triple of distinct points to its hook $(\beta_{ij}^{ik}, \alpha_{ij}^{ik})$, where $\beta_{ij}^{ik} > 0$. The second map, c_{ijk}, maps a hook $(\beta_{ij}^{ik}, \alpha_{ij}^{ik})$ to its class $[(\beta_{ij}^{ik}, \alpha_{ij}^{ik})]$ under the equivalence relation $\sim_k$. We have:

$$
\phi_{ijk}: \quad
\begin{array}{ccccc}
(\mathbb{R}^2)^3 \backslash \Delta_{ijk} & \overset{h_{ijk}}{\to} & [0,\infty] \times \mathbb{R}/2\pi\mathbb{Z} & \overset{c_{ijk}}{\to} & ([-\infty,\infty] \times \mathbb{R}/2\pi\mathbb{Z})/\sim_k, \\
(p_i, p_j, p_k) & \mapsto & (\beta_{ij}^{ik}, \alpha_{ij}^{ik}) & \mapsto & [(\beta_{ij}^{ik}, \alpha_{ij}^{ik})].
\end{array}
$$

Proposition 7.6
The map

$$
c_{ijk}^{-1}: \quad ([-\infty,\infty] \times \mathbb{R}/2\pi\mathbb{Z})/\sim_k \quad \to \quad [0,\infty] \times \mathbb{R}/2\pi\mathbb{Z},
$$

is 2 to 1 if β_{ij}^{ik} equals 0 or $\pm\infty$ and 1 to 1 else.

Proof. The inverse images of c_{ijk} are as follows:

(i) $c_{ijk}^{-1}(\ [(0,\alpha_{ij}^{ik})]\ ) = \{(0,\alpha_{ij}^{ik}),(0,\alpha_{ij}^{ik}+\pi)\}$;

(ii) $c_{ijk}^{-1}(\ [(\infty,\alpha_{ij}^{ik})]\ ) = \{(\infty,\alpha_{ij}^{ik}),(\infty,\alpha_{ij}^{ik}+\pi)\}$;

(iii) $c_{ijk}^{-1}(\ [(-\infty,\alpha_{ij}^{ik})]\ ) = \{(\infty,\alpha_{ij}^{ik}),(\infty,\alpha_{ij}^{ik}+\pi)\}$;

(iv) $c_{ijk}^{-1}(\ [(\beta_{ij}^{ik},\alpha_{ij}^{ik})]\ ) = (\beta_{ij}^{ik},\alpha_{ij}^{ik})$, if $0 < \beta_{ij}^{ik} < \infty$;

(v) $c_{ijk}^{-1}(\ [(\beta_{ij}^{ik},\alpha_{ij}^{ik})]\ ) = (-\beta_{ij}^{ik},\alpha_{ij}^{ik}+\pi)$, if $-\infty < \beta_{ij}^{ik} < 0$.   ■

Remark 7.7

Consider the image on the right in Figure 7.7. If we cut along $\beta_{ij}^{ik} = 0$, that is, along $\triangle$, we obtain a Möbius strip with $\beta_{ij}^{ik} = 0$ on the boundary. Cutting along $\beta_{ij}^{ik} = \infty$, that is, along $\wedge$, leaves us with two pieces joined along $\propto$. This results in a cylinder with $\beta_{ij}^{ik} = 0$ on one boundary component and $\beta_{ij}^{ik} = \infty$ on the other component.

7.3.5   The data map from $\mathbf{conf}_n$ to AH_n.

In this section we describe a map from a set of distinct points in the plane to all angles and hooks between pairs and triples of those points. Recall that in Definition 5.4 we have introduced the reduced configuration space $\mathbf{conf}_n$ as the space of n distinct points in the plane up to scaling and translations. For a representative c of a class $[c] \in \mathbf{conf}_n$, write the following data: for every pair of points $p_i, p_j \in c, i \neq j$, the undirected angle $\overline{\alpha}_{ij} = \overline{\alpha}_{ji}$; for every triple p_i, p_j, p_k of points in c, the six hooks h_{ij}^{ik}, h_{ik}^{ij}, h_{ji}^{jk}, h_{jk}^{ji}, h_{ki}^{ki}, and h_{ki}^{kj}. This gives $\binom{n}{2}$ unordered angles and $6\binom{n}{3}$ hooks. Note that the angles and hooks that we obtain are independent of the choice of a representative of a class $c \in \mathbf{conf}_n$.

Definition 7.8

AH_n *is the space of hooks and angles on n points:*

$$AH_n \quad := \quad (\mathbb{R}/\pi\mathbb{Z})^{\binom{n}{2}} \quad \times \quad (\ \mathbb{P}^1 \times (\mathbb{R}/2\pi\mathbb{Z})\ /\sim_k)^{6\binom{n}{3}},$$

where $\sim_k$ denotes the identification defined in 7.1.

Remark 7.9

Being a direct product of circles and Klein bottles, AH_n is smooth.

In the next definition, we introduce a **compactification** of the reduced configuration space $\mathbf{conf}_n$.

Definition 7.10

The **data map** ψ_{AH_n} *is the map*

$$\begin{aligned}
\psi_{AH_n}: &\quad \mathbf{conf}_n &\rightarrow&\quad AH_n, \\
\psi_{AH_n}: &\quad \mathbf{conf}_n &\rightarrow&\quad (\mathbb{R}/\pi\mathbb{Z})^{\binom{n}{2}} \quad \times \quad (\ \mathbb{P}^1 \times (\mathbb{R}/2\pi\mathbb{Z})/\sim_k\ )^{6\binom{n}{3}}, \\
&\quad [(p_1,\ldots,p_n)] &\mapsto&\quad ((\overline{\alpha_{ij}})_{1\leq i<j\leq n}, (\beta_{ij}^{ik},\alpha_{ij}^{ik})\mid i,j,k \text{ pairwise distinct}),
\end{aligned}$$

and XAH_n is the closure of the image of $\mathbf{conf}_n$ in AH_n.

Alternatively we could allow non-negative ratios only, construct a data map from $\mathbf{conf}_n$ to $(\mathbb{R}/\pi\mathbb{Z})^{\binom{n}{2}} \times ([0,\infty] \times (\mathbb{R}/2\pi\mathbb{Z}))^{6\binom{n}{3}}$, and define XAH_n as the closure of $\mathbf{conf}_n$ in this product. In this approach, however, 'jumps' occur in every hook h_{ij}^{ik}. Indeed, suppose that $p_j \neq p_k$ are fixed while p_i moves 'through' p_k. Then the ratio β_{ij}^{ik} stays close to zero, but α_{ij}^{ik} jumps to $\alpha_{ij}^{ik} + \pi$ at collision, as α_{ik} changes direction, while α_{ij} stays the same.

7.3.6   Example: a smooth compactification of $\mathbf{conf}_3$.

Consider three points p_1, p_2, and p_3 in the plane. Their configuration space is given by $\mathbf{conf}_3 = \{(p_1, p_2, p_3) \mid p_1 \neq p_2, p_1 \neq p_3, p_2 \neq p_3\}$. Then $\mathbf{conf}_3$ is mapped by ψ_{AH_n} to a rather big space:

$$\psi_{AH_n}: \quad \mathbf{conf}_3 \quad \rightarrow \quad S_{12} \times S_{13} \times S_{23} \times K_{12}^{13} \times K_{13}^{12} \times K_{21}^{23} \times K_{23}^{21} \times K_{31}^{32} \times K_{32}^{31}.$$

Indeed, we can make a smooth compactification of $\mathbf{conf}_3$ by mapping it to a much smaller space:

Lemma 7.11
Let ψ be the map $\psi: \mathbf{conf}_3 \rightarrow S_{12} \times K_{12}^{13}$ given by $(p_1, p_2, p_3) \mapsto (\alpha_{12}, \beta_{12}^{13})$. Then $\overline{\psi[\mathbf{conf}_3]} = S_{12} \times K_{12}^{13}$. Moreover, $S_{12} \times K_{12}^{13}$ is smooth.

Proof. We have to show that for every point $y \in S_{12} \times K_{12}^{13}$ and every neighbourhood U of y it holds that $U \cap \psi[\mathbf{conf}_3] \neq \emptyset$. Any point $y \in S_{12} \times K_{12}^{13}$ has coordinates:

$$y \quad = \quad (\alpha_{12}(y), \beta_{12}^{13}(y), \alpha_{12}^{13}(y)).$$

If $0 < |\beta_{12}^{13}(y)| < \infty$, then $(\alpha_{12}(y), \beta_{12}^{13}(y), \alpha_{12}^{13}(y)) = \psi(p_1, p_2, p_3)$, where $p_1 = (0,0)$, $p_2 = (\cos\alpha_{12}, \sin\alpha_{12})$, and $p_3 = \beta_{12}^{13}(\cos(\alpha_{12} + \alpha_{12}^{13}), \sin(\alpha_{12} + \alpha_{12}^{13}))$. If ratio $\beta_{12}^{13}(y) = 0, \pm\infty$, then in any neighbourhood of y there exists a point z such that $0 < |\beta_{12}^{13}(z)| < \infty$, so $z \in \psi[\mathbf{conf}_3]$. ∎

Later on we prove that $XAH[3]$ is another smooth compactification of $\mathbf{conf}_3$. Mapping of $\mathbf{conf}_3$ into AH_n has the advantage that there are no preferred labels.

7.4   Nests and screens.

The main result of this section is Theorem 7.21 that associates a nested set of subsets of $\{1, \ldots, n\}$ to an element $x \in XAH_n$. This is done by analyzing those ratios $\beta_{ij}^{ik}(x)$ that are equal to zero.

7.4.1 Clusters, nests, and screens.

Definition 7.12
Let Z be a collection of sets.
*(i) Z is **nested** iff either $A \subset B$ or $B \subset A$ or $A \cap B = \emptyset$ for any two elements $A, B \in Z$.*
*(ii) A set U is a **maximal subset** of a set W, w.r.t. some nested set Z iff $U, W \in Z$, $U \subsetneq W$ and there exists no $V \in Z$ with $U \subsetneq V \subsetneq W$.*
*(iii) A **nest** Z on $\{1 \ldots n\}$ is a nested set of subsets of $\{1, \ldots, n\}$ that includes the set $\{1, \ldots, n\}$ itself and all singleton sets $\{i\}$, where $i = 1, \ldots, n$.*
*(iv) The elements of a nest are called **clusters**. The singleton sets are called the **trivial clusters**.*

Example 7.13
The set $Z = \{\{1, 2, 3, 4, 5, 6\}, \{1, 2, 6\}, \{3, 5\}, \{1\}, \{2\}, \{3\}, \{4\}, \{5\}, \{6\}\}$ is a nest on $\{1 \ldots 6\}$. For simplicity, we often write only the non-obvious elements of Z. The obvious elements are the singleton sets and the total set $\{1, \ldots, n\}$. We indicate this by using the $\langle, \rangle$ brackets. In our example we would write $Z = \langle\{1, 2, 6\}, \{3, 5\}\rangle$.

Let $Z(n)$ be a nest. Associate a copy S_C of the plane to every non-trivial cluster $C \in Z(n)$. Every copy is labeled by its corresponding cluster. In this way we get a family of screens $\mathcal{S}_Z = \{S_C \mid C \in Z, \ C \text{ non-trivial}\}$, associated to the nest Z. In case there is only one non-trivial cluster, we have exactly one screen, $S_{[n]}$, where $[n]$ stands for $\{1, \ldots, n\}$. In Example 7.13 we have screens $S_{[6]}$, $S_{1,2,6,}$, and $S_{3,5}$.

In this section we show how to associate a nest Z to a point $x \in XAH[n]$. In the following sections we describe how to fill the family of screens $\mathcal{S}_Z$ corresponding to a nest Z in a meaningful way.

7.4.2 Properties of ratios.

Lemma 7.14
Let p_i, p_j, p_k, and p_l be distinct points in the plane. Then the following relations hold:
(i) $\beta_{ij}^{ik} \in (0, \infty)$;
(ii) $\beta_{ik}^{ij} = 1/\beta_{ij}^{ik}$;
(iii) $\beta_{ij}^{ik} + \beta_{ji}^{jk} \geq 1$;
(iv) $\beta_{il}^{ij} \cdot \beta_{ij}^{ik} = \beta_{il}^{ik}$;
(v) $\beta_{ij}^{ik} \cdot \beta_{ki}^{kl} = \beta_{ij}^{il} \cdot \beta_{li}^{lk}$.

Proof.
(i) Follows directly from the definition.
(ii) $1/\beta_{ij}^{ik} = \dfrac{|p_i - p_k|}{|p_i - p_j|} = \beta_{ik}^{ij}$.

(iii)   This is in fact the triangle inequality:

$$\beta_{ij}^{ik} + \beta_{ji}^{jk} = \frac{|p_i - p_k|}{|p_i - p_j|} + \frac{|p_j - p_k|}{|p_i - p_j|} = \frac{|p_i - p_k| + |p_j - p_k|}{|p_i - p_j|} \geq 1.$$

(iv) $\beta_{il}^{ij} \cdot \beta_{ij}^{ik} = \dfrac{|p_i - p_j|}{|p_i - p_l|} \cdot \dfrac{|p_i - p_k|}{|p_i - p_j|} = \dfrac{|p_i - p_k|}{|p_i - p_l|} = \beta_{il}^{ik}.$

(v)   Apply the definition.   ∎

Corollary 7.15
For $x \in XAH[n]$ and i, j, k, l distinct labels we have
  (i) $|\beta_{ij}^{ik}| \in [0, \infty]$;
  (ii) $|\beta_{ik}^{ij}| = 1/|\beta_{ij}^{ik}|$;
  (iii) $|\beta_{ij}^{ik}| + |\beta_{ji}^{jk}| \geq 1$;
  (iv) *If* $\max(|\beta_{il}^{ij}|, |\beta_{ij}^{ik}|) < \infty$, *then* $|\beta_{il}^{ij}| \cdot |\beta_{ij}^{ik}| = |\beta_{il}^{ik}|$.

Proof. The claims follow from Lemma 7.14 by taking limits, but notice that for $x \in XAH_n$ some β_{ij}^{ik} can be negative, see Definition 7.8.   ∎

7.4.3   Separating clusters.

Remark 7.16
For the rest of this section, we identify a site p_i with its label i.

Set

$$C_{ij} := \{p_k \mid |\beta_{ik}^{ij}| > 0\} \cup \{i, j\}. \tag{7.2}$$

Intuitively, think of the following. Recall the geometric interpretation of a hook h_{ik}^{ij} given in Section 7.3.2. Suppose we use h_{ij}^{ik} to draw a point p_j in the plane, given the points p_i and p_k. The ratio $|\beta_{ik}^{ij}|$ gives the distance between the points p_i and p_j, compared to the unit distance $p_i p_k$. Imagine an observer situated at p_k. When $|\beta_{ik}^{ij}|$ gets very small, p_j moves very close to p_i. But as long as $|\beta_{ik}^{ij}| > 0$, the observer at p_k still can distinguish p_i and p_j. Therefore one could say in this setting that C_{ij} consists of all points p_k such that $p_i \neq p_j$ w.r.t. p_k. We call C_{ij} the **separating cluster** of p_i and p_j.

Lemma 7.17
We have $C_{ij} = C_{ji}$.

Proof. Let us start with a heuristic proof: consider Figure 7.8. Note that $I = |p_k - p_j|$, $J = |p_k - p_i|$ and $K = |p_j - p_i|$. Therefore $|\beta_{ik}^{ij}| = K/J$ and $|\beta_{jk}^{ji}| = K/I$. We have to show that $K/J > 0$ implies that $K/I > 0$ as well. $K/J > 0$ only excludes that p_i and p_j coincide w.r.t. p_k. But this is also the only way to make K/I small. More formally: we have to prove that $|\beta_{ik}^{ij}| > 0$ implies that $|\beta_{jk}^{ji}| > 0$. First of all:
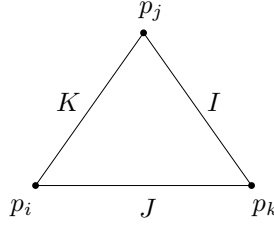
Figure 7.8: The triangle $p_i p_j p_k$.

as $|\beta_{ik}^{ij}| > 0$ it follows that $|\beta_{ij}^{ik}| < \infty$. Now suppose that $|\beta_{jk}^{ji}| = 0$. Then also $|\beta_{jk}^{ji}| \cdot |\beta_{ij}^{ik}| = |\beta_{kj}^{ki}| = 0$. This contradicts the triangle inequality applied to $|\beta_{kj}^{ki}|$ and $|\beta_{jk}^{ji}|$. ∎

Lemma 7.18
If $p_k \in C_{ij}$ and $p_l \notin C_{ij}$, then $p_l \notin C_{ik}, C_{jk}$.

Proof. First, $p_k \in C_{ij}$ implies that $|\beta_{ij}^{ik}| < \infty$. Secondly, as $p_l \notin C_{ij}$ it follows that $|\beta_{il}^{ij}| = 0$. So both $|\beta_{il}^{ij}|$ and $|\beta_{ij}^{ik}|$ are finite, which means that we can apply Corollary 7.15 and get $|\beta_{il}^{ik}| = |\beta_{il}^{ij}||\beta_{ij}^{ik}| = 0$. ∎

Lemma 7.19
Let i, j and k be distinct labels. Then

$$p_k \in C_{ij} \quad \Rightarrow \quad C_{ik} \subset C_{ij},$$
$$p_k \notin C_{ij} \quad \Rightarrow \quad C_{ij} \subset C_{ik}.$$

Proof. If $p_k \in C_{ij}$, then $C_{ik} \subset C_{ij}$ by Lemma 7.18. We are left with the case $p_k \notin C_{ij}$. We prove that in this case $C_{ij} \subset C_{ik}$. For this purpose, we fix $p_l \in C_{ij}$ and show that $p_l \in C_{ik}$. Since $p_k \notin C_{ij}$, it follows that $|\beta_{ik}^{ij}| = 0$. Due to $p_l \in C_{ij}$, one has $|\beta_{il}^{ij}| > 0$, and in particular $|\beta_{ij}^{il}|$ is finite. By Corollary 7.15, $|\beta_{ik}^{il}| = |\beta_{ik}^{ij}| \cdot |\beta_{ij}^{il}| = 0$. As a consequence $|\beta_{il}^{ik}| > 0$, so indeed $p_l \in C_{ik}$. ∎

Lemma 7.20
If $p_a, p_b \in C_{ij}$, then $C_{ab} \subset C_{ij}$.

Proof. If $p_b \in C_{ia}$, it follows from Lemma 7.19 that $C_{ab} \subset C_{ib} \subset C_{ij}$. Suppose that $p_b \notin C_{ia}$. Then Lemma 7.19 gives $C_{ia} \subset C_{ib}$. This implies that $p_a \in C_{ib}$. Therefore, $C_{ab} \subset C_{ib} \subset C_{ij}$. ∎

7.4.4 The clusters form a nest.

Theorem 7.21
Fix $x \in XAH_n$. Let $\mathcal{C}(x) := \{C_{ij}\}_{1 \leq i < j \leq n} \cup \{\{1\}, \ldots, \{n\}\}$. Then $\mathcal{C}(x)$ is a nest on n.

Proof. We have to show that for any clusters C_{st} and C_{ij} either $C_{st} \cap C_{ij} = \emptyset$ or one of them is contained in the other. Lemma 7.19 deals with the case $s = i$: it shows that the nest condition is fulfilled for C_{it} and C_{ij}. When $C_{st} \cap C_{ij} = \emptyset$ the nest condition is fulfilled as well. So, assume that s, t, i, and j are all distinct and that $p_m \in C_{st} \cap C_{ij}$. We have proved in Lemma 7.19 that the following inclusions hold:

$$
\begin{array}{ccc}
C_{im} & \star & C_{sm} \\
\cap & & \cap \\
C_{ij} & & C_{st} \\
\cup & & \cup \\
C_{jm} & * & C_{tm}
\end{array}
$$

The inclusions $\star$ and $*$ are still open. There are four possibilities:

$$
\begin{array}{ccccc}
 & 1 & 2 & 3 & 4 \\
\star & \subset & \supset & \subset & \supset \\
* & \subset & \supset & \supset & \subset
\end{array}
$$

In the first case, p_i and p_j are in C_{st}. So, $C_{ij} \subset C_{st}$ by Lemma 7.20. In the second case, $C_{st} \subset C_{ij}$. Concentrate on the case 3 now.

$$
\begin{aligned}
C_{im} \subset C_{sm} &\Rightarrow p_i \in C_{st}, \\
C_{jm} \supset C_{tm} &\Rightarrow p_t \in C_{ij}.
\end{aligned}
$$

If $p_j \in C_{sm}$, then $p_j \in C_{st}$, so both p_i and p_j are in C_{st}. This implies that $C_{ij} \subset C_{st}$. When $p_j \notin C_{sm}$, we can apply Lemma 7.18 as $p_i \in C_{sm}$ and conclude that $C_{is} \subset C_{ij}$. But this implies that $p_s \in C_{ij}$. As $p_t \in C_{ij}$ as well, it follows that $C_{st} \subset C_{ij}$. The fourth case follows from the third by relabeling. ∎

From Theorem 7.21 we obtain an important corollary.

Corollary 7.22
If $x \in XAH[n]$, then $\mathcal{C} = \mathcal{C}(x)$ forms a nest.

For $x \in XAH_n$, we call a cluster $C \in \mathcal{C}(x)$ an x-**cluster**. By now, the following statements are obvious.

Corollary 7.23
Let $\mathcal{C}$ be a nest. Then
 (i) C_{ij} is the smallest cluster of $\mathcal{C}$ that contains both i and j;
 (ii) i and j belong to distinct clusters in the screen $S_{C_{ij}}$.

Definition 7.24
Fix $x \in XAH_n$.

(i)   Let $M = \{i_1, \ldots, i_m\}$, for m in $2, \ldots, n$, be a subset of $\{1, \ldots, n\}$.   The **separating cluster** *C_M of M in x is the smallest cluster of $\mathcal{C}(x)$ that contains $i_1, \ldots, i_m$.   The* **separating screen** *S_M is the unique screen that contains exactly the elements of M.*

(ii)   Let $\mathcal{C}(x)$ be as in Theorem 7.21.   The **x-screens** *are the screens S_C for $C \in \mathcal{C}(x)$.*

7.5   The hooked tree.

Suppose we are given a point $x \in XAH_n$. By determining the clusters C_{ij} for x, we find the nest $\mathcal{C}(x)$ for x. From the nest, we get a list of screens $\mathcal{S}_{\mathcal{C}}$, the x-screens. In this section we introduce a data structure that enables us to fill the x-screens, the hooked tree. The hooked tree $ht(x)$ encodes both the nest $\mathcal{C}(x)$ of x and the relative positions of the underlying point set $p_1, \ldots, p_n$ of x. We define $ht(x)$ recursively.

7.5.1   Definition of hooked tree.

Definition 7.25
The **hooked tree** *$ht(x)$ of a point $x \in XAH_n$ is a rooted tree. Some of its edges have tags. The* **vertices** *of $ht(x)$ are the clusters of the nest $\mathcal{C}(x)$. The* **root** *is the cluster $\{1, \ldots, n\}$. The* **leaves** *are the clusters $\{1\}, \ldots, \{n\}$. Two clusters are connected by an* **edge** *if one of the clusters is maximal in the other.*

The **x-tags** *refer to hooks and angles in AH_n. Fix a cluster S. Order the maximal subclusters in S according to the smallest label in each maximal subcluster. Suppose S has maximal subclusters $c_1, \ldots, c_k$ with minimal labels*

$$j_1 \; < \; j_2 \; < \; \ldots \; < \; j_k.$$

If S is not the top cluster $[n]$, there exists a cluster T that contains S as one of its maximal subclusters. Suppose that T its maximal subclusters have minimal labels

$$i_1 \; < \; i_2 \; < \; \ldots \; < \; i_m.$$

Tag the edges from cluster S to its maximal subclusters as follows.

Edge to c_1. *If S is the top cluster $[n]$ then the edge from S to c_1 is tagged* **top**. *Else: no tag.*

Edge to c_2.
    (i)   If S is the top cluster $[n]$ then the edge to c_2 is tagged α_{1j_2}. Such tag is called an x-type **2.a** *tag.*
    (ii)   Else if $j_1 > i_1$ then tag the edge from S to c_2 by $h^{j_1 j_2}_{j_1 i_1}$. This is an x-type **2.b** *tag.*

(iii) Else if $j_1 = i_1$ then *tag the edge to c_2 by $h^{j_1 j_2}_{j_1 i_2}$. This is an x-**type 2.c** tag.*

Edge to c_t, for $t \geq 3$. *The edge from S to c_t, for $t > 3$, is tagged $h^{j_1 j_t}_{j_1 j_2}$. This is an x-**type 3** tag.*

The tag α_{ij} in x-tags does not stand for the value $\alpha_{ij}(x)$, but rather for a map $AH_n \rightarrow \mathbb{R}/\pi\mathbb{Z}$. The indices i and j indicate which particular factor of the form $\mathbb{R}/\pi\mathbb{Z}$ in AH_n is meant.

Definition 7.26
*Fix $x \in XAH_n$. Let q be an arbitrary point in AH_n. A q-coordinate $h^{ik}_{ij}(q)$, respectively, $\alpha_{ij}(q)$, $\alpha^{ik}_{ij}(q)$, $\beta^{ik}_{ij}(q)$ is a x-**type 2** hook, respectively, angle, angle, **ratio** iff h^{ik}_{ij}, α_{ij}, α^{ik}_{ij} or β^{ik}_{ij} occurs in x-tags; x-**type 3** hooks, angles, and ratios are defined in a similar way.*

7.5.2   The hooked path.

In this section we associate a unique x-tag to every site p_i. Moreover, we show that the hooked tree $ht(x)$ induces a partial ordering on the labels $1, \ldots, n$.

Definition 7.27
Fix $x \in XAH_n$.
(i)   To any site p_i, for $i = 1, \ldots, n$ we associate an x-tag $l_x(p_i)$: it is the first x-tag that one encounters when going up in $ht(x)$, starting from the leaf i.
*(ii)   The **predecessor** $p_x(p_i)$ of p_i with respect to x, for $i = 2, \ldots, n$ is defined as follows:*

    1. *p_1 has no predecessor.*
    2. *If $l_x(p_i)$ is an x-type 2 tag then $i = j_2$ in Definition 7.25.*

        • *In case of x-type 2.a, $p_x(p_i) = p_1$.*
        • *In case of x-type 2.b, $p_x(p_i) = p_{j_1}$.*
        • *In case of x-type 2.c, $p_x(p_i) = p_{i_2}$.*

    3. *If $l_x(p_i)$ is an x-type 3 tag then $i = j_t$ in Definition 7.25 and $p_x(p_i) = p_{j_2}$.*
*(iii)   To a site p_i, for $i = 1, \ldots, n$ we associate a **hooked path** $L_x(p_i)$:*

    1. *$L_x(p_1) = ()$.*
    2. *$L_x(p_i)$ equals $L_x(p_x(p_i))$ with p_i prepended.*

*If a site p_j occurs in $L_x(p_i)$, then we say that p_j is x-**above** p_i. If $p_j = p_x(p_i)$ or $p_i = p_x(p_j)$, then we call $p_i p_j$ an x-**leg**.*

Lemma 7.28
The predecessor relation gives a partial order on the set $p_1, \ldots, p_n$.

Proof. We have to show that there are no loops. For this purpose we define the **depth** of a site p_i as the number of edges from the root in $ht(x)$ to the node where the

edge that has $l_x(p_i)$ as its x-tag starts. Consider site p_i. Site p_1 has no predecessor. Assume that $i \neq 1$ and that p_j is its predecessor: $p_j = p_x(p_i)$. We claim that either depth$(p_j) <$ depth(p_i), or depth$(p_j) =$ depth(p_i) and $j < i$. Indeed, if $l_x(p_i)$ is of x-type 3, then the last case holds. And if $l_x(p_i)$ of x-type 2, then depth$(p_i) =$ depth$(p_j) + 1$.   ∎

Lemma 7.29
There is a 1 to 1 correspondence between the sites $p_1, \ldots, p_n$ and the x-tags.

Proof. In Definition 7.27 we have associated an x-tag with every site p_i: the x-tag $l_x(p_i)$ associated with p_i is the first tag one encounters going up from the leaf p_i in the hooked tree $ht(x)$. To finish the proof, we turn around the association: we show that for every x-tag l there is a unique path to a leaf of the hooked tree such that no other x-tag is encountered. If the edge tagged l is itself incident with a leaf we are done. So assume that the edge tagged l does not end in a leaf. Then it ends in a vertex of the hooked tree corresponding to a cluster S of at least two elements. By Definition 7.25 only the edge from S to its maximal subcluster M with minimal label j_1 has no tag. j_1 will also be the minimal label of every subcluster of M that contains j_1. Therefore there is a unique path without labels to p_{j_1}.   ∎

7.5.3 $\mathbf{Dom}_n(x)$ and $\mathbf{Rng}_n(x)$.

The x-tags define a factor of XAH_n.

Definition 7.30
Fix $x \in XAH_n$.
(i)   The factor $\mathbf{Dom}_n(x)$ is the factor of AH_n that corresponds to the angles and hooks in x-tags. The factor of AH_n complementary to $\mathbf{Dom}_n(x)$ is denoted by $\mathbf{Rng}_n(x)$.
(ii)   By tv_x, denote the projection of AH_n onto $\mathbf{Dom}_n(x)$; 'tv' stands for **tree values**. *The projection of AH_n onto $\mathbf{Rng}_n(x)$ is denoted by ctv_x, the complementary tree values.*

The following lemma states that dim$(\mathbf{Dom}_n(x)) =$ dim$(\mathbf{conf}_n)$. This shows that the hooked tree is optimal in the sense that it refers to as many coordinates of AH_n as the dimension requires.

Lemma 7.31
Let $x \in XAH_n$. Then dim$(\mathbf{Dom}_n(x)) = 2n - 3$.

Proof. The dimension of $\mathbf{Dom}_n(x)$ is given by the sum of the degrees of freedom in the hooks and angles referred to by x-tags. Every hook is defined by one angle α_{ij}^{ik} and one ratio β_{ij}^{ik}, so the dimension of one hook equals 2. The dimension of a single angle α_{ij} equals 1. The dimension of 'top' is zero. From Lemma 7.29 it follows that the x-tags refer to $n-2$ hooks and 1 angle as there are n sites and one 'top' tag.   ∎
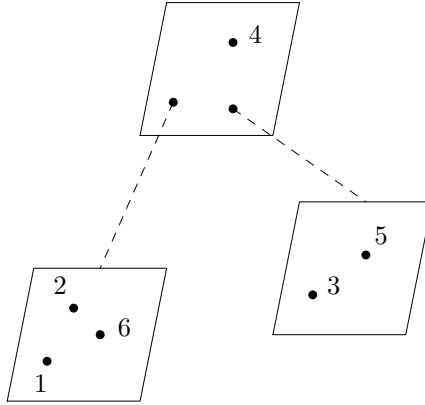
7.5.4 Example of a hooked tree.

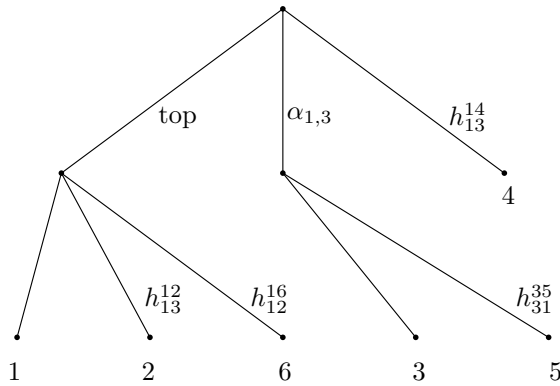Figure 7.9: The screens for the nest $\langle\{1,2,6\},\{3,5\}\rangle$.

Figure 7.10: The hooked tree for the nest $\langle\{1,2,6\},\{3,5\}\rangle$.

Example 7.32

Let us consider again, as in Example 7.13, the nest $Z = \langle\{1,2,6\},\{3,5\}\rangle$. A realization of Z consists of the three filled screens $S_{[6]}, S_{1,2,6}$ and $S_{3,5}$. Recall that $[6] = \{1,\ldots,6\}$. A possible realization is given in Figure 7.9. The hooked tree corresponding to Z is given in Figure 7.10. Note that the dimension of $\mathbf{Dom}_n(x)$ is indeed 9.

The first column of Table 7.2 gives all sites in Z. The x-tags corresponding to each site are shown in the second column. The third column gives for every x-tag its x-type. The fourth column gives $tv_x(x)$ coordinates corresponding to the way the x-screens are filled in Figure 7.9. How this filling is done exactly, and the meaning

of the fifth and sixth column will be explained later in this chapter.

From the data for the $tv_x(x)$ coordinates it follows, for example, that the length of the leg 12 is zero with respect to the length of the leg 13. And as the length of the leg 16 is of the same order as the length of the leg 12, it must vanish with respect to the length of the leg 13 too. Continuing in this way reveals the complete nest structure.

site	x-tag	x-type	$tv_x(x)$	$q \in \mathbf{Dom}_n(x)$	representatives
1	top	top			
3	$\alpha_{1,3}$	2.a	$-7°$	$69°$	same
2	$(\beta_{13}^{12}, \alpha_{13}^{12})$	2.c	$(0, 71°)$	$(.35, -91°)$	$(-.35, 89°)$
4	$(\beta_{13}^{14}, \alpha_{13}^{14})$	3	$(1.5, 50°)$	$(-1.92, 4°)$	same
5	$(\beta_{31}^{35}, \alpha_{31}^{35})$	2.b	$(0, 44°)$	$(-.34, 170°)$	$(.34, -10°)$
6	$(\beta_{12}^{16}, \alpha_{12}^{16})$	3	$(1, -37°)$	$(.91, -11°)$	same

Table 7.2: x-tags and values.

7.6   Filling x-screens.

In this section we present a method for filling x-screens, given a suitable point $q \in \mathbf{Dom}_n(x)$.

7.6.1   Standard form of $x \in XAH_n$.

First we put a fixed $x \in XAH_n$ in standard form: if necessary we change some representatives in Klein bottles K_{ij}^{ik} and/or change the representative for the top angle $\alpha_{1j_2}(x)$ modulo π. We only use the $\mathbf{Dom}_n(x)$ factor of AH_n in order to fill the x-screens. Therefore we only have to choose standard representatives for those angles and hooks that are referred to in x-tags.

Definition 7.33
$x \in XAH_n$ is represented in **standard form** iff

- α_{1j}, α_{ij}^{ik} of x-type 2 $\Rightarrow \alpha_{1j}(x)$, $\alpha_{ij}^{ik}(x) \in [-\pi/2, \pi/2)$ and

- β_{ij}^{ik} of x-type 3 $\Rightarrow \beta_{ij}^{ik}(x) > 0$.

By the following, we do not have to make a sign choice for any x-type 2 ratio $\beta_{ij}^{ik}(x)$.

Lemma 7.34
Fix $x \in XAH_n$.
(i) *If $h_{j_1 i_{1,2}}^{j_1 j_2}$ is an x-type 2 hook, then $\beta_{j_1 i_{1,2}}^{j_1 j_2}(x) = 0$.*
(ii) *If $h_{j_1 j_2}^{j_1 j_t}$ is an x-type 3 hook, then $0 < |\beta_{j_1 j_2}^{j_1 j_t}(x)| < \infty$.*

Proof. Follow the notation of Definition 7.25. We give a proof for the x-type 2.b case. The x-type 2.c case is similar and is omitted. From Definition 7.25 we know that there exists an x-screen S such that $p_{j_1}, p_{j_2} \in S$ but $p_{i_1} \notin S$. The claim follows from the definition of separating cluster, see in particular Equation 7.2. If $\beta_{j_1 j_2}^{j_1 j_t}$ is of x-type 3, then $p_{j_2} \in C_{j_1 j_t}$, so $|\beta_{j_1 j_2}^{j_1 j_t}(x)| > 0$. Suppose that $|\beta_{j_1 j_2}^{j_1 j_t}(x)| = \infty$. Then $|\beta_{j_1 j_t}^{j_1 j_2}(x)| = 0$, but this would imply that $p_{j_2} \notin C_{j_1 j_t}$. That is a contradiction. ∎

Changing an x-type 3 ratio $\beta_{ij}^{ik}(x)$ from negative to positive involves of course a swap $\alpha_{ij}^{ik}(x) = \alpha_{ij}^{ik}(x) + \pi$ for the corresponding x-type 3 angle: we have to oblige the Klein bottle identification 7.1.

Remark 7.35
We also refer to x-type 3 hooks, angles and ratios as **hooks on scale**, etc. The unique x-type 2.a angle is referred to as **top angle**. Hooks, angles and ratios of x-type 2.b or 2.c are also called **explosion hooks**, etc.

An explanation for these names can be found in the geometric interpretation of a hook h_{ij}^{ik}, given in Section 7.3.2. Think of what changes in the hook h_{ij}^{ik} as we start from the fixed value $x \in XAH_n$ and move away from this point in some general direction inside AH_n. If h_{ij}^{ik} is of x-type 2, then $\beta_{ij}^{ik}(x) = 0$. Perturbing x to $\tilde{x}$ implies in general that $|\beta_{ij}^{ik}(\tilde{x})| > 0$. In the geometric interpretation, this has the effect of an explosion. If h_{ij}^{ik} is of x-type 3, then $0 < |\beta_{ij}^{ik}(x)| < \infty$ and shifting x in general direction does not change this. In our geometric interpretation this means that the transformed leg, before and after perturbation, has finite but positive length. This explains the name 'hook on scale'. The name 'top angle' refers to the place of the x-tag 'top' in the hooked tree $ht(x)$.

Definition 7.36
*Let $x \in XAH_n$ be in standard form. A point $q \in \mathbf{Dom}_n(x)$ is **valid** with respect to x iff the following two conditions on the coordinates of q hold:*

non-orthogonality: *no explosion angle is orthogonal to the corresponding angle $\alpha_{ik}^{ij}(x)$. The top angle $\alpha_{1j_2}(q)$ is not orthogonal to the top angle $\alpha_{1j_2}(x)$.*

finiteness: *$|\beta_{ik}^{ij}(q)| < \infty$ for all ratio coordinates $\beta_{ik}^{ij}(q)$.*

Remark 7.37
$tv_x(x)$ is valid with respect to x..

Proof. The non-orthogonality is obvious, while the finiteness follows from Lemma 7.34.   ∎

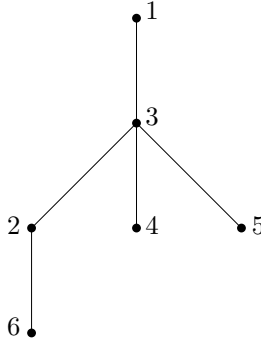### 7.6.2   Example: ordering the sites for the drawing process.

Figure 7.11: The poset induced by the predecessor relation.

Example 7.38
Figure 7.11 depicts the poset induced by the predecessor relation in our running example, see also Examples 7.13 and 7.32. This poset tells us, for example, that in order to draw p_6 in the top screen, we should draw p_1, p_3, and p_2 first and in that order and, moreover, that we can ignore p_4 and p_5. So, the hooked path $L_x(p_6)$ is given by $L_x(p_6) = (p_6, p_2, p_3, p_1)$.

This hooked path $L_x(p_6)$ tells us how to draw p_6 in the top x-screen using $ht(x)$. First p_1 is placed in the origin. Then p_3 is drawn using $l_x(p_3) = \alpha_{13}$. As by now the leg $p_1 p_3$ exists, we can apply $l_x(p_2) = h_{13}^{12}$ in order to add the leg $p_1 p_2$. Finally, the leg $p_1 p_6$ is formed by applying $l_x(p_6) = h_{12}^{16}$.

7.6.3   The construction $\mathrm{draw}_x(q)$.

Construction 7.42 indicates how to fill x-screens with sites $p_1, \ldots, p_n$, given a valid point $q \in \mathbf{Dom}_n(x)$. First we define an ordering on the x-screens.

Definition 7.39
*An x-screen T is **above** an x-screen S iff the set of labels of S is a subset of the set of labels of T.*

The following lemmas relate the x-type of a hook to clusters C in $\mathcal{C}(x)$.

Lemma 7.40
Let h_{ij}^{ik} be an x-tag.

(i)   If x-type(h_{ij}^{ik}) = 3 then $C_{ij} = C_{ijk} = C_{ik}$.
(ii) If x-type(h_{ij}^{ik}) = 2 then $C_{ij} \neq C_{ik}$ and moreover, C_{ij} is directly above C_{ik}.

Proof. We prove the two claims in the Lemma.

(i)   By construction, an x-type 3 hook involves the minimal labels of the first, the second, and another maximal cluster in a fixed cluster. Therefore

$$C_{ij} = C_{ijk} = C_{ik}.$$

(ii) Analyzing the cases in Definition 7.25 shows that i points to the minimal label in some cluster S and k points to the second lowest label in S. Moreover, i is a minimal label for one of the maximal clusters of T, the cluster directly above S, while j is the minimal label of one of the other maximal clusters in T. Therefore

$$C_{ij} \; = \; T \; \neq \; S \; = \; C_{ik}. \qquad \blacksquare$$

Lemma 7.41
Let C be a x-cluster. Let p_{m_1} and p_{m_2} be the sites with minimal labels in the first, resp., the second maximal cluster of C. Let $p_k \in C$, but $p_k \neq p_{m_1}, p_{m_2}$, and let $h_{ij}^{ik} = l_x(p_k)$. Then $p_i, p_j \in C$.

Proof. Let $M_1, M_2, \ldots, M_s$ be the maximal subclusters of C. Suppose that $p_k \in M_l$ for l in $\{1, \ldots, s\}$. Suppose that x-type(h_{ij}^{ik}) = 3. By Definition 7.25, there are two possibilities. Either p_k has minimal label in M_l, and in this case $l > 2$, $p_i = p_{m_1}$, and $p_j = p_{m_2}$ or, p_k, p_i and p_j belong all three to M_l. We are left with the case x-type(h_{ij}^{ik}) = 2. According to Definition 7.25, p_k has minimal label in the second maximal cluster of some cluster D. As $p_k \neq p_{m_2}$, this means that either D equals M_l or D is a subcluster of M_l. It follows from Lemma 7.40 that in both cases $p_i, p_j \in C$, since these two sites are contained in the cluster directly above D. $\qquad \blacksquare$

Construction 7.42 (draw$_\mathbf{x}$(q)).
Filling x-screens.

Input: x-screens, valid $q \in \mathbf{Dom}_n(x)$.
Output: x-screens filled with q, prescription $\mathbf{draw}_x(q)$.

Step 1. Choosing representatives.
Choose representatives for the top angle $\alpha_{1j_2}(q)$ and the explosion angles $\alpha_{ik}^{ij}(q)$ in $ht(q)$. Do so by changing the present value, if necessary, to the value modulo 2π most close to the corresponding value $\alpha_{1j_2}(x)$ or $\alpha_{ik}^{ij}(x)$ in $tv(x)$. This choice is unique because of the non-orthogonality condition in Definition 7.36. See also Figure 7.12, which demonstrates that there always exists a value of $\alpha(q)$ within distance $\pi/2$ of $\alpha(x)$.

Simultaneously, change the sign of an explosion ratio $\beta_{ij}^{ik}(q)$ whenever you change the explosion angle by $\alpha_{ij}^{ik}(q) = \alpha_{ij}^{ik}(q) + \pi$. Otherwise the K_{ij}^{ik} Klein bottle identification 7.1 is not obliged.
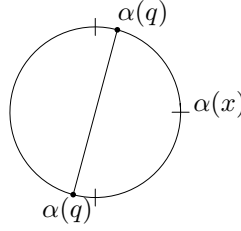
Figure 7.12: Non-orthogonality condition.

Step 2. Screen orientation.
We define the **screen orientation** of an x-screen $S = S_C$ by induction on the 'above' relation introduced in Definition 7.39. Assume that the screen orientation is defined for all x-screens above S. Let T be the screen directly above S. Following the labeling in Definition 7.25, the screen orientation $\mathcal{O}_S$ is defined by

$$
\mathcal{O}_S := \begin{cases}
\alpha_{1j_2}, & S \text{ is a top screen,} \\
\mathcal{O}_T + \alpha_{j_1 i_2}^{j_1 j_2}, & j_1 = i_1, \\
\mathcal{O}_T + \alpha_{j_1 i_1}^{j_1 j_2} + \pi, & j_1 = i_2, \\
\mathcal{O}_T + \alpha_{i_1 i_2}^{i_1 j_1} + \alpha_{j_1 i_1}^{j_1 j_2} + \pi, & j_1 = i_t,\ t = 3, \ldots, m, \quad \beta_{i_1 i_2}^{i_1 j_1} > 0, \\
\mathcal{O}_T + \alpha_{i_1 i_2}^{i_1 j_1} + \alpha_{j_1 i_1}^{j_1 j_2}, & j_1 = i_t,\ t = 3, \ldots, m, \quad \beta_{i_1 i_2}^{i_1 j_1} < 0.
\end{cases}
\tag{7.3}
$$

Step 3. Drawing the sites.
The recipe for drawing a site p_i in a screen $S = S_C$ for $i \in C$, is given inductively, by induction on the predecessor relation. Below, T denotes the screen directly above S.

1: Site p_1 is the first site in every path $L_x(p_i)$ and is drawn in 'the origin' in any screen where p_1 occurs.
2: Next suppose that $i \neq 1$ and that all sites p_m above p_i with $m \in C$ have already been drawn.
3: **if** p_i is the first site in the first cluster of C **then**
4:   p_i is drawn in the origin of S.
5: **else if** p_i is the first site in the second cluster of C **then**
6:   put p_i at $(\cos \mathcal{O}_S, \sin \mathcal{O}_S)$
7: **else**
8:   $l_x(p_i) = h_{jk}^{ji}$, where p_j and p_k are above p_i. By the induction hypothesis, the leg $p_j p_k$ is already present in S, see also Lemma 7.41. The leg $p_j p_i$ is constructed as follows:
9:   Rotate $p_j p_k$ over α_{jk}^{ji} around p_j.
10:   Scale the result by a factor β_{jk}^{ji} with respect to p_j.
11:   To summarize,

$$
p_i = \beta_{jk}^{ji} \, \mathbf{rot}_{\alpha_{jk}^{ji}} (p_k - p_j) + p_j.
\tag{7.4}
$$

12: By induction, the length of the leg $p_j p_k$ is finite. The finiteness condition in Definition 7.36 assures that the resulting leg $p_j p_i$ is finite as well.

Remark 7.43
Note that the legs $p_i p_j$ constructed in $\mathbf{draw}_x(q)$ while filling the screens are exactly the x-legs.

Some drawings are better than others.

Definition 7.44
*A valid $q \in \mathbf{Dom}_n(x)$ is **accepted** with respect to x iff in any x-screen S filled by $\mathbf{draw}_x(q)$, q-sites that belong to distinct maximal x-clusters of S do not coincide.*

Remark 7.45
Suppose that $q \in \mathbf{Dom}_n(x)$ is valid and accepted. If $\mathrm{type}_x(\beta_{ij}^{ik}) = 3$, then $|\beta_{ij}^{ik}(q)| > 0$.

Definition 7.46
Every valid and accepted $q \in \mathbf{Dom}_n(x)$ gives a filling of the x-screens consisting of n sites. The set of all filled x-screens that can be obtained in this way is denoted by $\mathbf{Scr}_n(x)$.

7.6.4   Example: filling x-screens.
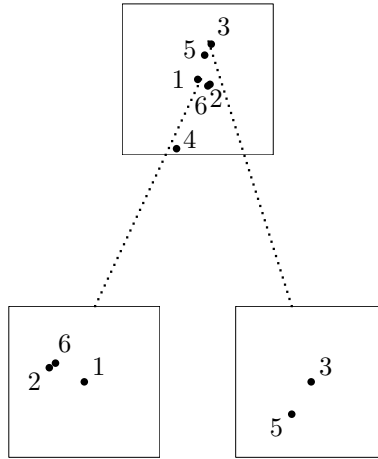
Figure 7.13: x-screens filled with some $q \in \mathbf{Dom}_n(x)$.

Example 7.47
In Figure 7.13 we have filled the x-screens of our running example, see Examples

7.13, 7.32 and 7.38, with the q-values present in the the fifth column in Table 7.2. The chosen representatives for the q-values are given in the last column. According to Step 2 in Construction 7.42, we have changed the representatives for h_{13}^{12} and h_{31}^{35}. Let us look more carefully at the relative positions of the sites p_1, p_2, and p_6 in the top screen $S_{[6]}$ and the screen $S_{1,2,6}$. It seems like the complete cluster $1, 2, 6$ has been rotated over π w.r.t. site p_1 in the bottom screen. In order to find an explanation, we compute the coordinates of p_2 in both $S_{[6]}$ and $S_{1,2,6}$. The hooked path $L_x(p_2)$ equals (p_2, p_3, p_1). In both screens $p_1 = (0,0)$. In the top screen, $p_3 = (\cos \mathcal{O}_{S_{[6]}}, \sin \mathcal{O}_{S_{[6]}})$, where $\mathcal{O}_{S_{[6]}} = \alpha_{13}$. We determine the position of p_2 in the top screen, using Equation 7.4:

$$p_2(S_{[6]}) \;=\; \beta_{13}^{12} \, \mathbf{rot}_{\alpha_{13}^{12}}(p_3) \;=\; \beta_{13}^{12} (\cos \alpha_{13} + \alpha_{13}^{12}, \sin \alpha_{13} + \alpha_{13}^{12}).$$

In $S_{1,2,6}$, however, p_2 is the first site in the second cluster, so

$$p_2(S_{1,2,6}) \;=\; (\cos \mathcal{O}_{S_{1,2,6}}, \sin \mathcal{O}_{S_{1,2,6}}).$$

According to Step 2 in Construction 7.42,

$$\mathcal{O}_{S_{1,2,6}} \;=\; \mathcal{O}_{S_{[6]}} + \alpha_{13}^{12} \;=\; \alpha_{13} + \alpha_{13}^{12},$$

as $i_1 = 1$, $i_2 = 3$ and $j_1 = 1, j_2 = 2$. We conclude that the only difference between the argument of p_3 in $S_{[6]}$ and $S_{1,2,6}$ can be caused by β_{13}^{12}: this ratio is used in drawing p_2 in $S_{[6]}$ but not used in drawing p_2 in $S_{1,2,6}$. Indeed, $\mathrm{sign}(\beta_{13}^{12}) = -1$, which causes a π shift in $\arg(p_2)$ from the top screen to the screen $S_{1,2,6}$.

7.7   Reading off data elements from filled screens.

Let $q \in \mathbf{Dom}_n(x)$. Suppose we have filled the x-screens with q-sites by applying $\mathbf{draw}_x(q)$. In this section we tell exactly how to read off angles and hooks coordinates from the q-filled x-screens. More precisely, we explain how to determine every angle $\overline{\alpha_{ij}}$ between two sites $p_i(q)$ and $p_j(q)$ and every hook h_{ik}^{ij} between three sites $p_i(q)$, $p_j(q)$, and $p_k(q)$. Basically we read off lacking coordinates in a suitable x-screen. Recall the notions of separating clusters and separating screens that were introduced in Definition 7.24. These notions are used for fixing the x-screens used for determining the angles and hooks coordinates.

Remark 7.48
The separating screen $S_{ij}(x)$ is the only x-screen in which it is guaranteed that $p_i(q) \neq p_j(q)$ for q being valid and accepted.

7.7.1   Determining hooks and angles from $\mathbf{draw}_x(q)$.

Definition 7.49
Let $q \in \mathbf{Dom}_n(x)$ be valid and accepted. From $\mathbf{draw}_x(q)$ we determine a point $\tilde{q} = \mathbf{read}_x(q) \in AH_n$ as follows.

(i) $\alpha_{ij}(\tilde{q}) \in \mathbb{R}/2\pi\mathbb{Z}$ is the angle of the directed line through $p_i(q)$ and $p_j(q)$ in the q-filled screen $S_{ij}(x)$.

(ii) $\alpha_{ij}^{ik}(\tilde{q}) = \alpha_{ik}(\tilde{q}) - \alpha_{ij}(\tilde{q})$.

(iii)   Read off all sites coordinates in screen S_{ijk}. If $p_i(q) \neq p_j(q)$ in S_{ijk}, then

$$\beta_{ij}^{ik}(\tilde{q}) \quad = \quad \frac{(p_k(q) - p_i(q)) \cdot (p'_j(q) - p_i(q))}{|p'_j(q) - p_i(q)|^2}, \tag{7.5}$$

where

$$p'_j(q) \quad = \quad \mathbf{rot}_{\alpha_{ij}^{ik}(\tilde{q})}(p_j(q) - p_i(q)) + p_i(q). \tag{7.6}$$

Else, $\beta_{ij}^{ik}(\tilde{q}) = 1/\beta_{ik}^{ij}(\tilde{q})$.

Note that by definition of separating screen, not all three sites p_i, p_j, and p_k coincide in S_{ijk}. Therefore $p_i(q) = p_j(q)$ in S_{ijk} implies that $p_i(q) \neq p_k(q)$.
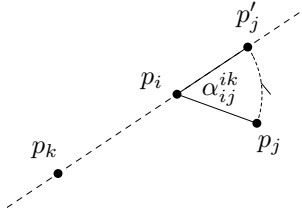
Figure 7.14: Determining β_{ij}^{ik}.

Remark 7.50

We give a geometric explanation for Definition 7.49. It is rather straightforward to read off $\alpha_{ij}(\tilde{q})$ and $\alpha_{ij}^{ik}(\tilde{q})$, so let us focus on $\beta_{ij}^{ik}(\tilde{q})$. Go to the separating screen $S_{ijk}(x)$. Write down the coordinates of $p_i(q)$, $p_j(q)$, and $p_k(q)$ in this screen. First consider the case where $p_i(q) \neq p_k(q)$. If proceeding through the definition in the right order, we know by now $\alpha_{ij}^{ik}(\tilde{q})$. See also Figure 7.14. Use $\alpha_{ij}^{ik}(\tilde{q})$ in order to rotate the leg $p_j - p_i$ onto the line l_{ik} through p_i and p_k, thereby fixing a point p'_j. Finally determine the coordinate of p_k on the ij'-axis with respect to the 'unit vector' $p_j - p_i$ as follows. Let $x = p_k - p_i$, $y = p'_j - p_i$, and θ the angle between x and y. From the definition of dot product $x \cdot y = |x||y| \cos \theta$, it follows that the quantity $\frac{|x|}{|y|} \cos \theta$ we look for is given by $(x \cdot y)/|y|^2$. Note that in our case θ always equals either 0 or π.

Proposition 7.51

The components of $\mathbf{read}_x(q)$ *are infinitely often differentiable* (C^∞) *on the set of valid and accepted* $q \in \mathbf{Dom}_n(x)$.

Proof. The main problem is the continuity of $\mathbf{read}_x(q)$, so this is stressed in the proof. To make the proof complete, replace every occurrence of 'continuous' by C^∞.

(i) AH_n is smooth as a direct product of circles and Klein bottles. $\mathbf{Dom}_n(x)$ is a factor of AH_n and is a product of circles and Klein bottles as well. $\mathbf{read}_x(q)$ determines a point in AH_n.

(ii) We restrict ourselves to valid $q \in \mathbf{Dom}_n(x)$. This means that we have imposed two conditions on q: the non-orthogonality condition, which is is an open condition as it assures that one point of a circle S^1 is avoided. The finiteness condition is open as well, as one point, infinity, of $\mathbb{P}^1$ is avoided.

(iii) For valid $q \in \mathbf{Dom}_n(x)$, the construction $\mathbf{draw}_x(q)$ is defined. The construction consists of three steps. First of all representatives are chosen for the top angle and explosion angles. The chosen representatives depend continuously on q. No jumps can occur due to the non-orthogonality condition. In step 2 screen orientations $\mathcal{O}_S$ are defined. The formulas presented in Equation 7.3, depend continuously on the chosen representatives for q. In the third step, points are drawn in the screen. The positions of these points depend continuously on the screen orientation $\mathcal{O}_S$ and the q coordinates, compare Equation 7.4.

(iv) Filled screens that are not accepted are thrown away. A filled screen is not accepted when certain clustering between sites occurs. Avoiding clustering is yet another open condition.

(v) For valid and accepted $q \in \mathbf{Dom}_n(x)$, the point $\mathbf{read}_x(q) \in AH_n$ is defined. The formulas for the coordinates of $\mathbf{read}_x(q)$ are given in Definition 7.49. All equations depend continuously on the position of the sites in accepted $\mathbf{draw}_x(q)$. ∎

7.7.2 Example: reading off hooked tree elements.

Example 7.52

Applying Definition 7.49, we read off the values of the angle and hooks in $\mathbf{Dom}_n(x)$ from Figure 7.13. These values are presented in Table 7.3. Next to the data elements to read off, the read off screen is given. Compare the values in Table 7.3 with the values of $q \in \mathbf{Dom}_n(x)$ in Table 7.2 used above to fill the x-screens. Note that these two sets of values are indeed the same but only up to identification in the appropriate Klein bottle.

angle	screen	value	angle	value	ratio	screen	value
$\alpha_{1,3}$	$S_{[6]}$	$69°$					
$\alpha_{1,2}$	$S_{1,2,6}$	$157°$	α_{13}^{12}	$88°$	β_{13}^{12}	$S_{[6]}$	-.35
$\alpha_{1,4}$	$S_{[6]}$	$-107°$	α_{13}^{14}	$-176°$	β_{13}^{14}	$S_{[6]}$	1.92
$\alpha_{3,5}$	$S_{3,5}$	$-123°$	α_{31}^{35}	$-12°$	β_{31}^{35}	$S_{[6]}$	.34
$\alpha_{1,6}$	$S_{1,2,6}$	$146°$	α_{12}^{16}	$-11°$	β_{12}^{16}	$S_{1,2,6}$	.91

Table 7.3: Read off values.

7.8   Consistency Theorem.

In this section we show that our construction of filling screens by means of hooked tree data is consistent with the procedure of reading off data from the filled screens.

7.8.1   Managing x-type 3 hooks.

Lemma 7.53
Let $q \in \mathbf{Dom}_n(x)$ be valid and accepted and put $\tilde{q} = \mathbf{read}_x(q) \in AH_n$. Suppose that $type_x(h_{ij}^{ik}) = 3$. Then

$$\alpha_{ij}^{ik}(\tilde{q}) = \begin{cases} \alpha_{ij}^{ik}(q), & \beta_{ij}^{ik}(q) > 0, \\ \alpha_{ij}^{ik}(q) + \pi, & \beta_{ij}^{ik}(q) < 0. \end{cases}$$

Figure 7.15: $\beta_{j_1 j_2}^{j_1 j_t}(q) > 0$ and $\beta_{j_1 j_2}^{j_1 j_t}(q) < 0$.

Proof. Follow the labeling in Definition 7.25: $i = j_1$, $j = j_2$, and $k = j_t$. For convenience we set $j_1 = 1$, $j_2 = 2$ and $j_t = t$. By Lemma 7.40, all evaluations take place in x-screen $S = S_{12} = S_{12t} = S_{1t}$. For an illustration of the proof, see Figure 7.15. As $p_1 = (0,0)$ and $p_2 = (\cos \mathcal{O}_S, \sin \mathcal{O}_S)$ it follows that

$$\alpha_{12}^{1t}(\tilde{q}) = \alpha_{1t}(\tilde{q}) - \alpha_{12}(\tilde{q}) = \arg(p_t) - \arg(p_2) = \arg(p_t) - \mathcal{O}_S.$$

If $\beta_{12}^{1t}(q) > 0$, then $\arg(p_t) = \mathcal{O}_S + \alpha_{12}^{1t}(q)$, so $\alpha_{12}^{1t}(\tilde{q}) = \alpha_{12}^{1t}(q)$. If, on the other hand, $\beta_{12}^{1t}(q) < 0$, then $\arg(p_t) = \mathcal{O}_S + \alpha_{12}^{1t}(q) + \pi$. So, $\alpha_{12}^{1t}(\tilde{q}) = \alpha_{12}^{1t}(q) + \pi$ as required. ∎

Lemma 7.54
Let $q \in \mathbf{Dom}_n(x)$ be valid and accepted. Set $\tilde{q} := \mathbf{read}_x(q) \in AH_n$. Suppose that $type_x(\beta_{ij}^{ik}) = 3$. Then
  (i) $|\beta_{ij}^{ik}(\tilde{q})| = |\beta_{ij}^{ik}(q)|$.
  (ii) $\beta_{ij}^{ik}(\tilde{q}) > 0$.

Proof. As in the proof of Lemma 7.53 set $i = 1, j = 2, k = t$ and conclude from Lemma 7.40 that the read off screen is given by screen $S = S_{12} = S_{1t}$. We use Equation 7.5 for determining $\beta_{j_1 j_2}^{j_1 j_t}(\tilde{q})$, while remembering that $p_1 = (0, 0)$.

$$\beta_{12}^{1t}(\tilde{q}) \quad = \quad \frac{p_t \cdot p_2'}{p_2' \cdot p_2'}. \tag{7.7}$$

p_2' is given by

$$p_2' \quad = \quad \mathbf{rot}_{\alpha_{12}^{1t}} p_2 \quad = \quad (\cos[\mathcal{O}_S + \alpha_{12}^{1t}(\tilde{q})], \sin[\mathcal{O}_S + \alpha_{12}^{1t}(\tilde{q})]).$$

Therefore $|p_2'| = 1$, so $\beta_{12}^{1t}(\tilde{q})$ reduces to $\beta_{12}^{1t}(\tilde{q}) = p_t \cdot p_2'$. Observe that $p_2 = (\cos \mathcal{O}_S, \sin \mathcal{O}_S)$ and apply Lemma 7.53. If $\beta_{12}^{1t}(q) > 0$, then $\alpha_{12}^{1t}(\tilde{q}) = \alpha_{12}^{1t}(q)$ and by evaluating Equation 7.7 it follows that $\beta_{12}^{1t}(\tilde{q}) = \beta_{12}^{1t}(q)$. If, on the other hand, $\beta_{12}^{1t}(q) < 0$, then $\alpha_{12}^{1t}(\tilde{q}) = \alpha_{12}^{1t}(q) + \pi$, so $p_t = -\beta_{12}^{1t}(q)p_2'$, which implies that $\beta_{12}^{1t}(\tilde{q}) = -\beta_{12}^{1t}(q)$, as claimed. ∎

Example 7.55

In the hooked tree in our running example, see Examples 7.13, 7.32, 7.38, 7.47 and 7.52, two x-type 3 hooks occur, h_{13}^{14} and h_{12}^{16}. The q-values, that are those values that where used to *fill* the x-screens, and the $\mathbf{read}_x(q)$-values, the values that where *read off* from the filled x-screens, are collected in Table 7.4.

	q coordinate	$\mathbf{read}_x(q)$ coordinate
h_{13}^{14}	$(-1.92, 4°)$	$(1.92, -176°)$
h_{12}^{16}	$(.91, -11°)$	$(.91, -11°)$

Table 7.4: Swap of representatives for type$_x$ 3 hooks.

Note that $\beta_{13}^{14}(q) < 0$. According to Lemmas 7.53 and 7.54 this implies that the representative in K_{13}^{14} swaps. Indeed, β_{13}^{14} changes sign, while $\alpha_{13}^{14}(\tilde{q}) = \alpha_{13}^{14}(q) + \pi$. Ratio $\beta_{12}^{16}(q)$ is positive so here nothing should change and this is reflected in the values in the table.

7.8.2   Managing x-type 2 hooks.

Next lemma shows that in case of a x-type 2 hook, the representative in the Klein bottle stays the same.

Lemma 7.56

Let $q \in \mathbf{Dom}_n(x)$ be valid and accepted. Put $\tilde{q} = \mathbf{read}_x(q) \in AH_n$. Suppose that x-type(h_{ij}^{ik}) = 2. Then

$$(\beta_{ij}^{ik}(\tilde{q}), \alpha_{ij}^{ik}(\tilde{q})) \quad = \quad (\beta_{ij}^{ik}(q), \alpha_{ij}^{ik}(q))$$

Proof. Throughout the proof, we label as in Definition 7.25. The screen orientations $\mathcal{O}_S$ for the different cases are defined in Equation 7.3. Set $k = j_2$ and $i = j_1$. We distinguish three possibilities for the hinge point p_{j_1}.

(i) $j_1 = i_1$. In this case, $j = i_2$. First we show that $\alpha_{i_1 i_2}^{i_1 j_2}(\tilde{q}) = \alpha_{i_1 i_2}^{i_1 j_2}(q)$. In order to determine $\alpha_{i_1 i_2}(\tilde{q})$, we need the coordinates $p_{i_1}(T) = (0,0)$ and $p_{i_2}(T) = (\cos\mathcal{O}_T, \sin\mathcal{O}_T)$ in $T = S_{i_1 i_2}$. It follows that $\alpha_{i_1 i_2}(\tilde{q}) = \arg(p_{i_2}) = \mathcal{O}_T$. For determining $\alpha_{i_1 j_2}(\tilde{q}) = \alpha_{j_1 j_2}(\tilde{q})$ we compute in screen S the coordinates of $p_{j_1}(S) = (0,0)$ and:

$$p_{j_2}(S) = (\cos\mathcal{O}_S, \sin\mathcal{O}_S) = (\cos\mathcal{O}_T + \alpha_{i_1 i_2}^{i_1 j_2}, \sin\mathcal{O}_T + \alpha_{i_1 i_2}^{i_1 j_2}).$$

We get that $\alpha_{i_1 i_2}^{i_1 j_2}(\tilde{q}) = \mathcal{O}_T + \alpha_{i_1 i_2}^{i_1 j_2}(q) - \mathcal{O}_T = \alpha_{i_1 i_2}^{i_1 j_2}(q)$.

Next we determine $\beta_{i_1 i_2}^{i_1 j_2}(\tilde{q})$. For this purpose we compute the coordinates of p_{i_1}, p_{i_2}, p'_{i_2}, and p_{j_2} in $S_{i_1 i_2 j_2} = T$. We gave the first two above, the latter two are given by

$$p'_{i_2}(T) = (\cos\mathcal{O}_T + \alpha_{i_1 i_2}^{i_1 j_2}, \sin\mathcal{O}_T + \alpha_{i_1 i_2}^{i_1 j_2}),$$
$$p_{j_2}(T) = \beta_{i_1 i_2}^{i_1 j_2} p'_{i_2}.$$

By substituting those coordinates in Equation 7.5 we obtain that $\beta_{i_1 i_2}^{i_1 j_2}(\tilde{q}) = \beta_{i_1 i_2}^{i_1 j_2}(q)$, as claimed.
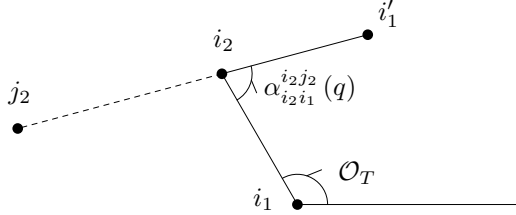
Figure 7.16: $\beta_{i_2 j_2}^{i_2 i_1}(\tilde{q}) = \beta_{i_2 j_2}^{i_2 i_1}(q)$. In the picture, $\beta_{i_2 j_2}^{i_2 i_1}(q) < 0$.

(ii) $j_1 = i_2$. In this case, $j = i_1$. Again we start by showing that $\alpha_{i_2 i_1}^{i_2 j_2}(\tilde{q}) = \alpha_{i_2 i_1}^{i_2 j_2}(q)$. For an illustration of what happens in screen $T = S_{i_1 i_2}$, consult Figure 7.16. As in the case $j_1 = i_1$ it holds that $\alpha_{i_1 i_2}(\tilde{q}) = \mathcal{O}_T$. Therefore, $\alpha_{i_2 i_1}(\tilde{q}) = \mathcal{O}_T + \pi$. Angle $\alpha_{i_2 j_2}(\tilde{q}) = \alpha_{j_1 j_2}(\tilde{q})$ is determined from $p_{j_1}(S) = (0,0)$ and $p_{j_2}(S) = (\cos\mathcal{O}_S, \sin\mathcal{O}_S)$ in $S = S_{j_1 j_2} = S$: screen orientation $\mathcal{O}_S$ is given by $\mathcal{O}_S = \mathcal{O}_T + \alpha_{j_1 i_1}^{j_1 j_2} + \pi$. Therefore $\alpha_{j_1 j_2}(\tilde{q}) = \arg(p_{j_2}) = \mathcal{O}_T + \alpha_{j_1 i_1}^{j_1 j_2} + \pi$. So

$$\alpha_{i_2 i_1}^{i_2 j_2}(\tilde{q}) = \alpha_{i_2 j_2}(\tilde{q}) - \alpha_{i_2 i_1}(\tilde{q}) = \mathcal{O}_T + \alpha_{j_1 i_1}^{j_1 j_2} + \pi - \mathcal{O}_T + \pi = \alpha_{j_1 i_1}^{j_1 j_2}(q).$$

For determining $\beta_{i_2 i_1}^{i_2 j_2}(\tilde{q})$, which occurs in the x-screen T, we apply Equations 7.5

and 7.6 directly:

$$
\begin{aligned}
\beta_{i_2 i_1}^{i_2 j_2}(\tilde{q}) &= \frac{(p_{j_2} - p_{i_2}) \cdot (p'_{i_1} - p_{i_2})}{|p'_{i_1} - p_{i_2}|^2}, \\
&= (p_{j_2} - p_{i_2}) \cdot (p'_{i_1} - p_{i_2}), \\
&= (\beta_{i_2 i_1}^{i_2 j_2}(q)(p'_{i_1} - p_{i_2}) + p_{i_2} - p_{i_2}) \cdot (p'_{i_1} - p_{i_2}), \\
&= \beta_{i_2 i_1}^{i_2 j_2}(q)(p'_{i_1} - p_{i_2}) \cdot (p'_{i_1} - p_{i_2}), \\
&= \beta_{i_2 i_1}^{i_2 j_2}(q).
\end{aligned}
$$

(iii) $j_1 = i_t, t = 3, \ldots m$. In this case $j = i_1$. We start by analyzing $\alpha_{i_t i_1}^{i_t j_2}$. For determining $\alpha_{i_t i_1}(\tilde{q})$ we compute in $T = S_{i_1 i_t}$ coordinates $p_{i_1}(T) = (0,0)$, $p_{i_2}(T) = (\cos \mathcal{O}_T, \sin \mathcal{O}_T)$, and

$$
\begin{aligned}
p_{i_t}(T) &= \beta_{i_1 i_2}^{i_1 i_t}(q) \mathbf{rot}_{\alpha_{i_1 i_2}^{i_1 i_t}(q)}(p_{i_2}), \\
&= \beta_{i_1 i_2}^{i_1 i_t}(q)(\cos(\mathcal{O}_T + \alpha_{i_1 i_2}^{i_1 i_t}(q)), \sin(\mathcal{O}_T + \alpha_{i_1 i_2}^{i_1 i_t}(q))).
\end{aligned}
$$

Therefore,

$$
\alpha_{i_t i_1}(\tilde{q}) = \begin{cases} \mathcal{O}_T + \alpha_{i_1 i_2}^{i_1 i_t}(q), & \beta_{i_1 i_2}^{i_1 i_t}(q) > 0, \\ \mathcal{O}_T + \alpha_{i_1 i_2}^{i_1 i_t}(q) + \pi, & \beta_{i_1 i_2}^{i_1 i_t}(q) < 0. \end{cases}
$$

We use the coordinates, $p_{i_t}(S) = p_{j_1}(S) = (0,0)$ and $p_{j_2}(S) = (\cos \mathcal{O}_S, \sin \mathcal{O}_S)$ in $S = S_{i_t j_2} = S_{j_1 j_2}$ for determining $\alpha_{i_t j_2}(\tilde{q})$. From Equation 7.3 it follows that

$$
\mathcal{O}_S = \begin{cases} \mathcal{O}_T + \alpha_{i_1 i_2}^{i_1 i_t}(q) + \alpha_{j_1 i_1}^{j_1 j_2}(q) + \pi, & \beta_{i_1 i_2}^{i_1 i_t}(q) > 0, \\ \mathcal{O}_T + \alpha_{i_1 i_2}^{i_1 i_t}(q) + \alpha_{j_1 i_1}^{j_1 j_2}(q), & \beta_{i_1 i_2}^{i_1 i_t}(q) < 0. \end{cases}
$$

After subtracting it follows that $\alpha_{i_t i_1}^{i_t j_2}(\tilde{q}) = \alpha_{i_t i_1}^{i_t j_2}(q)$. We only have to show that $\beta_{i_t i_1}^{i_t j_2}(\tilde{q}) = \beta_{i_t i_1}^{i_t j_2}(q)$. We do so by filling in coordinates in Equation 7.5. The relevant coordinates in screen $S_{i_1 i_t j_2} = T$ are as follows.

$$
\begin{aligned}
p_{i_1} &= (0,0), \\
p_{i_2} &= (\cos \mathcal{O}_T, \sin \mathcal{O}_T), \\
p_{i_t} &= \beta_{i_1 i_2}^{i_1 i_t}(q) \mathbf{rot}_{\alpha_{i_1 i_2}^{i_1 i_t}}(p_{i_2} - p_{i_1}) + p_{i_1}, \\
&= \beta_{i_1 i_2}^{i_1 i_t}(q) \mathbf{rot}_{\alpha_{i_1 i_2}^{i_1 i_t}}(p_{i_2}), \\
p'_{i_1} &= \mathbf{rot}_{\alpha_{i_t i_1}^{i_t j_2}}(p_{i_1} - p_{i_t}) + p_{i_t}, \\
&= \mathbf{rot}_{\alpha_{i_t i_1}^{i_t j_2}}(-p_{i_t}) + p_{i_t}, \\
p_{j_2} &= \beta_{i_t i_1}^{i_t j_2} \mathbf{rot}_{\alpha_{i_t i_1}^{i_t j_2}}(p_{i_1} - p_{i_t}) + p_{i_t}, \\
&= \beta_{i_t i_1}^{i_t j_2} \mathbf{rot}_{\alpha_{i_t i_1}^{i_t j_2}}(-p_{i_t}) + p_{i_t}.
\end{aligned}
$$

Therefore

$$\beta_{i_t i_1}^{i_t j_2}(\tilde{q}) \;=\; \frac{\beta_{i_t i_1}^{i_t j_2}(q)\,\mathbf{rot}_{\alpha_{i_t i_1}^{i_t j_2}}(-p_{i_t}) \cdot \mathbf{rot}_{\alpha_{i_t i_1}^{i_t j_2}}(-p_{i_t})}{\mathbf{rot}_{\alpha_{i_t i_1}^{i_t j_2}}(-p_{i_t}) \cdot \mathbf{rot}_{\alpha_{i_t i_1}^{i_t j_2}}(-p_{i_t})} \;=\; \beta_{i_t i_1}^{i_t j_2}(q). \qquad \blacksquare$$

Example 7.57
In our running example we have two type$_x$2 hooks, h_{13}^{12} and h_{31}^{35}. The reader is invited to check that the representatives computed for $\mathbf{read}_x(q)$ in K_{13}^{12} and K_{31}^{35} that are the same as those for q itself. See in particular Example 7.47 and Example 7.52.

7.8.3 Consistency theorem for hooked tree elements.

Theorem 7.58
Fix $x \in XAH_n$. Let $q \in \mathbf{Dom}_n(x)$ be valid and accepted. Then

$$\mathbf{Dom}_n(x) \quad \rightarrow \quad \mathbf{Scr}_n(x) \quad \rightarrow \quad AH_n \quad \rightarrow \quad \mathbf{Dom}_n(x),$$

$$q \quad \mapsto \quad \mathbf{draw}_x(q) \quad \mapsto \quad \mathbf{read}_x(q) \quad \overset{tv_x}{\mapsto} \quad \tilde{q}.$$

is the identity map.

Proof. We analyze the three types of data elements present in $ht(x)$, see Definition 7.25. The type$_x$ 3 hooks are dealt with in Lemma 7.53 and the type$_x$ 2 hooks in Lemma 7.56. We are left with the type$_x$ 2.a angle between the top screen and its second maximal cluster. In Definition 7.25 this angle is labeled α_{1j_2}. The separating screen of p_1 and p_{j_2} is the top screen $S_{[n]}$, so we have to read off in this screen. The coordinates of p_1 and p_{j_2} in $S_{[n]}$ are $p_1 = (0,0)$ and $p_{j_2} = (\cos\alpha_{1j_2}(q), \sin\alpha_{1j_2}(q))$. The read off value $\alpha_{1j_2}(\tilde{q})$ equals $\arg(p_{j_2}) = \alpha_{1j_2}(q)$. This completes the proof of the theorem. $\blacksquare$

7.9 XAH_n is smooth.

Lemma 7.59
Fix $x \in XAH_n$. Let $q \in XAH_n$ be such that:
  (i) $tv_x(q)$ is valid and accepted;
  (ii) $q = \psi_{AH_n}([c_q])$ for some $[c_q] \in \mathbf{conf}_n$.
Then $q = \mathbf{read}_x(tv_x(q))$.

Proof. The consistency theorem, Theorem 7.58, proves the claim for those q coordinates that belong to $\mathbf{Dom}_n(x)$. In the rest of the proof, we analyze $\alpha_{ij} \mod \pi$ and h_{ik}^{ij}. Write $\tilde{q} := \mathbf{read}_x(tv_x(q))$.

First we show that $\alpha_{ab}(q) = \alpha_{ab}(\tilde{q})$ for $a, b \in 1, \ldots, n$, with $a \neq b$. Definition 7.49 tells that we have to determine $\alpha_{ab}(q)$ in the screen S_{ab}. Let j_1 and j_2 be the first label in the first cluster and the first label in the second cluster of screen S_{ab}. Then p_{j_1} and p_{j_2} are the sites drawn first and second in Construction 7.42. If $a \neq j_1, j_2$, then p_a was constructed out of the x-leg $p_{j_1 j_2}$ by repeatedly applying hooks from $ht(x)$ in the order indicated by the hooked path $L_x(p_a)$. The same holds for p_b. For hooks h_{ij}^{ik} that are referred to in $ht(x)$ one has $h_{ij}^{ik}(q) = h_{ij}^{ik}(\tilde{q})$. As a consequence, the positions of p_a and p_b relative to p_{j_1} and p_{j_2} are the same in S_{ab} as in any configuration $c_q \in [c_q]$.

The angle of the directed line passing first through p_{j_1} and then through p_{j_2} in S_{ab} is exactly the screen orientation $\mathcal{O}_{S_{ab}} = \mathcal{O}_{S_{j_1 j_2}}$. Writing out any screen orientation according to the recursion in Equation 7.3 gives a list of data elements corresponding exactly to the hooked path $L_x(p_b)$. As all angles occurring in the screen orientation definition are coordinates of $\mathbf{Dom}_n(x)$, Theorem 7.58 applies again. At any type 2 angle α_{ij}^{ik} however a π switch can occur: the corresponding type 2 ratio β_{ij}^{ik} is not used in the definition. Moreover, representatives might swap in Step 1 of Construction 7.42. It follows that

$$\mathcal{O}_{S_{j_1 j_2}} \;=\; \begin{cases} \alpha_{j_1 j_2}(q), \\ \alpha_{j_1 j_2}(q) + \pi \end{cases}$$

To show that $h_{ij}^{ik}(q) = h_{ij}^{ik}(\tilde{q})$ is easy now. The proof consists of three observations:

(i)   Any q-filled x-screen S is just a copy of the original configuration, due to the Consistency Theorem. But, it also satisfies the following: points not belonging to cluster $C(S)$ corresponding to screen S are omitted; points in S are scaled such that the distance from p_{j_1} to p_{j_2} equals one; points in S are possibly rotated over π according to Construction 7.42, Step 1.

(ii)   By Definition 7.49, $\alpha_{ij}^{ik}(\tilde{q}) = \alpha_{ik}(\tilde{q}) - \alpha_{ij}(\tilde{q})$. From the proof of part 1. of this lemma it follows that the angle $\alpha_{ij}^{ik}(\tilde{q})$ equals $\alpha_{ij}^{ik}(q)$ up to π.

(iii)   In case $\alpha_{ij}^{ik}(\tilde{q}) = \alpha_{ij}^{ik}(q) + \pi$ this π-switch is automatically corrected by the sign of β_{ij}^{ik}, as $\alpha_{ij}^{ik}(\tilde{q})$ is used in Equation 7.6.   ∎

Lemma 7.60
Fix $x \in XAH_n$. Let $U \subset AH_n$ be the set of points in AH_n such that $tv_x(u)$ is valid and accepted for all $u \in U$. Then

$$XAH_n \cap U \;=\; graph(ctv_x(\mathbf{read}_x)). \tag{7.8}$$

Proof. We prove the two inclusions. First let $y \in XAH_n \cap U$. Then its projection $q_y := tv_x(y) \in \mathbf{Dom}_n(x)$ is valid and accepted with respect to x. There always exist points $z \in XAH_n \cap U$ of the form $z = \psi_{AH_n}([c_z])$, for $[c_z] \in \mathbf{conf}_n$, that are arbitrary close to y. For such points z expression (7.8) holds by Lemma 7.59. So these points can be expressed as the image of a configuration consisting of non-coinciding points. Therefore these points z belong to the graph of graph($ctv_x(\mathbf{read}_x)$). This implies

that y itself belongs to the graph as well, as y can be constructed as limit point of points of the form $z = \psi_{AH_n}([c_z])$, for $[c_z] \in \mathbf{conf}_n$ in XAH_n.

Secondly, suppose we start with a point g_q on the graph. This implies that $q = tv_x(g_q) \in \mathbf{Dom}_n(x)$ is valid and accepted. As both conditions (valid, accepted) are open conditions, there exists ϵ with $0 < \epsilon << 1$, such that if we replace all q-ratios that vanish by ϵ that then $q(\epsilon)$ is still valid and accepted. But this means that $\mathbf{draw}_x(q(\epsilon))$ produces a filling of the x-screens in which all sites in the top screen are distinct. Writing down the coordinates gives a class $[c_{q(\epsilon)}] \in \mathbf{conf}_n$. Then

$$\psi_{AH_n}([c_{q(\epsilon)}]) \quad = \quad (q(\epsilon); ctv_x(\mathbf{read}_x(q(\epsilon)))).$$

The claim follows by observing that XAH_n is the closure of $\psi_{AH_n}(\mathbf{conf}_n)$ in AH_n. ∎

Theorem 7.61
XAH_n is a submanifold of AH_n.

Proof. Being a submanifold of a manifold can be determined locally, see [BG], section 6.2. Lemma 7.60 shows that XAH_n can locally be written as the graph of a function, and this is one of the characterizations of submanifold. See [BG], Theorem 2.1.2. notably part (iv). ∎

7.10 Voronoi diagrams in the x-screens.

So far in this chapter we have introduced the space XAH_n in order to model configurations of coinciding sites in the plane. We have seen that we can associate with every $x \in XAH_n$ a family of x-screens. Moreover, for almost all $q \in XAH_n$, we can fill the x-screens with q-sites so that for any two q sites $p_i(q)$ and $p_j(q)$ there exists an x-screen where $p_i(q)$ and $p_j(q)$ are distinct.

In this section we add Voronoi diagrams to the x-screens. As in any x-screen at least two sites are distinct, we could apply the ordinary definition of Voronoi diagram. But there is an ambiguity in the screen model, as we take angles α_{ij} between pairs of points in $\mathbb{R}/\pi\mathbb{Z}$ and allow negative ratios β_{ik}^{ij}.

Example 7.62
Recall Example 7.47. This example demonstrates that q-clusters can get rotated over π in distinct x-screens.

7.10.1 Connection with Kontsevich-Soibelman space.

We nail down the clusters in such a way that they cannot get swapped over π in distinct x-screens. We do this by taking angles between pairs of points in $\mathbb{R}/2\pi\mathbb{Z}$

and allowing ratios $\beta_{ij}^{ik} \in [0, \infty]$ only. That is, we consider the map

$$\psi_{EDAH_n} : \quad \mathbf{conf}_n \quad \rightarrow \quad (\mathbb{R}/2\pi\mathbb{Z})^{\binom{n}{2}} \times ([0, \infty] \times \mathbb{R}/2\pi\mathbb{Z})^{6\binom{6}{3}},$$
$$[(p_1, \ldots, p_n)] \quad \mapsto \quad ((\alpha_{ij})_{1 \leq i < j \leq n}, (\beta_{ij}^{ik}, \alpha_{ij}^{ik})).$$

where i, j, and k are pairwise distinct indices. Denote by $EDAH_n$ the product $(\mathbb{R}/2\pi\mathbb{Z})^{\binom{n}{2}} \times ([0, \infty] \times \mathbb{R}/2\pi\mathbb{Z})^{6\binom{6}{3}}$. Recall the manifold with corners $FM_2(n)$ introduced by Kontsevich and Soibelman, see [KS] and described in Section 7.1.2.

Proposition 7.63
Let $XEDAH_n$ denote the closure of $\psi_{EDAH_n}(\mathbf{conf}_n)$ in $EDAH_n$. Then

$$XEDAH_n \quad \cong \quad FM_2(n).$$

Proof. FM_2 is defined as the closure of the image of $\mathbf{conf}_n$ under the map

$$[\{p_1, \ldots, p_m\}] \quad \mapsto \quad ((\alpha_{ij})_{1 \leq i < j \leq n}, \beta_{ij}^{ik}),$$

where i, j, and k are pairwise distinct indices and $\beta_{ij}^{ik} = \frac{|p_i - p_k|}{|p_i - p_j|}$. As $\alpha_{ij}^{ik} = \alpha_{ik} - \alpha_{ij}$, the claim follows directly. ∎

Figure 7.17: The Voronoi diagram of $p_1(t)$, $p_2(t)$ and $p_3(t)$. On the left for negative t, on the right for positive t.

Example 7.64
Consider $p_1(t) = t(1, 0)$, $p_2(t) = t(-\frac{1}{2}, \frac{1}{2}\sqrt{3})$, and $p_3(t) = t(-\frac{1}{2}, -\frac{1}{2}\sqrt{3})$. We compare the angles associated to p_1, p_2, and p_3 in $XAH[3]$ and $FM_2(3)$ for positive and negative t. First we consider $XAH[3]$. The undirected angles $\overline{\alpha_{12}} = -\frac{\pi}{3}$, $\overline{\alpha_{13}} = \frac{\pi}{3}$ and $\overline{\alpha_{23}} = \frac{\pi}{2}$ do not change at $t = 0$. In $FM_2(3)$, however, angles α_{12}, α_{13} and α_{23} change by π at $t = 0$. Think of this as moving into another corner in the manifold with corners. In Figure 7.17 the Voronoi diagram of $p_1(t)$, $p_2(t)$ and $p_3(t)$ is shown. On the left for any negative value of t, on the right for any positive value of t. Note the jump in the diagram at $t = 0$. It demonstrates the need of the directed angles in the screen model if we want to use it for displaying Voronoi diagrams.

$$\alpha = \alpha_0 \qquad\qquad \alpha = \alpha_0 + \pi$$
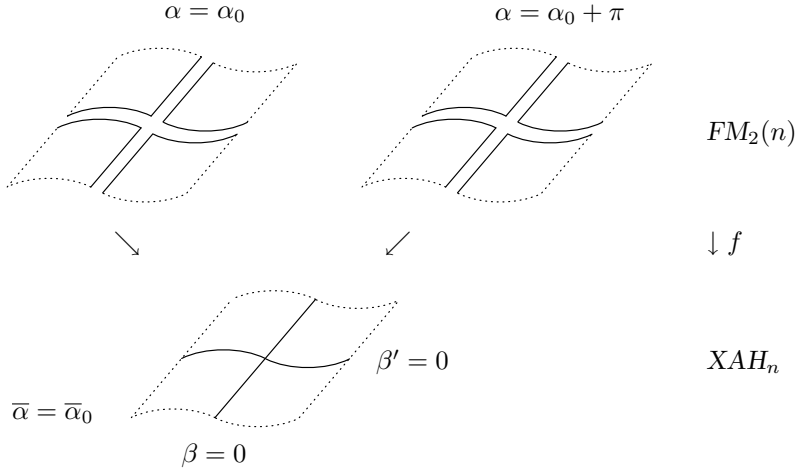
Figure 7.18: The manifold with corners $FM_2(n)$ above the smooth manifold XAH_n, with $\overline{\alpha}$, β, and β' in $\mathbf{Dom}_n(x)$. That slice is presented where all coordinates are fixed except for β and β'.

Theorem 7.65

See also Figure 7.18. Consider the map

$$
\begin{array}{rccl}
f : & FM_2(n) & \to & XAH_n, \\
& ((\alpha_{ij})_{1 \le i < j \le n}, (\beta_{ij}^{ik}, \alpha_{ij}^{ik})) & \mapsto & ((\overline{\alpha_{ij}}_{1 \le i < j \le n}), [(\beta_{ij}^{ik}, \alpha_{ij}^{ik})]),
\end{array}
$$

where [.] denotes the class of $[(\beta_{ij}^{ik}, \alpha_{ij}^{ik})]$ in the Klein bottle K_{ij}^{ik} with respect to the equivalence relation $\sim_k$. Fix $x \in XAH_n$. Let m be the number of $\beta_{ij}^{ik}(x)$ in $\mathbf{Dom}_n(x)$ such that $\beta_{ij}^{ik}(x) = 0$. Then

$$|f^{-1}(x)| \quad = \quad 2^{m+1}.$$

Proof. Fix a class $[(\beta_{ij}^{ik}(x), \alpha_{ij}^{ik}(x))]$ such that $\beta_{ij}^{ik}(x) = 0$. Any such class has two elements, $(0, \alpha_{ij}^{ik})$ and $(0, \alpha_{ij}^{ik} + \pi)$. By Lemma 7.60, XAH_n can be written as the graph of a function on $\mathbf{Dom}_n(x)$. Therefore those β_{ij}^{ik} components that are not in $\mathbf{Dom}_n(x)$ are a function of those components that are in $\mathbf{Dom}_n(x)$. Moreover, $\mathbf{read}_x(x)$ even determines the representative for those β_{ij}^{ik} components that are not in $\mathbf{Dom}_n(x)$. For any $\beta_{ij}^{ik} \in \mathbf{Dom}_n(x)$, the two representatives correspond to two distinct pieces of the boundary in $FM_2(n)$. We conclude that we can use the signvector of those $\beta_{ij}^{ik}(x) \in \mathbf{Dom}_n(x)$ with $\beta_{ij}^{ik}(x) = 0$ as a coordinate system pointing to the distinct corners in the fiber of the map f. The additional 1 in 2^{m+1} comes from the two representatives of the unique α_{ij}-component in $\mathbf{Dom}_n(x)$. ∎

Example 7.66

Consider $x \in XAH_3$ given by

$\overline{\alpha}_{12}$	$\overline{\alpha}_{13}$	$\overline{\alpha}_{23}$	$(\beta_{12}^{13}, \alpha_{12}^{13})$	$(\beta_{21}^{23}, \alpha_{21}^{23})$	$(\beta_{31}^{32}, \alpha_{31}^{32})$
$\frac{\pi}{6}$	$\frac{\pi}{6}$	$\frac{\pi}{4}$	$(1, 0)$	$(0, -\frac{5\pi}{12})$	$(0, \frac{\pi}{12})$

Theorem 7.21 associates to x the nest $\langle \{1, 2, 3\}, \{2, 3\} \rangle$. The factor $\mathbf{Dom}_3(x)$ consists of the two components $\overline{\alpha}_{12}(x)$ and $h_{21}^{23}(x)$. The standard form of x restricted to $\mathbf{Dom}_3(x)$ is given by the representatives $\alpha_{12}(x) = \frac{\pi}{6}$ and $\alpha_{21}^{23}(x) = -\frac{5\pi}{12}$, compare Definition 7.33. The fiber $f^{-1}(x)$ consists exactly of those points in $FM_2(3)$ that are mapped on the same standard form in XAH_n. We obtain these points by analyzing the four distinct representatives for α_{12} and α_{21}^{23}. Choose for example $\alpha_{12} = -\frac{5\pi}{6}$ and $\alpha_{21}^{23} = -\frac{5\pi}{12}$. It follows from the nest structure that $\alpha_{13} = \alpha_{12}$, while $\alpha_{23} = \alpha_{21}^{23} + \alpha_{21} = -\frac{5\pi}{6} + \frac{\pi}{6} = -\frac{\pi}{4}$. The four points $f_1, \ldots, f_4$ in $FM_2(3)$ obtained in this way with coordinates $(\alpha_{12}, \alpha_{13}, \alpha_{23}, \beta_{12}^{13}, \beta_{23}^{21}, \beta_{32}^{31})$, are given by

$$
\begin{aligned}
f_1 &= (\tfrac{\pi}{6}, \tfrac{\pi}{6}, \tfrac{3\pi}{4}, 1, 0, 0), \\
f_2 &= (\tfrac{\pi}{6}, \tfrac{\pi}{6}, -\tfrac{\pi}{4}, 1, 0, 0), \\
f_3 &= (-\tfrac{5\pi}{6}, -\tfrac{5\pi}{6}, -\tfrac{\pi}{4}, 1, 0, 0), \\
f_4 &= (-\tfrac{5\pi}{6}, -\tfrac{5\pi}{6}, \tfrac{3\pi}{4}, 1, 0, 0).
\end{aligned}
$$

Remark 7.67

In Chapter 5 we have encountered a similar situation in comparing the spaces CUA_3 and CDA_3 of undirected and directed angles on three points. Recall particularly Examples 5.30 and 5.31.

We can define and fill x-sreens in $FM_2(n)$ as well. Fix a point $x \in FM_2(n)$. The set of vanishing ratios $\beta_{ij}^{ik}(x)$ for x defines a family of x-clusters and corresponding x-screens by applying the methods of Section 7.4. A stripped version of Construction 7.42 fills the x-screens, given some $q \in \mathbf{Dom}_n(x)$. In short, we discuss the adaptations in Construction 7.42.

Ad Step 1.   We do not have representatives in $EDAH_n$, so we skip Step 1.

Ad Step 2.   The definition of $\mathcal{O}_S$ still holds, but negative ratios β_{ij}^{ik} do not occur in $EDAH_n$.

Ad Step 3. In Step 3 nothing changes.

7.10.2   Adding Voronoi diagrams in the x-screens.

In this section we define a Voronoi diagram $V_{FM}(x)$ for $x \in FM_2(n)$.

Definition 7.68

Let $x \in FM_2(n)$. The Voronoi diagram $V_{FM}(x)$ is defined in terms of the x-screens filled by $draw_x(x)$. Fix an x-screen T filled by $draw_x(x)$. Let C be the cluster corresponding to T. Its maximal subclusters are denoted by $C_1, \ldots, C_m$. Suppose that the coordinates of $C_1, \ldots, C_m$ in T are given by $t_1, \ldots, t_m$.

Initialization. *$V(T)$ is defined as the Voronoi diagram $V(\{t_1, \ldots, t_m\})$.*

Completion. *This is a recursive step from the screens displaying single sites up to the top screen. Assume that the maximal subscreens $S_1, \ldots, S_m$ of T have been completed. Denote the completed diagram in S_i by $V_{FM}(S_i)$. After the initialization step, any cluster C_i lives in a Voronoi cell $V(t_i)$ in T. Define*

$$V_{FM}(t_i) \quad = \quad V(t_i) \cap V_{FM}(S_i),$$

and

$$V_{FM}(T) \quad = \quad \bigcup_{i=1 \ldots m} V_{FM}(t_i).$$

The Voronoi diagram $V_{FM}(x)$ is the rooted tree of all $V_{FM}(T)$, where T runs over all x-screens. The ordering on $V_{FM}(T)$ is inherited from the ordering on the x-screens.
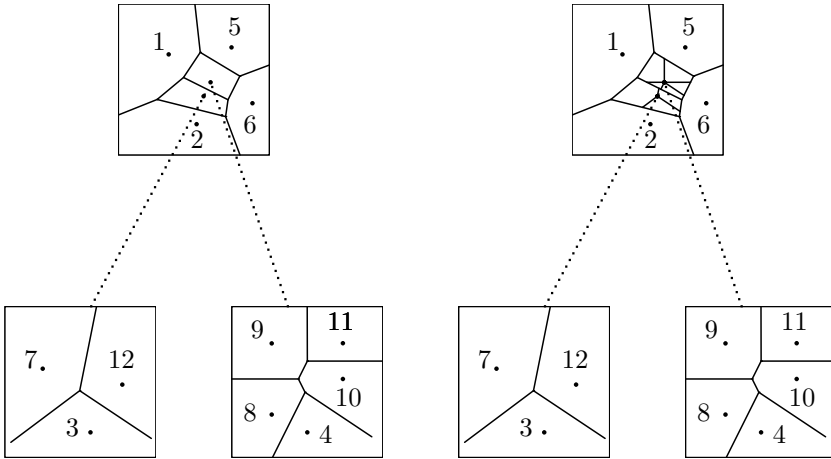
Figure 7.19: Constructing $V_{FM}(x)$: on the left, initialization; on the right, completion.

Example 7.69

Recall Example 4.42. In this example we consider an ordered set of sites in $\mathbb{R}[t] \times \mathbb{R}[t]$ given by

$$
\begin{aligned}
S(t) \quad = \quad & ((-6, 4), (-2, -6), (-1, -2 - 3t), (0, -3t), (3, 5), (6, -3), \\
& (-1 - 3t, -2 + t), (-2t, -2t), (-2t, 2t), (2t, 0), (2t, 2t), (-1 + 2t, -2)).
\end{aligned}
$$

For any pair of sites $p_i(t)$ and $p_j(t)$ we have defined an angle or direction $\alpha_{ij}(t)$ at $t = 0$. In a similar way we can define a ratio

$$\beta_{ij}^{ik}(0) \quad = \quad \lim_{t \downarrow 0} \frac{|p_i(t) - p_k(t)|}{|p_i(t) - p_j(t)|}.$$

This establishes a map χ from a set $S(t)$ of n sites in $\mathbb{R}[t] \times \mathbb{R}[t]$ to a point $x :=$ $\chi(S(0)) \in FM_2$. We construct the Voronoi diagram $V_{FM}(x)$ by applying Definition 7.68. The nest of x is given by $\langle \{3, 7, 12\}, \{4, 8, 9, 10, 11\}\rangle$. Figure 7.19 shows on the left the three filled screens together with the Voronoi diagrams added in the initialization step. On the right the diagram $V_{FM}(x)$ is shown. It is constructed by adding the two diagrams corresponding to clusters $3, 7, 12$ and $4, 8, 9, 10, 11$ in the cells of those clusters in the top screen.

Example 7.70
We analyze an example where the maximal depth of a site equals 2. We start with the ordered set of sites in $\mathbb{R}[t] \times \mathbb{R}[t]$ given by $S(t) = \{p_1, p_2, p_3, p_4\}$, where

$$
\begin{aligned}
p_1 &= (0, 0), \\
p_2 &= t(\cos \tfrac{\pi}{3}, \sin \tfrac{\pi}{3}), \\
p_3 &= p_2 + t^2(\cos \tfrac{\pi}{6}, \sin \tfrac{\pi}{6}), \\
p_4 &= p_3 + t^3(\cos \tfrac{\pi}{2}, \sin \tfrac{\pi}{2}).
\end{aligned}
$$

As in Example 7.69, one can construct a point $y = \chi(S(0)) \in FM_2$. The nest of y is given by $\langle 234, 34\rangle$. In Figure 7.20 the tree of filled screens for y is shown: on the left after the initialization step but before the completion step of Definition 7.68; on the right after the completion step. In this example one can see clearly how the Voronoi diagram $V_{FM}(T)$ of the top screen T is built up recursively out of the screens corresponding with the subclusters of $\{1, 2, 3, 4\}$.

Remark 7.71
Note the compatibility with the construction of limit Voronoi diagram for sites in $\mathbb{R}[t] \times \mathbb{R}[t]$ as constructed in Chapter 3. Compare also Examples 7.69 and 7.70.

7.11   Conclusion.

7.11.1   An easy model to remember.

In this chapter we have presented a real version of the Fulton-MacPherson compactification $X[n]$. An advantage of our approach is that we do not need any machinery from algebraic geometry neither in constructing our compactification space XAH_n nor in proving that it is a smooth manifold. Instead of algebraic blowups we have used the angles between two points and the hooks between three points. This idea was already proposed by Kontsevich and Soibelman. We have shown how to adapt their approach so that the resulting modified compactification space is a smooth manifold instead of just a manifold with corners. Moreover, we have shown that an explicit analysis of the ratios on triples of points gives a combinatorial counterpart of Fulton-MacPherson's description of degenerated configurations in terms of screens.

Because of its nature, the construction and description of the space XAH_n can serve as a illustrative example to the theory of configuration spaces that has attracted a
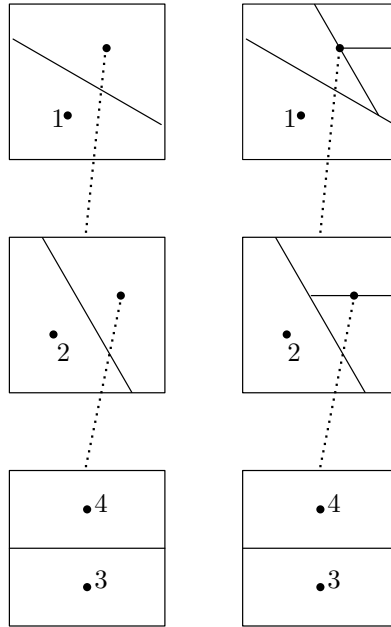
Figure 7.20: Constructing $V_{FM}(y)$: on the left, initialization; on the right, completion.

lot of interest in recent years. The setup in terms of screens can serve as a general framework for studying properties of point sets in the plane. Especially for point sets that contain almost coinciding points, a description by angles and hooks can be a more robust alternative for storing the relative positions of the points. Another advantage of working with hooks and angles is that translations and scalings are already eliminated. That is, one concentrates on point configuration up to affine transformations.

[FM], Theorem 2 states that the Fulton-MacPherson compactification $X[n]$ equals the closure of $CONF_n$ in the product of those $\mathrm{Bl}_\Delta(X^S)$ for $S \subset \{1, \ldots, n\}$ of cardinality 2 and 3. Note that our model also supports this 'three is enough' motto: we only consider properties of pairs of points (the angles) and triples of points (the hooks).

7.11.2 Relation to earlier chapters.

A first application is given by studying limits of Voronoi diagrams: we have introduced a method to associate a collection of filled x-screens to a point $x \in XAH_n$. In the final sections it turned out that this method can be ported to the manifold with

corners $FM_2(n)$, introduced by Kontsevich-Soibelman. Just because of its corners, the screen structure associated to a point x in $FM_2(n)$ is well suited for modeling a possibly degenerated Voronoi diagram for x. Recall the description of Voronoi diagrams of polynomial sites, presented in Chapter 4: we have by now two notions of degenerated Voronoi diagram that match both combinatorially and according to shape with the notion of classic Voronoi diagram.

From a set $S(t)$ of n distinct sites $\{p_1(t), \ldots, p_n(t)\}$ in $\mathbb{R}[t] \times \mathbb{R}[t]$ we can construct a point $s \in XAH_n$ at $t = 0$, compare Example 7.69. A construction in the other direction can be made as well. Suppose we are given some $x \in XAH_n$. And suppose the x-screens are filled by x-sites $p_1(x), \ldots, p_n(x)$. Define the **depth** of a screen S as:

$$\mathrm{depth}(S) \quad = \quad 1 + \# \text{ screens above } S.$$

Let p_j be the site directly above p_i with respect to the predecessor relation defined in Definition 7.27. The polynomial site $p_i(t)$ representing $p_i(x)$ is defined as:

$$\begin{aligned} p_1(t) &= (0,0), \\ p_i(t) &= p_j(t) + t^{\mathrm{depth}(S_{ij})} \left(\text{coordinates}(\, p_i(x)\,) \text{ in } S_{ij} \right). \end{aligned}$$

Mapping a set $S(t)$ of polynomial sites to a point $s \in XAH_n$ and back results in this way in a normal form for $S(t)$.

In Chapters 5 and 6 we have studied the compactification CDA_n. This compactification is the closure of the graph of the directed angle map, cf. Definition 5.11. One of the drawbacks of considering only directed angles is that collinear configurations can not be reconstructed from just these angles, compare Section 5.2. This problem is solved in the compactification XAH_n by adding the hooks between triples of points.

In Chapter 6, Theorem 6.11 we prove essentially that two data sets $\gamma_n, \eta_n \in CDA_n$ that are Euclidean close have Voronoi diagrams $V(\gamma_n), V(\delta_n)$ that are Hausdorff close. As there is an obvious continuous map (forget all ratios) from $FM_2(n)$ to CDA_n, this continuity result also holds for the top screen of the Voronoi diagram $V_{FM}(x)$. More precisely: suppose we have some $x \in FM_2(n)$. Fill the top screen $S_{[n]}$ by x. The coordinates of the sites $p_1(x), \ldots, p_n(x)$ can be read off from $S_{[n]}$, while the directed angles between pairs of sites are part of x. These data together determine a point $\gamma_n \in CDA_n$. This establishes a map $f : FM_2 \to CDA_n$. We have the following situation:

$$\begin{array}{ccccc} FM_2(n) & \overset{f}{\to} & CDA_n & \overset{\text{Voronoi map}}{\to} & \text{diagram space,} \\ x & \mapsto & \gamma_n & \mapsto & V(\gamma_n). \end{array}$$

As both f and the 'Voronoi map' are continuous, the composition is continuous as well. In this short analysis, we have left out the incorporation of the compactness condition on the Voronoi map. This is left as an exercise to the reader.

Bibliography

[AAHSW] Andrzejak, A., Aronov, B., Har-Peled, S., Seidel, R., Welzl, E. – Results on k-sets and j-facets via continuous motions, in: Proc. 14th Annual ACM Symposium on Computational Geometry, (1998) 192-199.

[AG] Abrams, A., Ghrist, R. – Finding Topology in a Factory: Configuration Spaces, American Math. Monthly, **109**, no 2, (2002), 140-150.

[AGMR] Albers, G., Guibas, L.J., Mitchel, J.S.B., Roos, R. – Voronoi Diagrams of Moving Points, Internat. J. Comput. Geom. Appl., **8** (1998), 365-380.

[AK] Aurenhammer, F., Klein, R. – Voronoi diagrams, in: Handbook of Computational Geometry (eds. J. Sack, J. Urrutia), Elsevier, (2000).

[AS] Aurenhammer, F., Schwarzkopf, O. – A Simple On-Line Randomized Incremental Algorithm for Computing Higher-Order Voronoi Diagrams, International Journal of Computational Geometry & Applications **4**, (1992), 363-381.

[BKOS] De Berg, M., Van Kreveld, M., Overmars, M., Schwarzkopf, O. – Computational Geometry, Springer, (1997).

[BG] Berger, M., Gostiaux, B. – Differential Geometry: Manifolds, Curves, and Surfaces, Springer, (1988).

[Bj] Björner, A. – Topological Methods, in: Handbook of Combinatorics (eds. R. Graham, M. Grötschel, L. Lovász), Elsevier, (1995).

[Ca] Cain, G.L. – Introduction to General Topology, Addison-Wesley, (1994).

[CF] Conway, J.H., Fung, F.Y. – The Sensual (Quadratic) Form, Math. Assoc. America, (1997).

[CM] Coxeter, H.S.M., Moser, W.O.J. – Generators and Relators for discrete groups, Springer, (1957).

[CS] Clarkson, K.L., Shor, P.W. – Applications of Random Sampling in Computational Geometry II, Discrete and Computational Geometry, **4** (1989), 387-421.

[De] Dehne, F. – An $O(n^4)$ algorithm to construct all Voronoi diagrams for k-nearest neighbor searching in the Euclidean plane, Proc. Int. Col. on Automata, Languages and Programming, Barcelona(Spain), (1983), Springer, Lecture Notes in Computer Science, Vol 154.

[De1] Devados, S.L., – Tessellations of Moduli Spaces and the Mosaic Operad, Contemporary Mathematics **239** (1999), 91-114.

[De2] Devados, S.L., – A Space of Cyclohedra, Discrete and Computational Geometry, submitted, (2001).

[DEG] Dey, T.K., Edelsbrunner, H., Guha, S. – Computational topology, invited paper in Advances in Discrete and Computational Geometry, eds. B. Chazelle, J.E. Goodmann and R. Pollack. Contemporary Mathematics, AMS, (1998).

[Ed] Edelsbrunner, H. – Algorithms in Combinatorial Geometry, Springer, (1987).

[Ed2] Edelsbrunner, H. – Geometry and Topology of Mesh Generation, Cambridge University Press, (2001).

[EM] Edelsbrunner, H., Mücke, E.P. – Simulation of simplicity: a technique to cope with degenerate cases in geometric algorithms, ACM Transactions on Graphics, **9** (1990), 66-104.

[FM] Fulton, W., MacPherson, R. – A compactification of configuration spaces, Annals of Mathematics, **139** (1994), 183-225.

[Go] Goldstein, H. – Classical Mechanics, 2nd ed., Addison-Wesley, (1980).

[GHK] Gudmundsson, J., Hammar, M., Van Kreveld, M. – Higher order Delaunay Triangulations, Comput. Geom. Theory Appl., accepted.

[Ha] Hartshorne, R. – Algebraic Geometry, Springer, (1977).

[Ke1] Kendall, D. G. – A survey of the statistical theory of shapes, Statistical Science, Vol. 4, No. 2, 87-120, (1989).

[Ke2] Kendall, W.S. – Geometry, statistics and shape, in: Geometry in present-day science (eds. O.E.Barndorff-Nielsen, E.B. Vedel Jensen), World Scientific, (1999).

[Ko] Kontsevich, M. – Operads and Motives in Deformation Quantization, `xxx-QA/9904055`, (1999).

[KS] Kontsevich, M., Soibelman, Y., – Deformation of algebras over operads and Deligne's conjecture, `xxx-QA/0001151`, (2000).

[Kr] Kreyszig, E. – Advanced Engineering Mathematics, 8th edition, Wiley, (1999).

[Le] Lee, D.T. – On k-nearest neighbor Voronoi diagrams in the plane. IEEE Trans. Comput., C-31: 478-487, 1982.

[Ma] Mathematica, version 4, Wolfram Research, Inc., Champaign, IL (1999).

[Mu] Munkres, J.R. – Elements of Algebraic Topology, Addison-Wesley, (1984).

[OBS] Okabe, A., Boots, B., Sugihara, K. – Spatial Tessellations, Wiley, (1992).

[OT] Orlik, P., Terao, H. – Arrangements of Hyperplanes, Springer, (1992).

[R] Rees, E.G. – Notes on Geometry, Springer, Corrected 2nd printing, (1988).

[Sh] Sharir, M. – k-Sets and random hulls, Combinatorica, **13** (1993), 483–495.

[Si] Siersma, D. – Isolated line singularities, Proc. Symp. Pure Mathematics Vol. 40, part 2, (1983), 485-496.

[Vo] Voronoi, G. – Nouvelles applications des paramètres continus à la théorie des formes quadratiques. Deuxième mémoire. Recherches sur les parallélloèdres primitifs. J. Reine Angew. Math. **136**, 198-287, (1909).

[Wa] Walker, J. W. – Homotopy Type and Euler Characteristic of Partially Ordered Sets, Europ. J. Combinatorics, **2** (1981), 373-384.

[Ya] Yap, C.K. – Robust geometric computation, CRC Handbook in Discrete and Computational Geometry (eds. J.E. Goodman and J. O'Rourke), CRC Press, (1997).

[Zi] Ziegler, G. M. – Lectures on Polytopes, Springer, (1994).

Index

Samenvatting.

Voronoi diagrammen.

Stel je alle supermarkten in een stad voor. De stad is te verdelen in sectoren door naar de dichtstbijzijnde supermarkt te kijken: alle mensen die wonen in de sector van een bepaalde supermarkt wonen dichter bij die supermarkt dan bij welke andere supermarkt dan ook. Het *Voronoi diagram* van de supermarkten is de onderverdeling van de stad in zulke sectoren. Een voorbeeld van een Voronoi diagram van zes supermarkten, genummerd 1 t/m 6, wordt gegeven door de doorgetrokken lijnstukken in Figuur 7.21.
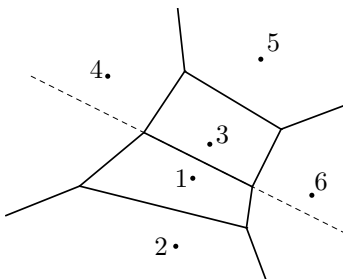

Figuur 7.21: Het Voronoi diagram van zes supermarkten, genummerd 1 t/m 6.

Dit proefschrift gaat over Voronoi diagrammen. Daarom bekijken we Figuur 7.21 wat preciezer. In de afbeelding zien we grenzen, zoals de grens tussen de sector 1 en sector 3. Mensen die op deze grens wonen, wonen net zo dicht bij supermarkt 1 als bij supermarkt 3. We zien dat de grens op een gestippelde lijn ligt. Deze lijn heet de *bisector* van de punten 1 en 3. Aan de ene kant van de lijn wonen de mensen dichter bij supermarkt 1, terwijl mensen aan de andere kant van de lijn dichter bij supermarkt 3 wonen.

Met behulp van deze bisectoren kunnen we bijvoorbeeld sector 1 beschrijven: mensen wonen in sector 1 precies als ze aan de goede kant van alle bisectoren tussen supermarkt 1 en elk van de andere supermarkten wonen. Op deze manier kunnen we alle sectoren beschrijven en daarmee ook het Voronoi diagram.

Limieten van Voronoi diagrammen.

Na het voorafgaande zal het niemand verbazen dat Voronoi diagrammen veel toege-
past worden buiten de wiskunde, bijvoorbeeld bij planningsproblemen, maar ook
bij het tekenen van hoogtelijnen op stafkaarten. In Hoofdstuk 2 worden een aantal
bekende feiten over Voronoi diagrammen en verwante constructies op een rijtje gezet.
Zoals uit de titel blijkt, willen we in dit proefschrift *limieten* van Voronoi diagrammen
beschrijven. Deze introduceren we met behulp van SRV-wagens.
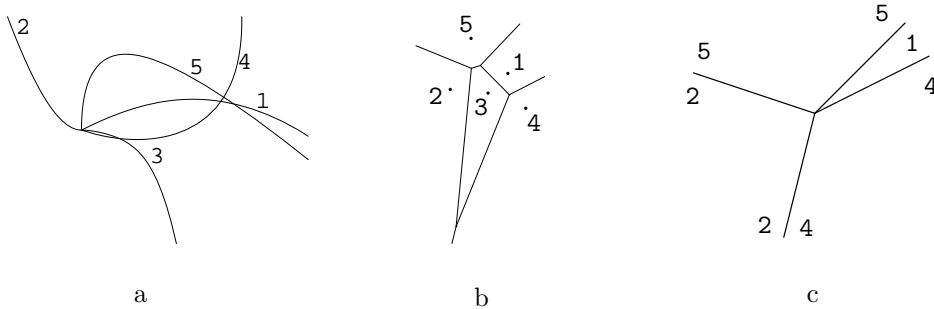
Figuur 7.22: a. Vijf SRV-wagens op weg naar een botsing. b. Het Voronoi diagram
van de SRV-wagens vlak voor de botsing. c. Het limiet Voronoi diagram tijdens de
botsing.

In Figuur 7.22.a zien we de routes die vijf SRV-wagens op zekere dag afleggen.
Zolang de SRV-wagens op verschillende plekken in het land zijn, zoals in Figuur
7.22.b, kunnen we het Voronoi diagram van de SRV-wagens bepalen, net als we
eerder met de supermarkten hebben gedaan. Maar wanneer de SRV-wagens op een
ongelukkig moment botsen, is het niet zo duidelijk wat het Voronoi diagram van
de SRV-wagens op dat moment is. In Hoofdstuk 4 laten we zien hoe we toch een
Voronoi diagram kunnen uitrekenen op het moment van de botsing als we maar
weten met welke relatieve snelheid en onder welke hoek ze botsen. Op die manier
verkrijgen we een *limiet* Voronoi diagram zoals in Figuur 7.22.c.

Hoe een limiet is opgebouwd, wordt geïllustreerd in Figuur 7.23. Twee punten (SRV-
wagens) vallen samen. Zolang de twee punten verschillen, zoals in Figuren 7.23.a
en 7.23.b, is het Voronoi diagram van de punten 1 en 2 precies de bisector van de
twee punten. Maar zodra twee punten samenvallen is de bisector en dus het Voronoi
diagram niet gedefiniëerd. We lossen dit probleem eenvoudigweg op door op het
samenvalmoment toch een bisector te definiëren: dit is de lijn die enerzijds door de
twee samenvallende punten gaat en anderzijds loodrecht staat op de hoek waaronder
de twee punten botsen. Bovendien geven we de lijn een richting, bijvoorbeeld zo dat
punt 1 links van de lijn ligt vlak voor de botsing.

Ook als we meerdere punten hebben, zoals in Figuur 7.22, kunnen we op deze manier
een bisector definiëren tussen elk tweetal punten. Eerder hebben we al gezien dat

elke Voronoi sector en daarmee dus ook het Voronoi diagram volledig wordt bepaald door alle bisectoren.
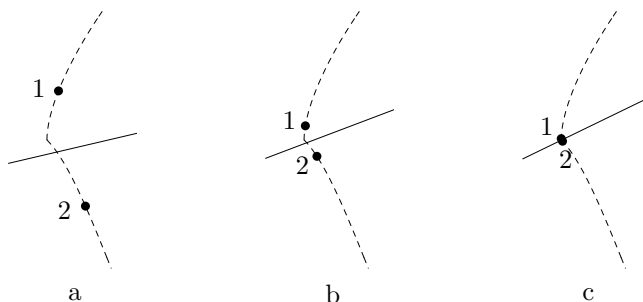
Figuur 7.23: Een Voronoi diagram van twee samenvallende punten.
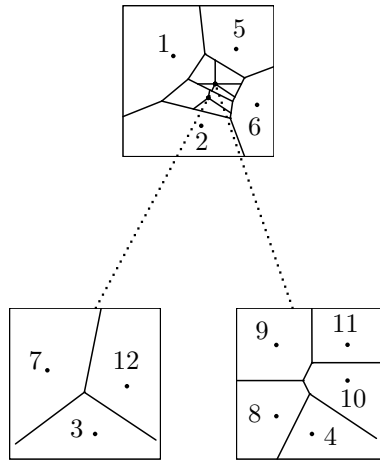
Compactificaties van configuratie ruimten.

Een verzameling verschillende punten in het vlak wordt vaak een *configuratie* genoemd. En de *configuratie ruimte* is het object waarin alle verschillende configuraties te vinden zijn. Een element van de configuratie ruimte is dus een verzameling verschillende punten. Voor zo'n element kunnen we alle hoeken tussen deze punten opschrijven. Zo verkrijgen we een uitgebreid element, bestaande uit zowel punten als hoeken. Al deze uitgebreide elementen brengen we onder in een punten- en hoeken-ruimte. Deze punten-en hoeken-ruimte is een object met veel dimensies dat randen heeft, denk aan de rand van een tafel. Elementen die op zo'n rand leven, corresponderen met gedegenereerde configuraties. Dit zijn configuraties waarin sommige punten samenvallen en zulke configuraties behoren dus niet a priori tot de punten- en hoeken-ruimte. De *compactificatie* van de de punten- en hoeken-ruimte is nu juist de oorspronkelijke punten- en hoeken-ruimte waaraan alle randen zijn toegevoegd.

In Hoofdstuk 5 definiëren we zo'n punten- en hoeken-compactificatie en gaan we voor kleine configuraties na welke hoeken mogelijk zijn tussen punten. Bovendien bekijken we een algebraïsche variant van de punten- en hoeken-compactificatie door te rekenen met de bekende vergelijking $y = ax + b$ van een lijn. Door elk tweetal punten van een configuratie van verschillende punten kunnen we immers een lijn trekken.

Met behulp van de bisector methode kunnen we voor elk element van de punten- en hoeken-compactificatie een Voronoi diagram definiëren. In Hoofdstuk 6 bewijzen we dat de representatie van een Voronoi diagram door middel van punten en hoeken in zekere zin robuust is. Namelijk, als twee elementen dicht bij elkaar liggen in de punten- en hoeken-compactificatie, dan lijken de Voronoi diagrammen van deze twee elementen ook erg op elkaar.

Klikbare Voronoi diagrammen.

In het limiet Voronoi diagram in Figuur 7.22.c is de sector van SRV-wagen 3 niet meer terug te vinden. In feite bestaat deze sector uit één punt. Als we deze sector toch beter willen bekijken, zullen we het plaatje oneindig moeten uitvergroten. Dit is mogelijk als we met *klikbare* configuraties werken. Een nieuw voorbeeld is gegeven in Figuur 7.24. In het top scherm zijn zes punten zichtbaar. Echter, twee punten in het midden zijn geen losse punten maar clusters van punten: door op het onderste van die clusters te klikken verschijnt een scherm dat de punten 3, 7 en 12 toont. Merk op dat in alle drie de schermen verschillende punten zichtbaar zijn. Dit maakt het mogelijk in elk scherm het Voronoi diagram van die verschillende punten toe te voegen. De Voronoi diagrammen uit de onderste twee schermen zijn in het klein zichtbaar in de corresponderende sectoren in het top scherm.

Figuur 7.24: Een klikbaar Voronoi diagram in een klikbare configuratie.

In Hoofdstuk 7 definiëren we klikbare Voronoi diagrammen met behulp van een hoeken- en haken-compactificatie. Ten opzichte van de vorige twee hoofdstukken zijn nu de punten in de punten- en hoeken-ruimte vervangen door haken. Zo'n haak is te zien in Figuur 7.25. Deze haak geeft aan waar punt 3 getekend moet worden, gegeven de punten 1 en 2. Daartoe draaien we eerst de poot 12 over een hoek α_{12}^{13} en verlengen (of verkorten) de aldus verkregen poot met een ratio β_{12}^{13}. Stel nu dat de ratio β_{12}^{13} gelijk is aan nul. Poot 13 krijgt dan lengte nul en dus vallen de punten 1 en 3 samen.

Voor een configuratie bestaande uit louter verschillende punten kunnen we alle haak ingrediënten, bestaande uit hoeken en ratio's, zo opschrijven. Door te compactificeren worden elementen bestaande uit hoeken en haken corresponderend met configuraties die samenvallende punten bevatten toegevoegd. Door slim te compactificeren kunnen we zelfs een hoeken- en haken-compactificatie verkrijgen die als
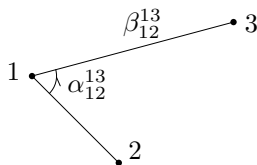
Figuur 7.25: De haak die uit de punten 1 en 2 het punt 3 construeert.

hoog-dimensionaal object glad is, en dus geen scherpe randen bevat. Het bewijs van die gladheid is tegelijk een constructie die aangeeft hoe schermen als in Figuur 7.24 te definiëren en vervolgens te vullen met punten. Onze compactificatie is verwant aan een aantal bekende andere compactificaties en deze verbanden worden ook besproken.

Hogere order Voronoi diagrammen.

Hoofdstuk 3 staat qua inhoud enigszins los van de rest van dit proefschrift. Hier gaat het om hogere order Voronoi diagrammen. Bij het tweede orde Voronoi diagram bijvoorbeeld, kijken we niet alleen naar de dichtstbijzijnde supermarkt, maar naar de twee dichtstbijzijnde supermarkten. Deze hogere order diagrammen kunnen ook worden gedefiniëerd in termen van bisectoren. Wij beschouwen voor een vaste configuratie van punten alle mogelijke zoveelste orde Voronoi diagrammen: het gewone, eerste orde diagram, het tweede orde, het derde orde, enzovoort.

Dankwoord

Op deze plek wil ik graag allen bedanken die hebben geholpen bij het schrijven van dit proefschrift: Rody Aldenhoven, Sergei Anisov, Martijn van Manen, Dima Pasechnik en Richard Vink hebben hele hoofdstukken in een vroegtijdig stadium doorgelezen en van kritische kanttekeningen voorzien; Marcia da Inda, Wim Bomhof, Ellen Meijerink, Behrooz Mirzaii en Yaroslav Kondratyuk hebben altijd voor een goede sfeer op kamer 6.17 gezorgd; de leden van de leescommissie, Prof. Frits Beukers, Dr. Otfried Cheong, Prof. Eduard Looijenga, Prof. Ieke Moerdijk en Dr. Gert Vegter wil ik bedanken voor hun interesse, vragen en opmerkingen; mijn collega's, familie en vrienden wil ik bedanken voor hun belangstelling, geduld en wat dies meer zij; tenslotte wil ik mijn begeleiders, Dirk Siersma en Wilberd van der Kallen, hartelijk bedanken: bijna wekelijks vonden er de afgelopen jaren bijeenkomsten van ons drieën plaats waarbij menige wiskundige noot gekraakt is en steeds weer nieuwe uitdagingen op tafel kwamen.

Curriculum Vitae

Roderik Lindenbergh was born on 12th June 1970 in Aerdenhout. He visited the Eerste Christelijk Lyceum in Haarlem to get his diploma in 1987. After one year of physics he studied mathematics at the Universiteit van Amsterdam until his graduation in 1994. The final half year of his studies were spent at Lehrstuhl D für Mathematik at the RWTH Aachen. Next few months he was the first ever service desk employee of internet provider Planet Internet while waiting for the start of his alternative military service. During his one year service he worked on an interactive algebra book at the Research Institute for Applications of Computer Algebra, then based at Amsterdam and Eindhoven. In April 1996 he went for eight months to London for being a research assistant in computational group theory at QMW College. In 1997 he started to work on the PhD project 'Geometry and Topology of conflict sets of distance functions' as an OIO, Onderzoeker in Opleiding, at the Mathematical Institute of Utrecht University. This work has resulted in the PhD thesis you are reading now.